RATIONAL SOLUTIONS OF NONLINEAR PARTIAL DIFFERENTIAL EQUATIONS

A THESIS SUBMITTED TO

THE UNIVERSITY OF KENT AT CANTERBURY

IN THE SUBJECT OF MATHEMATICS

FOR THE DEGREE

OF DOCTOR OF PHILOSOPHY

By

Ellen Dowie

March 2018

Abstract

The work in this thesis considers rational solutions of nonlinear partial differential equations formed from polynomials. The main work will be on the Boussinesq equation and the Kadomtsev-Petviashvili-I (KP-I) equation, the nonlinear Schrödinger equation will also be included for completeness.

Rational solutions of the Boussinesq equation model rogue wave behaviour. These solutions are shown to be highly structured which, it is hypothesised, is due to the inherent structure and form of integrable differential equations. Rogue wave solutions have been observed in equations such as the nonlinear Schrödinger equation, KP equation and the Boussinesq equation, to name but a few. By examining the form of these solutions and considering the behaviour of the roots, the aim is to establish the behaviour of this family of solutions. All solutions are bounded and real.

Additionally, since a generating function for the KP equation solutions already exists, a characterisation of the solutions will be made along with an attempt at understanding the current generating function in order to improve its adaptability.

Links between solutions of the three equations will be shown as well as a function that can solve all three equations subject to certain criteria on the parameters.

Acknowledgements

I would like to thank my supervisor Peter Clarkson for all the help and encouragement he has provided to me during this experience, as well as the initial introduction to nonlinear waves. This has been an enlightening time for me and you have helped me every step of the way. Additionally to Ana Loureiro for being my second supervisor and aiding me in this process. I would also like to thank the School of Mathematics, Statistics and Actuarial Science at the University of Kent for my PhD studentship.

Thank you to all the friends I have made along the way. I am indebted to Jenny, Mark, Christoph and Mingjie for being such wonderful office mates for the vast majority of this. Thank you for random ice cream trips and the slither scoreboard! Also to Neal for being a surrogate office mate who never failed to make me look at things in a new light. A great thanks to my best friend Fox for the stories, writing and drawing days that kept me calm.

A special thanks goes to Claire Carter, I honestly don't know how I will be without your hugs and laughter. You are irreplaceable.

To my parents, who have always pushed me to be the best that I can be, you gave me the confidence to keep trying when few others believed in me. To my brother, who, no matter how far away he is, has always been there for me. Finally to Ash, for having an uncanny ability to make me smile no matter the situation. I love you all, thank you for all you have done for me.

List of Figures

Contents

Chapter 1

Introduction

This chapter will begin with some motivation for consideration of rational solutions and their applications. Real world events will be used to highlight the importance of the study of these solutions and summarise some current research in the field.

Moving on to the next section, the three equations that will be considered will be given. These are the focusing nonlinear Schrödinger (NLS) equation,

$$\mathrm{i}u_t + u_{xx} + 2|u|^2 u = 0, \tag{1.1}$$

the Boussinesq equation,

$$u_{tt} + u_{xx} - (u^2)_{xx} - \tfrac{1}{3}u_{xxxx} = 0, \tag{1.2}$$

and the Kadomstev-Petviashvili-I (KP-I) equation

$$u_{tx} + 6u_x^2 + 6uu_{xx} + u_{xxxx} + 3\sigma^2 u_{yy} = 0. \tag{1.3}$$

The NLS equation will only be considered briefly through the thesis while the

main work will be related to the Boussinesq and the KP-I equations.

The symmetry reductions will be briefly discussed and how they relate to these types of equations as well as detailing why different methods are used to retrieve solutions. Finally, an outline of the thesis will be provided.

Unless solutions contained within one chapter will be referred to in another, then there will be no superscript notation used; u will usually denote the solution of the differential equation and F will usually denote the polynomial that drives this solution. In the event that solutions are compared they will be referred to as e.g. u^{BE} to denote which equation they solve.

1.1 Motivation

"Rogue waves" have become of more interest in recent decades as further experimentation and monitoring has occurred [10, 51, 54]. They have also been referred to as "freak waves" or "monster waves" to name a few characterisations. Despite an origination in folklore, it has now been proved [35] that not only do these waves occur but they do so more frequently than originally imagined. Given the force and unexpected formation of these waves, they present a significant problem to the safety of ships and crew should they encounter such a phenomenon. The waves have also been found to occur in lakes not only in oceans. One pivotal hypothesised occurrence is that relating to the sinking of the SS Edmund Fitzgerald on Lake Superior in America in 1975. A sighting of 3 rogue waves; a phenomenon known as the "Three Sisters", was reported during a storm in the vicinity of the ship. The ship was sunk and the wreckage found had the bow and stern separated and embedded at the bottom of the lake some 52m away from each other. The bow upright in the mud and the stern capsized. While it could not be proven that the rogue waves were the cause of the ship's destruction the

theory was supported by a sighting of at least 2 rogue waves by a nearby ship.

Evidence of the waves existence was found in 1995 at an oil rig in the North Sea. The rig had measuring equipment for the purpose of checking the stability of the structure itself but it was this equipment that recorded the 26m high wave despite the local sea state only having waves of up to 12m in height.

Though these waves can have a devastating effect, the formal definition does not mean that all rogue waves are the largest waves in the water. They are defined as waves that are twice the height of the mean of the top third highest waves in the surrounding water. Thus they can occur in calm waters and may be much lower than those that cause destruction to ships. However they will still be surprising given the local water behaviour.

This thesis will be concerned with rogue water waves but the waves have also been discovered in other media, namely optical fibres [29, 30, 43, 57], Bose-Einstein condensates [13], superfluids [34], the atmosphere [59] and finance [62, 63].

1.2 The Equations

The three equations that will be considered are all nonlinear partial differential equations (PDEs) known to have soliton solutions. These soliton equations have been studied for some time and can be shown to have rich structures and significant behaviours with their solutions. While the equations are all nonlinear, they have also all been shown to be solvable by the inverse scattering method which is known to have equations with interesting solutions and a hierarchy.

Not only do these equations permit solitary waves, but rational solutions of them elicit rogue wave type behaviour. It also transpires that when there are no parameters, the degree of the polynomial is twice the number of waves that are present. The situation with parametrised equations varies case by case so these

will be explored in each individual chapter.

1.2.1 The Focussing NLS Equation

As mentioned, the NLS equation (1.1) is solvable by the inverse scattering method [65], and has been found to have rogue wave solutions. The solutions are only in terms of 2 variables which does restrict the analysis of the physical behaviour to 1-dimension and time. These rational solutions of the NLS can be described via a Wronskian formation which has still not been characterised for the Boussinesq rational solutions. This formation for the NLS is detailed in [28]. This is the equation that is most frequently studied when considering soliton waves and rogue waves but this thesis will only consider it briefly.

1.2.2 The Boussinesq Equation

The Boussinesq equation (1.2) also gives rise to solutions which result in soliton waves and its rational solutions appear as rogue waves. It is an equation that is solvable by the inverse scattering method [2, 3, 5, 26, 65] and at present there is no generating function for such solutions but the first 6 will be explicitly detailed in Appendix B.1.

As a PDE, the Boussinesq equation is derived from the Navier-Stokes equation for an incompressible fluid combined with a continuity equation. Solutions of the Boussinesq equation model long, shallow water waves; that is where the wave depth is negligible in comparison to the wavelength. It was discovered in 1872 by Joseph Boussinesq following a physical experiment by John Scott Russell conducted in a canal.

Historically it was Russell's chance discovery of the "wave of translation" that is now referred to as a "soliton wave" while conducting an experiment regarding canal boats that led to Boussinesq's derivation of the PDE named after him.

1.2.3 The KP-I Equation

The KP-I equation (1.3) is the final equation that will be considered. Once more, it is a nonlinear PDE that is solvable by the inverse scattering method [31, 47] and thus permits soliton solutions but its rational solutions model rogue waves.

The equation was discovered by Boris Kadomtsev and Vladimir Petviashvili in 1970 as a generalisation of the KdV equation

$$u_t + u_{xxx} - 6uu_x = 0, \tag{1.4}$$

to two dimensions. It was the first integrable equation in $(2+1)$-dimensions to be discovered [45] and has important physical applications. These applications include weakly two-dimensional long waves in shallow water [4, 56], ion-acoustic waves in plasma [38] and sound waves in ferromagnetic media [60].

1.3 Symmetry Reductions

In order to calculate a symmetry reduction of a PDE with dependant variable u and independent variables x and t, it is required that the solutions of this PDE are left invariant under the following transformation

$$\begin{aligned} x^* &= x + \epsilon\xi(x,t,u) + \mathcal{O}(\epsilon^2), \\ t^* &= t + \epsilon\tau(x,t,u) + \mathcal{O}(\epsilon^2), \\ u^* &= u + \epsilon\phi(x,t,u) + \mathcal{O}(\epsilon^2), \end{aligned}$$

where ξ, τ and ϕ are called infinitesimals.

We define the infinitesimal generator as

$$\mathbf{v} \equiv \xi(x,t,u)\frac{\partial}{\partial x} + \tau(x,t,u)\frac{\partial}{\partial t} + \phi(x,t,u)\frac{\partial}{\partial u}. \tag{1.5}$$

This is equivalent to requiring that the n'th prolongation is 0 when u and u^* satisfies the PDE and where n is the order of the PDE and the prolongation is defined as

$$\mathrm{pr}^{(n)}\mathbf{v} \equiv \sum_{\substack{i+j\leq n \\ i,j\geq 0}} \phi^{[x^i t^j]}\frac{\partial}{\partial u_{x^i t^j}} + \mathbf{v}, \tag{1.6}$$

with $\phi^{[r]}$ the infinitesimal associated with $\dfrac{\partial u^*}{\partial r^*}$. Consider the operator $\mathbf{D}$ as differentiation but dependant on what it acts on depends on whether we have to use the chain rule for differentiation given that u is a function of x and t as well.

We define $\phi^{[x]}$ as

$$\phi^{[x]} = \frac{\mathbf{D}\phi}{\mathbf{D}x} - \frac{\mathbf{D}\xi}{\mathbf{D}x}\frac{\partial u}{\partial x} - \frac{\mathbf{D}\tau}{\mathbf{D}x}\frac{\partial u}{\partial t}. \tag{1.7}$$

Here, $\phi^{[t]}$ is merely the above equation with with Dx replaced by Dt and $\phi^{[xx]}$ is the above equation with ϕ replaced by $\phi^{[x]}$ and the u terms being differentiated by x again.

All of these calculations can be verified by making the substitutions into the PDE and simplifying on the basis that u and u^* solve the PDE.

Once we apply the prolongation to obtain an infinitesimal equation and use the original PDE to remove the highest derivative then we can generate a system of equations for ξ, τ and ϕ by equating any derivatives of u to 0 in the infinitesimal equation. Solving this system of equations gives the infinitesimals which we use in the following characteristic equation to obtain the symmetry,

$$\frac{\mathrm{d}x}{\xi} = \frac{\mathrm{d}t}{\tau} = \frac{\mathrm{d}u}{\phi}. \tag{1.8}$$

Symmetry reductions can be used to find new solutions of nonlinear PDEs from previously discovered ones. The pivotal point about the solutions that will be found throughout this thesis is that they are not solutions that can be obtained in this way since the highest power of x and t, or indeed, x, t and y in the $(2+1)$ dimensional case, is the same.

It will be shown that the soliton equations being considered in this thesis have high structure and symmetry. In the case of nonlinear PDEs that are solvable via inverse scattering, one finds that there are interesting behaviours that are not found in non-integrable PDEs. This could be a reason as to why the integrable PDEs have so many symmetries.

1.4 Thesis Outline

Beginning with Chapter 2 and the NLS equation as an introductory equation. This chapter aims to cover some of the methods that will be expanded to apply to later equations. Some background and history of the equation will be given along with some exploration of a parametrised solution which the polynomial complex roots of can be investigated. Trying to ascertain the effect of the parameters on the solutions is something that will be completed for later equations as well.

Moving to Chapter 3 and one of the main equations. The Boussinesq equation will be given along with some history and its bilinear form. There will be an examination of what the rational solutions may look like. Both the behaviour of the solutions of the equation and that of the complex roots of the polynomials that drive the solutions will be explored and similarities identified. Rogue wave solutions are also defined as the limit of some travelling wave solution. §3.5 is concerned with the physical behaviour of waves. An examination of where any saddle points occur is conducted along with an attempt to understand what

behaviours are common, for example is the average height of the waves uniform thus the more waves there are the higher the central wave must be?

In §3.6 investigation of the behaviour of the roots of the F functions particularly around the pivotal cases of t close to 0 and plot these alongside their corresponding functions u. The relationship between the behaviour of the roots and its effect on the solution u for the known functions F is examined.

In Chapter 4, a more general form of the solutions is considered with the addition of two parameters, α and β. Once more, the root structure and 3D graphs are examined to understand the underlying behaviour.

Chapter 6 considers the final equation of KP-I. While a generating function for KP-I has already been found, the methodology behind why it works seems lacking. As such, this chapter aims to understand where the functions come from in order to relate this to a generating function for the Boussinesq equation in the future. Alongside this, a characterisation of the solutions of KP-I given the change of a variable is considered.

Chapter 7 then ties together solutions of all three equations as a single function in terms of parameters. Choices of specific parameters relate to solutions of the different equations.

Chapter 2

The Focusing NLS Equation

This chapter will explore the focusing NLS equation

$$\mathrm{i}u_t + u_{xx} + 2|u|^2 u = 0, \tag{2.1}$$

mainly through the work by Dubard and Matveev [28]. The solutions that will be considered are rational solutions constructed from 3 polynomials F, G and H, the main one of concern being F whereby

$$u_n(x,t) = \left\{1 - 4\frac{G_n(x,t) + \mathrm{i}tH_n(x,t)}{F_n(x,t)}\right\} \exp\left(\tfrac{1}{2}\mathrm{i}t\right), \tag{2.2}$$

and $G_n(x,t)$ and $H_n(x,t)$ are polynomials of degree $\frac{1}{2}(n+2)(n-1)$ in both x^2 and t^2, and $F_n(x,t)$ is a polynomial of degree $\frac{1}{2}n(n+1)$ in both x^2 and t^2 and has no real zeros.

The work will begin with a brief introduction to the background and derivation of the equation, along with its bilinear form. After this there will be consideration of the Wronskian form as defined in [28] and an exploration into how this method produces solutions and whether it will be possible to extrapolate this to different equations. Within this, there will be an investigation into how the roots

of the polynomial that relates to the rational solution influences the shape of the waves and a consideration of some plots in relation to this and the changing of parameters.

The purpose of this chapter is to bridge the gap between current research in the field and less investigated equations. There will be a brief discussion at the end of the chapter as to the possibilities of further research.

2.1 Introduction

The NLS equation (2.1) is a $(1+1)$-dimensional complex equation that is, historically, the main equation used to model water waves. It has also been widely used in the modelling of optical fibres. Named after Erwin Schrödinger, the equation is a nonlinear variation of the Schrödinger equation used in quantum mechanics.

2.1.1 Background

In 1972, Zakharov and Shabat discovered the inverse scattering method to solve the equation [65]. Prior to this, it had been used in various studies into water waves [11, 12].

The NLS equation (2.1) permits "Bright solitons" which decay in the infinite spatial limit. On the other hand, the de-focusing NLS equation, where the sign in front of the modulus is changed, has "Dark soliton" solutions. These solutions do not decay in the same limit.

It was hypothesised in [7] that for solutions of the NLS ψ_n, there is a relation that

$$\frac{1}{8\pi}\int_{-\infty}^{\infty}\int_{-\infty}^{\infty}(|\psi_n(x,t)|^2-1)^2\mathrm{d}t\mathrm{d}x=\tfrac{1}{2}n(n+1)=Q_n, \tag{2.3}$$

where Q_n represents the number of distinct waves. This is an integral relation

that links the function to the number of waves.

2.1.2 Invariants and Symmetries

Invariants and symmetries of nonlinear PDE's are often a way to find new solutions. While the solutions found using the methods in this thesis differ from those that can be obtained from reductions, the invariants and symmetries will be given.

2.1.2.1 Invariants

Making the substitutions

$$u \to \alpha u^* + \beta, \qquad x \to \gamma x^* + \delta, \qquad t \to \xi t^* + \epsilon, \tag{2.4}$$

in (2.1) results in

$$\mathrm{i}\tfrac{\alpha}{\xi} u^*_{t^*} + \tfrac{\alpha}{\gamma^2} u^*_{x^*x^*} + 2\alpha^3|u^*|^2u^* + 2\alpha^2\beta(u^*)^2 + 4\alpha^2\beta|u^*|^2 + 4\alpha\beta^2u^* + 2\alpha\beta^2\bar{u^*} + 2\beta^3 = 0. \tag{2.5}$$

It is clear that $\alpha \neq 0$ to keep terms such as $|u^*|^2u^*$, so this is divided throughout the whole equation to result in

$$\tfrac{\mathrm{i}}{\xi} u^*_{t^*} + \tfrac{1}{\gamma^2} u^*_{x^*x^*} + 2\alpha^2|u^*|^2u^* + 2\alpha\beta(u^*)^2 + 4\alpha\beta|u^*|^2 + 4\beta^2u^* + 2\beta^2\bar{u^*} + 2\tfrac{\beta^3}{\alpha} = 0. \tag{2.6}$$

In order for the substitutions to leave the equation invariant it is required that

$$\xi = 1, \qquad \gamma^2 = 1, \qquad \alpha^2 = 1, \qquad \alpha\beta = 0, \qquad \beta^2 = 0, \qquad 2\tfrac{\beta^3}{\alpha} = 0. \tag{2.7}$$

Solving these equations gives the following invariants

$$u \to \pm u^*, \tag{2.8a}$$

$$x \to \pm x^* + \delta, \tag{2.8b}$$

$$t \to t^* + \epsilon. \tag{2.8c}$$

As such, all translations in x and t and no possible translations of u that are invariant. There are also no time scalings that maintain invariance.

2.1.2.2 Symmetries

If the following transformation is made then the calculation of the symmetries can be considered as easier

$$u \to \tfrac{\mathrm{i}}{2}\sqrt{2}\bar{u} \tag{2.9a}$$

$$x \to \mathrm{i}\bar{x} \tag{2.9b}$$

$$t \to \bar{t} \tag{2.9c}$$

Under this transformation the (2.1) becomes

$$\mathrm{i}\bar{u}_{\bar{t}} - \bar{u}_{\bar{x}\bar{x}} + |\bar{u}|^2\bar{u} = 0 \tag{2.10}$$

and the following accelerating wave reductions are found

$$\bar{u_1} = \omega_1(z)\exp(\mathrm{i}[\Theta(z) + \mu\bar{t}(\bar{x} - \tfrac{2}{3}\mu\bar{t}^2)]) \qquad z = \bar{x} - \mu\bar{t}^2, \tag{2.11a}$$

$$\bar{u_2} = \omega_2(z)\exp(-\mathrm{i}[\Theta(z) + \mu\bar{t}(\bar{x} - \tfrac{2}{3}\mu\bar{t}^2)]) \qquad z = \bar{x} - \mu\bar{t}^2, \tag{2.11b}$$

where both $\omega(z)$ and $\Theta(z)$ satisfy some specific ordinary differential equations and μ is a parameter.

2.2 Bilinear Form

To find the bilinear form for the NLS we make the substitution $u = G/F$ where G is complex and F is real. Once this has been used in (2.1), the solution written in terms of the Hirota 'D' operator is [44]

$$F\left[(\mathrm{i}\mathrm{D}_t + \mathrm{D}_x^2)G \cdot F\right] - G\left[\mathrm{D}_x^2 F \cdot F - 2|G|^2\right] = 0, \tag{2.12}$$

such that this can be written as a system for the NLS as

$$\begin{cases} (\mathrm{i}\mathrm{D}_t + \mathrm{D}_x^2)G \cdot F = 0, \\ \mathrm{D}_x^2 F \cdot F = 2|G|^2, \end{cases} \tag{2.13}$$

where the operators D_x and D_t are given by

$$\mathrm{D}_x^m \mathrm{D}_t^n a(x,t) \cdot b(x',t') = (\partial_x - \partial_{x'})^m (\partial_t - \partial_{t'})^n a(x,t) b(x',t') \mid_{x=x',t=t'} . \tag{2.14}$$

The form (2.13) will be used frequently as it is often that polynomials which solve the bilinear form can be constructed as rational solutions of the equation. Rational solutions then model rogue waves.

2.3 Lax Pair

The NLS hierarchy that has been worked through yields rational-oscillatory solutions since they are all multiples of $\mathrm{e}^{\mathrm{i}t/2}$. Beginning with the Lax pair of the focusing NLS equation which has been taken from [25] with some alterations; the matrix σ_3 has been multiplied by -1 and the translations $u \to u/2$ and $v \to -v/2$ have been imposed. For the proceeding equations the notation change from the

book is $u \to u^*$ and $v \to u$. Also, $c_2 = 1$ and $c_3 = 0$. The Lax pair is thus

$$\begin{pmatrix} \psi \\ \phi \end{pmatrix}_x = \begin{pmatrix} -\mathrm{i}\lambda & -\frac{1}{2}u \\ \frac{1}{2}u^* & \mathrm{i}\lambda \end{pmatrix} \begin{pmatrix} \psi \\ \phi \end{pmatrix}, \tag{2.15}$$

$$\begin{pmatrix} \psi \\ \phi \end{pmatrix}_t = \begin{pmatrix} \mathrm{i}(\frac{1}{4}uu^* - 2\lambda^2) & -(\frac{1}{2}\mathrm{i}u_x + \lambda u) \\ -(\frac{1}{2}\mathrm{i}u_x^* - \lambda u^*) & -\mathrm{i}(\frac{1}{4}uu^* - 2\lambda^2) \end{pmatrix} \begin{pmatrix} \psi \\ \phi \end{pmatrix} \tag{2.16}$$

where u solves (2.1) and u^* is the complex conjugate of u.

If λ is left arbitrary and the Lax pair is solved for the simple seed solution $u_0 = \mathrm{e}^{\mathrm{i}t/2}$, then the solutions ψ_0 and ϕ_0 are both multiples of

$$\exp\left(\frac{\sqrt{-4\lambda^4 - \lambda^2}x}{2\lambda}\right). \tag{2.17}$$

From this, it is clear that letting $\lambda = \pm\mathrm{i}/2$ will yield special and simpler solutions of the equation. For simplicity, $\lambda = \mathrm{i}/2$ is selected.

Using this value of λ and the simple solution u_0 in the Lax pair gives a system of first order differential equations which need to be solved. Namely,

$$\frac{\partial\psi}{\partial x} - \frac{1}{2}\psi = -\frac{1}{2}\exp\left(\frac{1}{2}\mathrm{i}t\right)\phi, \tag{2.18}$$

$$\frac{\partial\phi}{\partial x} + \frac{1}{2}\phi = \frac{1}{2}\exp\left(-\frac{1}{2}\mathrm{i}t\right)\psi. \tag{2.19}$$

By differentiating (2.18) once with respect to x and substituting in (2.19) results in,

$$\frac{\partial^2\psi}{\partial x^2} = \frac{1}{2}\frac{\partial\psi}{\partial x} - \frac{1}{4}\psi + \frac{1}{4}\exp\left(\frac{1}{2}\mathrm{i}t\right)\phi. \tag{2.20}$$

Now it is possible to add half (2.18) to (2.20) to give,

$$\frac{\partial^2\psi}{\partial x^2} = 0 \Longrightarrow \frac{\partial\psi}{\partial x} = f(t) \Longrightarrow \psi = xf(t) + g(t), \tag{2.21}$$

with f and g some currently unknown functions. This can then be used to determine ϕ from (2.19) in terms of $f(t)$ and $g(t)$. In order to establish what f and g are it is necessary to use (2.16). One solution is

$$\psi_0 = (x + 1 + \mathrm{i}t) \exp\left(\frac{1}{4}\mathrm{i}t\right) \qquad \phi_0 = (x - 1 + \mathrm{i}t) \exp\left(-\frac{1}{4}\mathrm{i}t\right), \tag{2.22}$$

where $|\psi_0|^2 + |\phi_0|^2 = 2F_1$ and F_1 is the polynomial solution. Then u_0, ψ_0, ϕ_0, F_0 and F_1 are used in the following equation

$$u_{n+1} = \frac{4\psi_n \phi_n^* F_n}{F_{n+1}} - u_n, \tag{2.23}$$

to determine u_1 and then substitute this back into the Lax pair to get ψ_1, ϕ_1 and thus F_2 so that u_2 can be retrieved.

When solving the second order differential equations there are always two arbitrary integration constants. In the first 3 functions they have been chosen so that the leading order of the denominator has coefficient 1 and the second constant can then be calculated via $|\psi|^2 + |\phi|^2$ where the constant is chosen so that any odd powers of x and t are removed. This is in order to simplify the solutions found and keep them of even order.

2.4 Wronksian Form

A method of generating solutions u of (2.1) is detailed. The solutions considered are quasi-rational solutions, in this case rational solutions in terms of x and t with some additional parameters, all multiplied by $\mathrm{e}^{2\mathrm{i}t}$. The solutions are generated through Wronskians of particular functions with additional specific scalar multiples.

A Wronskian is a determinant of a square matrix with a given structure. Con-

sider the Wronskian denoted W of functions $f_1(x)$ up to $f_n(x)$, then this is

$$W(f_1,...,f_n)(x) = \begin{vmatrix} f_1(x) & f_2(x) & \dots & f_n(x) \\ f_1'(x) & f_2'(x) & \dots & f_n'(x) \\ \vdots & \vdots & \ddots & \vdots \\ f_1^{(n-1)}(x) & f_2^{(n-1)}(x) & \dots & f_n^{(n-1)}(x) \end{vmatrix}, \tag{2.24}$$

where superscripts denote differentiation.

The solutions as given in [28] are of the form

$$u = -q_{2n}(0)B^{1-2n}\mathrm{e}^{2\mathrm{i}B^2t}\frac{W_2|_{k=0}}{W_1}. \tag{2.25}$$

The definitions of which are given below.

Working term by term; $q_{2n}(0)$ is a constant. The function $q_{2n}(k)$ is a polynomial in k of degree $2n$ and defined as follows

$$q_{2n}(k) = \prod_{j=1}^{n}\left(k^2 - \frac{\omega^{2m_j+1}+1}{\omega^{2m_j+1}-1}B^2\right), \tag{2.26}$$

with

$$\omega = \exp\left(\frac{\mathrm{i}\pi}{2n+1}\right), \tag{2.27}$$

and the m_j's integers satisfying $0 \leq m_j \leq 2n-1$ and $m_l \neq 2n - m_j$ for all l and j.

Since it is necessary to have $0 \leq m_j \leq 2n-1$ and $m_l \neq 2n - m_j$ for all l and j then there are only 4 cases for $n = 3$. Always take $m_1 = 0$, since it is possible to interchange any of the m_j's and trying $m_1 = 1$ has no solutions. When $m_2 = 1$ then $m_3 = \{2, 4\}$, when $m_2 = 2$ then it must be that $m_3 = 5$ and when $m_2 = 4$ it must be that $m_3 = 5$. It seems that increasing the m_j's just results in the roots moving further away from the origin in a vertical direction.

The element B is a constant such that if $x^2 + t^2 \to \infty$ then $|u|^2 \to B^2$. Since the NLS equation is invariant under the transformation $v(x,t) \to Bv(Bx, B^2t)$ then we choose $B = 1$ without loss of generality. After this, (2.25) becomes

$$u = -q_{2n}(0)\mathrm{e}^{2it}\frac{W_2|_{k=0}}{W_1}. \tag{2.28}$$

The term W_2 is a Wronksian of size $2n+1$ such that

$$W_2 = W(f_1, ..., f_{2n}, f). \tag{2.29}$$

If we consider $j = 1, ..., n$ then the functions f_j and f_{n+j} are defined as

$$f_j(x,t) = D_k^{2j-1} f(k,x,t)|_{k=1}, \tag{2.30}$$

$$f_{n+j}(x,t) = D_k^{2j-1} f(k,x,t)|_{k=-1}, \tag{2.31}$$

where D_k is an operator of the form

$$D_k = \frac{k^2}{k^2+1}\frac{\partial}{\partial k}, \tag{2.32}$$

such that

$$D_k^2(A) = \frac{k^3\left(k\dfrac{\mathrm{d}^2A}{\mathrm{d}k^2} + k^3\dfrac{\mathrm{d}^2A}{\mathrm{d}k^2} + 2\dfrac{\mathrm{d}A}{\mathrm{d}k}\right)}{(k^2+1)^3}. \tag{2.33}$$

The function $f(k,x,t)$ is then

$$f(k,x,t) = \frac{\exp(kx + \mathrm{i}k^2t + \Phi(k))}{q_{2n}(k)}, \tag{2.34}$$

where $\Phi(k)$ is a polynomial of degree $2n$ in k with coefficients that are parameters

ψ through

$$\Phi(k) = \mathrm{i}\sum_{l=1}^{2n} \psi_l (\mathrm{i}k)^l. \tag{2.35}$$

Due to the form of $f(k,x,t)$ and its differentials, $W_2|_{k=0}$ is equivalent to only considering the expansion of the determinant in the last column of which only the first term is non-zero. The denominator W_1 in (2.25) is a Wronskian of size $2n$ as,

$$W_1 = W(f_1, ..., f_{2n}). \tag{2.36}$$

It is possible to relate the u_1 solution of this to that given in Appendix A by making the following substitutions

$$\psi_1 = 0, \qquad \psi_2 = \frac{\sqrt{3}}{4}, \qquad t \to \frac{t}{4}, \qquad x \to \frac{x}{2}.$$

Other cases have not been investigated but it is likely that a similar substitutions will suffice.

This method works for the NLS equation but given that there are a lot of questions regarding it, many of which will be discussed in §2.5, it does not seem realistic to think that this can be adjusted to use for the Boussinesq or KP-I unless these questions are answered. The use of a dummy variable will be a pivotal method that will be employed again, however the intricacies of the remainder of the method are somewhat convoluted.

2.4.1 Root and Solution Behaviour

Having tried to understand the methodology and achieved some progress but not enough to conclusively explain all the functions used, perhaps there will be something to discover from considering plots of the solutions. As has been mentioned previously, there are parameters introduced by the method which it will

be interesting to see how these affect the solution. The roots that will be referred to are the complex zeros of the polynomials F that form the solutions u.

The hope is that these graphs will be a good comparison for Boussinesq and potentially KP-I, though obviously additional dimensions in KP-I will greatly affect the behaviour, later in the thesis. Given that the solutions will be complex, it becomes necessary to identify whether taking the real part, the imaginary part, or the modulus of the solutions will relate best to later equation solutions. Originally it seemed that taking the imaginary part of u and plotting this related to the roots the most, however for $n = 1$ it seems that $|u|$ works best actually showing a wave unlike either the imaginary or the real part of u. At $n = 1$, the imaginary plot shows no wave at $t = 0$, the real plot only shows a trough at $t = 0$ and the modulus shows the wave at $t = 0$ as expected. These three options are shown in Figure 2.1.

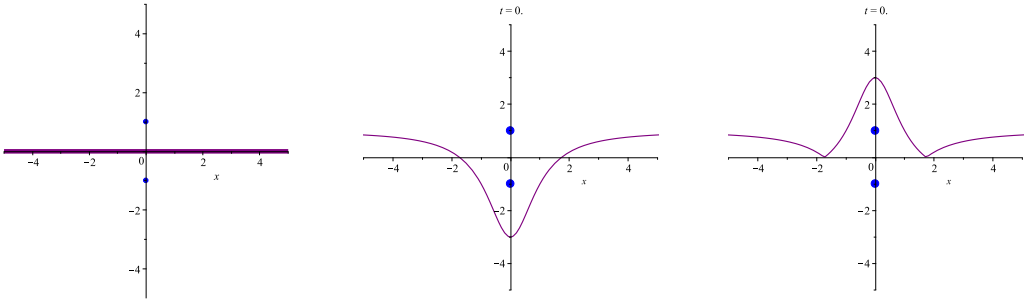

Figure 2.1: Plot of the imaginary part of u_1, the real part and the modulus in purple, along with the complex roots of F_1 in blue.

The graphs in Figure 2.2 are using the form of u_3 as detailed in Appendix A.

The movement of these roots is quite interesting where the oval and central roots morph into a star like formation. This change takes the original 3 wavelets to then form one wave (as at $t = -0.2$) before the waves reform in a complex manner before resulting in the high central wave and then 2 subsequent waves on either side of it. The solutions have multiple joining and separating behaviours in a narrow space of time before the final system becomes apparent at $t = 0$.

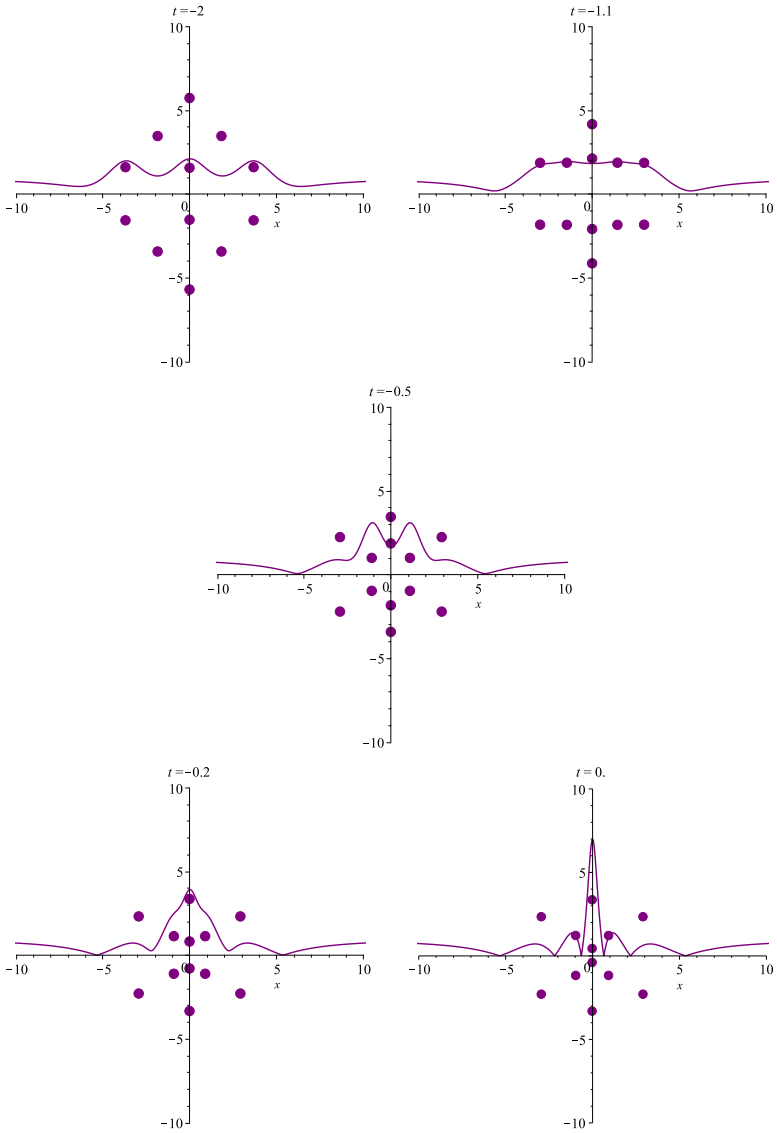

Figure 2.2: $|u_3|$ for different values of negative t plotted with the complex roots of F_3.

2.4.2 Altering the Parameters ψ_i

When $n = 1$ there are only two parameters with ψ_1 and ψ_2, these relate to positive translations on the real and imaginary axis, i.e $\psi_1 = 10$ relates to a positive shift on the real axis by 10 whereas $\psi_1 = -10$ to a negative shift.

When considering ψ_2, taking $\psi_2 = 10$ means that the roots start at roughly ± 40i instead of ± 20i. This means that at $t = 0$, since the speed of the roots

movement does not change, instead of having reached the vicinity of the real axis and having been repelled away, the roots are still travelling towards it. In this manner ψ_2 seems partially related to the time t rather than a spatial shift.

With ψ_3, this moves the roots in a negative shift along the the real axis with the roots having a greater distance between them as well. There is also a slight rotation occurring which can be seen in Figure 2.3 for both $t = -10$ and $t = 0$.

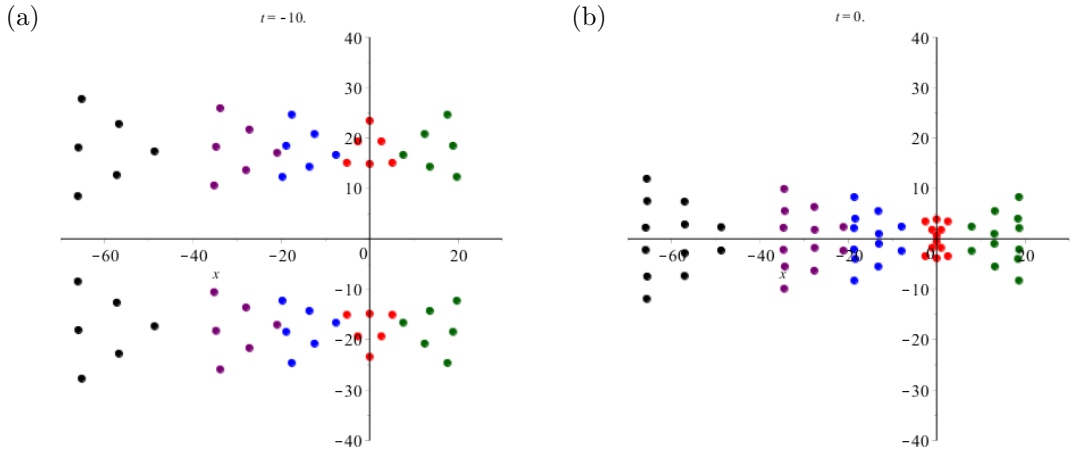

Figure 2.3: $\psi_3 = 0$ (red), 5 (blue), -5 (green), 10 (purple) and 20 (black).

Much like with ψ_2, ψ_4 seems to do more of a time-shift. When $\psi_4 = 20$ the roots are moving away from the axes on $-10 \leq t \leq 10$ so they have already met near the real axis at a greater negative time. This can be seen in Figure 2.4.

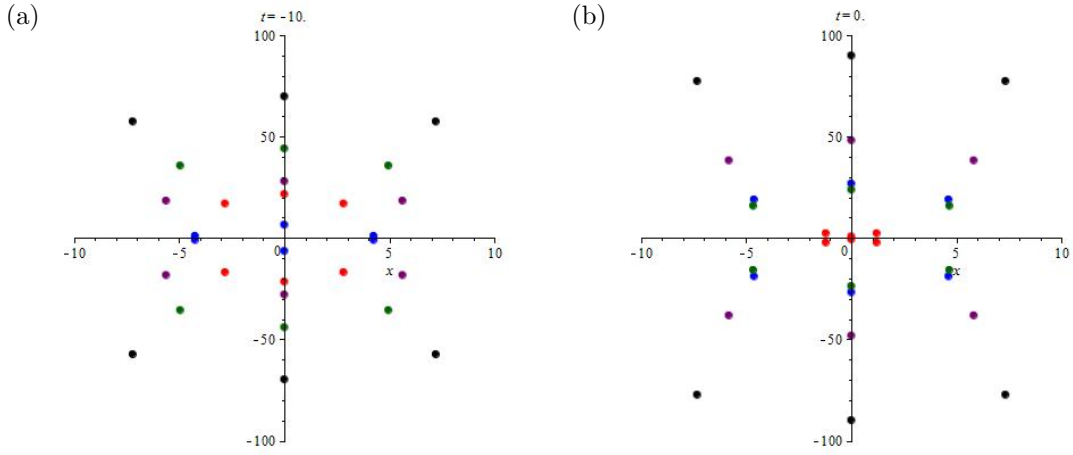

Figure 2.4: $\psi_4 = -5$ (green), 0 (red), 5 (blue), 10 (purple) and 20 (black).

It may be that these parameters represent some movement up the NLS hierarchy; often it is found that the parameters can relate to new time variables.

2.5 Discussion

It is prudent to note that this chapter is not an in-depth exploration into the rational solutions of the NLS equation. There has been much work and methods that have not been mentioned or explored here including [9, 21, 32].

The discovery of the Wronskian form of rational solutions for the NLS equation enforces the belief that there may be solutions for other soliton equations such as the Boussinesq equation. While it will be seen later that the structure of the solutions for the NLS equation differs greatly from that of the Boussinesq and KP-I equations, it may be possible to adjust the Wronskian form of the NLS in order to find solutions for these equations. It is worth noting that there are pivotal differences with these solutions, namely that the bilinear form is derived not by the second logarithmic derivative in x but by the ratio of a complex and a real polynomial. Also, the fact that the equation is primarily dealt with as a system will alter its comparability to the Boussinesq and KP-I which we chose not to work with in its system form.

In later chapters there will also be comparison of the functions F^{NLS} to the polynomials that form the rational solutions of the Boussinesq and KP-I equations. It will be seen that all of these solutions have many similarities and a high amount of structure. This further supports the possible existence of a Wronskian generating function for all of these solutions.

There are many questions that can be asked of this style of generating solutions of the NLS equation. It is not clear as to why $q(2n)$ works and what its relation is to the equation as a whole. It is possible that it has some relation to the complex

roots of the polynomials that solve the bilinear form. When working with the generating function, it has $m_j = j - 1$ but there is no exploration of what would happen if this was a different function or simply random selection. If it was known how D_k was found this would surely help in applying a similar method to other equations. Also a justification for f being of its form and similarly for f_j. It would additionally be interesting to know what impact Φ has on the solutions other than introducing parameters. Given that it is a function of the dummy variable k, this is not a trivial matter.

A pivotal question is how the complex roots of the polynomials F inform the behaviour of the solutions u. This is a query that relates to the whole thesis as it is a common method for exploring the solution behaviour and yet there is no concrete understanding of how all the roots affect the solutions. While it has been mentioned that complex roots nearing the real line create the waves, the impact that the other roots have is not known.

As mentioned, there are many things that could be extended from this chapter but it is not the main concern of this thesis.

Chapter 3

The Boussinesq Equation

In this chapter the Boussinesq equation is considered,

$$u_{tt} + u_{xx} - (u^2)_{xx} - \tfrac{1}{3}u_{xxxx} = 0. \tag{3.1}$$

After introducing the equation and its derivation along with some of its symmetries, we discuss the form that will be used in this chapter.

There will be some initial work that assesses the most common type of solutions that are gained from the Boussinesq equation and how these are formed before progressing on to a discussion of the family of solutions we seek. These solutions will be categorised and their physical behaviour explored in a variety of different methods.

The chapter will finish with some more combinatorial work on the conservation laws as well as discussing the relation of the Boussinesq equation to other nonlinear PDE's.

3.1 Introduction

The Boussinesq equation is a $(1+1)$-dimensional equation suitable for modelling a variety of waves. It is primarily an equation that models wave propagation at shallow depth but can be altered to produce stable long wave or stable short wave solutions dependent on a sign change. Our main focus will be on the stable long waves and this will be described by the equation we use.

In Chapter 4 it will be shown that parameters can be introduced into (3.1) under specific conditions which extends the Boussinesq equation to a generalised form.

3.1.1 Background

Joseph Boussinesq derived the Boussinesq equation [15, 16] in 1871 after the experiment conducted by John Scott Russell. The well-known experiment was the first recorded observation of a "wave of translation", also known as a soliton or solitary wave, in which the size and shape of a constructed wave travelled a significant distance down a channel before it began to dissipate. This was a leading discovery that lead to much research into soliton waves.

This equation can be solved via the inverse scattering method [14, 48] making it an integrable equation which gives rise to many forms of interesting behaviour.

3.1.2 Derivation

To derive the Boussinesq equation, begin with the Navier-Stokes (N-S) equations, move to the shallow water wave equations and then arrive at the Boussinesq.

The N-S equations model movement of fluids. They can be concisely summarised as

$$\frac{\partial \mathbf{v}}{\partial t} + (\mathbf{v}.\nabla)\mathbf{v} - \nu\nabla^2\mathbf{v} = -\nabla\omega + \mathbf{g}, \tag{3.2}$$

with $\mathbf{v}$ the flow velocity, ν the kinematic viscosity, ω the thermodynamic work and $\mathbf{g}$ any body forces including gravity. In 3-dimensions these are explicitly

$$\frac{\partial v_1}{\partial t} + v_1\frac{\partial v_1}{\partial x} + v_2\frac{\partial v_1}{\partial y} + v_3\frac{\partial v_1}{\partial z} - \nu\left(\frac{\partial^2 v_1}{\partial x^2} + \frac{\partial^2 v_1}{\partial y^2} + \frac{\partial^2 v_1}{\partial z^2}\right) = -\frac{\partial \omega}{\partial x} + g_1, \quad (3.3a)$$

$$\frac{\partial v_2}{\partial t} + v_1\frac{\partial v_2}{\partial x} + v_2\frac{\partial v_2}{\partial y} + v_3\frac{\partial v_2}{\partial z} - \nu\left(\frac{\partial^2 v_2}{\partial x^2} + \frac{\partial^2 v_2}{\partial y^2} + \frac{\partial^2 v_2}{\partial z^2}\right) = -\frac{\partial \omega}{\partial y} + g_2, \quad (3.3b)$$

$$\frac{\partial v_3}{\partial t} + v_1\frac{\partial v_3}{\partial x} + v_2\frac{\partial v_3}{\partial y} + v_3\frac{\partial v_3}{\partial z} - \nu\left(\frac{\partial^2 v_3}{\partial x^2} + \frac{\partial^2 v_3}{\partial y^2} + \frac{\partial^2 v_3}{\partial z^2}\right) = -\frac{\partial \omega}{\partial z} + g_3. \quad (3.3c)$$

Given that the Boussinesq equation is concerned with 1 directional flow then the N-S reduces to,

$$\frac{\partial v}{\partial t} + v\frac{\partial v}{\partial x} - \nu\frac{\partial^2 v}{\partial x^2} = -\frac{\partial \omega}{\partial x} + g_1, \quad (3.4)$$

where we have replaced v_1 with v as there is no longer any need for subscripts.

Since we are dealing with 1 directional flow then we have no sheer forces affecting the modelling and as such $\nu = 0$ reducing the equation farther to

$$\frac{\partial v}{\partial t} + v\frac{\partial v}{\partial x} = -\frac{\partial \omega}{\partial x} + g_1. \quad (3.5)$$

For incompressible flow such as the Boussinesq models there is $\nabla\omega \equiv \frac{1}{\rho}\nabla p$ for ρ the density of the fluid and p the pressure. Additionally, subject to hydrostatic pressure $p = \rho g h$ with g gravity and h the distance from bed to surface.

The N-S equation now becomes

$$\frac{\partial v}{\partial t} + v\frac{\partial v}{\partial x} = -g\frac{\partial h}{\partial x} + g_1, \quad (3.6)$$

which is essentially one of the shallow water wave equations in 1 dimension. Ad-

ditionally there needs to be conservation of mass which can be expressed as

$$\frac{\partial h}{\partial t} + \frac{\partial (hu)}{\partial x} = 0, \tag{3.7}$$

with h the area of the flow at point x. The combination of these two equations under additional calculations will result in the Boussinesq equations

$$\frac{\partial u_0}{\partial t} = g\frac{\partial h}{\partial x} + \frac{g}{2}\frac{\partial}{\partial x}\left(\frac{h^2}{H} + H^2\frac{\partial^2 h}{\partial x^2}\right), \tag{3.8a}$$

$$\frac{\partial h}{\partial t} = -H\frac{\partial u_0}{\partial x} - \sqrt{gH}\frac{\partial}{\partial x}\left(\frac{h^2}{H} - \frac{H^2}{6}\frac{\partial^2 h}{\partial x^2}\right), \tag{3.8b}$$

as given in [16].

From previous work in [16] we know that $h = f(x - t\sqrt{gH})$ and thus

$$\frac{h^2}{H} - \frac{H^2}{6}\frac{\partial^2 h}{\partial x^2} = g(x - t\sqrt{gH}), \tag{3.9}$$

for f and g some undetermined functions. As such we can establish that

$$\frac{\partial}{\partial t}\left(\frac{h^2}{H} - \frac{H^2}{6}\frac{\partial^2 h}{\partial x^2}\right) = -\sqrt{gH}\frac{\partial}{\partial x}\left(\frac{h^2}{H} - \frac{H^2}{6}\frac{\partial^2 h}{\partial x^2}\right). \tag{3.10}$$

Using this equality and solving (3.8) to eliminate differentials of u_0 retrieves the following, singular equation

$$\frac{\partial^2 h}{\partial t^2} + gH\frac{\partial^2 h}{\partial x^2} + gH\frac{\partial^2}{\partial x^2}\left(\frac{3}{2}\frac{h^2}{H} + \frac{H^2}{3}\frac{\partial^2 h}{\partial x^2}\right). \tag{3.11}$$

Subject to the translation $x \to \mathrm{i}x$, this can be changed to the same form as written in [16] as

$$\eta_{\tau\tau} - gH\eta_{\xi\xi} - \frac{3g}{2}(\eta^2)_{\xi\xi} - \frac{gH^3}{3}\eta_{\xi\xi\xi\xi} = 0, \tag{3.12}$$

with η the vertical displacement, ξ the horizontal displacement, H the height of the

water at rest, τ time and g the gravitational acceleration. These are represented in Figure 3.1. This equation models long waves in shallow water; this can be shallow seas, lakes or harbours to name some situations. The fluid is considered to be incompressible and irrotational. Rotational fluid introduces turbulence and other mitigating factors that will complicate the equation.

For a full work through of how the equations are derived, please see [16].

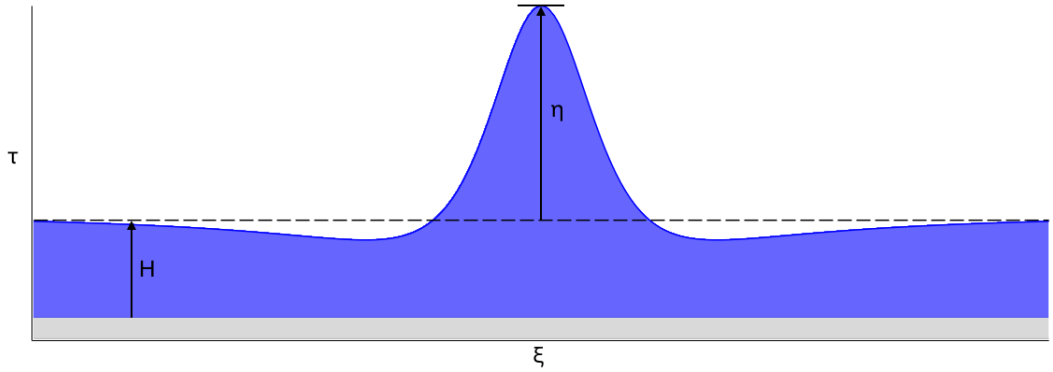

Figure 3.1: Representation of some of the variables in (3.12)

This equation can be nondimensionalised by making the following transformations

$$\xi = \mathrm{i}Hx, \qquad \tau = \frac{\sqrt{H}t}{\sqrt{g}}, \qquad \eta = -\tfrac{2}{3}Hu, \tag{3.13}$$

which results in the dimensionless equation (3.1) which we will be working with in this chapter. It is worth noting that there is another transformation that will give (3.1) without the need for a complex scaling. This transformation is

$$\xi = Hx, \qquad \tau = \frac{\sqrt{H}t}{\sqrt{g}}, \qquad \eta = \tfrac{2}{3}H(u-1). \tag{3.14}$$

It is possible to change many of the signs in (3.12) through simple scaling and translation of ξ, τ and η. While doing so will change the boundary conditions that may be imposed on the equation, it is not a matter that will affect us given that we only require solutions to decay as $(x,t) \to \infty$.

The Boussinesq equation in the form (3.1) is used to model incompressible and irrotational flow of fluid. It can be derived from the coupled shallow water wave equations, which, despite the name, can still model deep waves. The restrictions of the shallow water wave equations require that the horizontal dynamics are the driving force of wave behaviour and the vertical dynamics are negligible. This explains why the Boussinesq equation can still model waves out at sea or in large lakes.

3.1.3 Invariants and Symmetries

As seen by the two dimensionless transformations in the §3.1.2, (3.12) is invariant under

$$u \to -u - \tfrac{2}{3}H \qquad x \to -\mathrm{i}x \qquad t \to t, \tag{3.15}$$

however, the main concern is the invariants of the dimensionless equation.

3.1.3.1 Invariants

Making the substitutions

$$u \to \alpha u^* + \beta, \qquad x \to \gamma x^* + \delta, \qquad t \to \xi t^* + \epsilon, \tag{3.16}$$

in (3.1) and recalling that

$$u_t = \frac{\partial u}{\partial u^*}\frac{\partial u^*}{\partial t^*}\frac{\partial t^*}{\partial t} \qquad \text{and} \qquad u_x = \frac{\partial u}{\partial u^*}\frac{\partial u^*}{\partial x^*}\frac{\partial x^*}{\partial x}, \tag{3.17}$$

we can establish the following equation

$$\alpha\xi^2 u^*_{t^*t^*} + \alpha\gamma^2 u^*_{x^*x^*} - 2\alpha^2\gamma^2 (u^*_{x^*})^2 - 2(\alpha u^* + \beta)\alpha\gamma^2 u^*_{x^*x^*} - \tfrac{1}{3}\alpha\gamma^4 u^*_{x^*x^*x^*x^*} = 0. \tag{3.18}$$

Rearranging the equation and noting that $\alpha \neq 0$ in order to retain terms like $u^*_{t^*t^*}$, we simplify this to

$$\xi^2 u^*_{t^*t^*} + (\gamma^2 - 2\beta\gamma^2)u^*_{x^*x^*} - \alpha\gamma^2(u^*)^2_{x^*x^*} - \tfrac{1}{3}\gamma^4 u^*_{x^*x^*x^*x^*} = 0. \tag{3.19}$$

Similarly $\xi \neq 0$ so we can divide through by this giving

$$u^*_{t^*t^*} + \left(\frac{\gamma^2 - 2\beta\gamma^2}{\xi^2}\right) u^*_{x^*x^*} - \frac{\alpha\gamma^2}{\xi^2}(u^*)^2_{x^*x^*} - \frac{1}{3}\frac{\gamma^4}{\xi^2} u^*_{x^*x^*x^*x^*} = 0. \tag{3.20}$$

In order for the substitutions to leave the equation invariant, we require

$$\frac{\gamma^2}{\xi^2}(1 - 2\beta) = 1, \qquad \frac{\alpha\gamma^2}{\xi^2} = 1, \qquad \frac{\gamma^4}{\xi^2} = 1. \tag{3.21}$$

Consequently we see that $\gamma \neq 0$ as well. Solving these equations gives the following invariants

$$u \to \alpha u^* + \left(\frac{1-\alpha}{2}\right), \qquad x \to \pm\sqrt{\alpha}x^* + \delta, \qquad t \to \pm\alpha t^* + \epsilon. \tag{3.22}$$

This establishes that any translations in x and t will keep the equation invariant and providing that the scaling in x is the square root of the scaling in t then we can interchange the sign without affecting the equation. Any scaling in u need be of the same factor as that of t and the translation in u is directly related to its scaling.

3.1.3.2 Symmetries

Since calculating the symmetries can be a complicated process we will simplify (3.1) by making a different change of variables. We can remove the u_{xx} term and

make all the factors 1 through

$$u \to \tfrac{1}{2}\bar{u} + \tfrac{1}{2}, \qquad x \to \sqrt{3}\bar{x}, \qquad t \to \mathrm{i}\sqrt{3}\bar{t}. \tag{3.23}$$

Under this transformation (3.1) becomes

$$\bar{u}_{\bar{t}\bar{t}} + \bar{u}\bar{u}_{\bar{x}\bar{x}} + \tfrac{1}{2}(\bar{u}_{\bar{x}})^2 + \bar{u}_{\bar{x}\bar{x}\bar{x}\bar{x}} = 0. \tag{3.24}$$

Using the method as described in §1.3 we have the following infinitesimals

$$\xi = \alpha\bar{x} + \beta, \qquad \tau = 2\alpha\bar{t} + \gamma, \qquad \phi = -2\alpha\bar{u},$$

for α, β and γ constants. Then by solving the characteristic equation derived from these to give the following classical symmetry reductions

$$\bar{u_1} = \omega_1(z) \qquad z = \gamma\bar{x} - \beta\bar{t} \tag{3.25}$$

$$\bar{u_2} = \frac{\omega_2(z)}{\bar{t} + \gamma/(2\alpha)} \qquad z = \frac{\bar{x} + \beta/\alpha}{(\bar{t} + \gamma/(2\alpha))^{1/2}}. \tag{3.26}$$

Additionally there are non-classical symmetry reductions [24] of

$$\bar{u_3} = \omega_1(z) - 4\gamma^2\bar{t}^2 \qquad z = \bar{x} + \gamma\bar{t}^2 \tag{3.27}$$

$$\bar{u_4} = \bar{t}^2\omega(z) - \frac{\bar{x}^2}{\bar{t}^2} \qquad z = \bar{x}\bar{t} \tag{3.28}$$

$$\bar{u_5} = \bar{t}^2\omega(z) - \frac{(x + \lambda\bar{t}^5)^2}{\bar{t}^2} \qquad z = \bar{x}\bar{t} + \tfrac{1}{6}\lambda\bar{t}^6 \tag{3.29}$$

$$\bar{u_6} = \bar{t}^{-1}\omega(z) - \tfrac{1}{4}\bar{t}^{-2}(\bar{x} - 3c_1\bar{t}^2)^2 \qquad z = \bar{x}\bar{t}^{-1/2} + c_1\bar{t}^{3/2}. \tag{3.30}$$

The rational solutions that will be discussed in this thesis are not obtainable by symmetry reductions.

If we make the inverse transformation of (3.23) then we have a classical sym-

metry for (3.1).

3.2 Bilinear Form

Given that we are considering rational solutions of the Boussinesq equation that are real and bounded, then we can state that we require our solutions of the equation u and its derivatives to tend to 0 as $(x,t) \to \infty$. We use this in the following section to set all integration constants to 0.

By setting $u = \omega_x$ and substituting into (3.1) it is possible to then integrate through the whole equation and set the constant to 0. This retrieves a different formulation of (3.1) into which we can substitute $w = 2F_x$, where F is a polynomial solution, and integrate once more. Multiplying through by F^2, the final equation is the Bilinear form of (3.1) and is as follows:

$$FF_{tt} - F_t^2 + FF_{xx} - F_x^2 - \frac{1}{3}FF_{xxxx} + \frac{4}{3}F_xF_{xxx} - F_{xx}^2 = 0. \tag{3.31}$$

It is worth noting that $F(x,t) = 0$ only when it is the constant 0 function since we can have no real roots in F if we require bounded solutions in u.

Finding solutions of (3.31) in terms of polynomials is equivalent to finding rational solutions of (3.1). In §3.6 we will consider the complex roots of these functions F. The information that the roots provide can give us an indication of how the solution will behave and expectations of higher order behaviour.

The Boussinesq equation in Hirota bilinear form can also be written as,

$$\left(\mathrm{D}_x^2 + \mathrm{D}_t^2 - \frac{1}{3}\mathrm{D}_x^4\right) F \cdot F = 0. \tag{3.32}$$

In [6] the Hirota bilinear form is used with an asymptotic expansion

$$F_n = 1 + \epsilon F_N^{(1)} + \epsilon^2 F_N^{(2)}, \tag{3.33}$$

to determine special solutions. It is then established that the bilinear form truncates, that is the order 1 terms of ϵ vanish for any N, when

$$F_N^{(1)} = \sum_{i=1}^{N} \exp(k_i x - k_i t^3 + \eta_i^0). \tag{3.34}$$

This gives some soliton solutions of the equation. Hirota then detailed a general formula for F_n which, after taking the long wave limit, can produce rational solutions which relate to rogue waves. We have employed this method in §3.4.

Initially we shall restrict our consideration of solutions to even power polynomials for F. It is possible afterwards to extend this into a general form. However doing so either introduces parameters as in §4 or leads to complex solutions, see Appendix B.2. The six known even power polynomial functions can be found in Appendix B.1. As can be seen from these, it is not only even power polynomials but each function F_n is of degree $n(n+1)$ as well.

The leading order terms, of combined x and t, of the polynomial have coefficients that are binomial coefficients $\binom{n(n+1)/2}{k}$ where n represents how far up the hierarchy we are and k relates to the half power of t that the coefficient corresponds to. Hence it is possible to express the leading order terms as a power of the function $(x^2 + t^2)$, indeed one could also consider the functions as a power of $(x^2 + t^2 + 1)$, i.e. a power of F_1 plus lower order terms.

A formula for the other coefficients remains to be found, i.e all the coefficients of degree less than the degree of the polynomial. Currently it should be noted that if they are rational coefficients then the denominator is a power of 3; a situation most likely encountered due to the coefficient of u_{xxxx} in (3.1). A compact form

of the solution is

$$F_n = (x^2 + t^2 + 1)^N + \sum_{\substack{i+j \leq 2(N-1) \\ i,j \geq 1}} a_{ij} x^i t^j, \tag{3.35}$$

where $N = \dfrac{n(n+1)}{2}$ and a_{ij} are constants to be determined.

3.3 BE Hierarchy

Let us consider the Lax pair of the Boussinesq equation where in all following calculations ψ_n is considered to be a function of x and t. The Lax pair provides much information relating to the equation and has historic applications in generating functions for a number of integrable equations. Given that the Boussinesq equation is a fourth order PDE with two time derivatives though, does result in a more complex Lax pair than, for example, the NLS equation.

The Lax pair of (3.31) is,

$$\frac{\partial}{\partial t}\psi_n = -\mathrm{i}\frac{\partial^2}{\partial x^2}\psi_n - \mathrm{i}\psi_n \frac{\partial}{\partial x}\omega_n, \tag{3.36}$$

$$\frac{\partial^3}{\partial x^3}\psi_n = -\frac{3}{2}\left(\frac{\partial}{\partial x}\omega_n - \frac{1}{2}\right)\frac{\partial}{\partial x}\psi_n - \frac{3}{4}\left(\frac{\partial^2}{\partial x^2}\omega_n + \mathrm{i}\frac{\partial}{\partial t}\omega_n\right)\psi_n + \lambda\psi_n, \tag{3.37}$$

where $\dfrac{\partial}{\partial x}\omega_n = u_n$ as found in [3, 18, 19, 26, 64]. It can be verified that

$$\frac{\partial^4}{\partial t \partial x^3}\psi_n = \frac{\partial^4}{\partial x^3 \partial t}\psi_n, \tag{3.38}$$

when u_n satisfies (3.1), as required.

Taking $u_0 = 0$; a known solution of (3.1), in (3.37) establishes,

$$\frac{\partial^3}{\partial x^3}\psi_0 - \frac{3}{4}\frac{\partial}{\partial x}\psi_0 = \lambda\psi_0. \tag{3.39}$$

Solving this results in an equation in terms of λ gives solutions where the term

$\exp(A\sqrt{16\lambda^2-1})$ appears often for A some function. Therefore setting $\lambda = \pm\frac{1}{4}$ will simplify the function ψ_0 significantly. As λ is some parameter we will opt to take $\lambda = \frac{1}{4}$ for the proceeding calculations and work with a much simpler set of differential equations that we can solve.

The solution to (3.37) when $n = 0$ is

$$\psi_0 = G_1(t)\exp(x) + G_2(t)\exp\left(-\tfrac{1}{2}x\right) + G_3(t)\exp\left(-\tfrac{1}{2}x\right)x. \tag{3.40}$$

At this point there are two functions of the three that have the same coefficient of an exponential and two functions that have the same degree of x. An interesting solution can be found by setting $G_1(t) = 0$ when compared to the NLS hierarchy. Firstly the solution of the simultaneous differential equations (3.37) and (3.36) is

$$\psi_0(x,t) = \{(x+\mathrm{i}t)c_3 + c_2\}\exp\left(-\tfrac{1}{2}x - \tfrac{1}{4}\mathrm{i}t\right) + c_1\exp(x-\mathrm{i}t), \tag{3.41}$$

for c_1, c_2 and c_3 constants. We can identify similarities with this equation and that of ϕ_0 from NLS hierarchy by taking $c_1 = 0, c_2 = -1$ and $c_3 = 1$ with the additional factor of $\mathrm{e}^{-x/2}$. This gives another comparable relation between the Boussinesq equation and the NLS when looking for rational solutions.

While it is possible to take a general solution of (3.37) for $n = 1$ the solution is much more complex than for $n = 0$ and so creates troubles for finding a simultaneous solution for (3.36)

The solution to (3.37) for $n = 2$ has coefficients of $\mathrm{e}^{-x/2}$ and e^{x}. In order to simplify, consider taking only the parts of the solution for (3.37) that multiply $\mathrm{e}^{-x/2}$ and setting the parameter in front of the other exponential to 0. However, the solution needs to also satisfy (3.36) and ideally the coefficient of the highest power of x or t we want to set to 1 to give a monic polynomial. This can be achieved by setting one of the integration constants to 1 so that we arrive at the

equation,

$$\psi_1 = \frac{\exp(-\frac{1}{2}x - \frac{1}{4}\mathrm{i}t)}{t^2+x^2+1}\Big\{x^4 - t^4 - 2t^2x + 2x^3 - 2t^2 + 4x^2 - 7 + c_4 t \\ +\mathrm{i}(2t^3x + 2tx^3 + 4tx^2 + 10tx + c_4x + 6t + c_4)\Big\}. \tag{3.42}$$

It is useful to consider how else to group these functions. Since c_4 is a constant it could also be imaginary so similarly it is possible to have

$$\psi_1 = \frac{\exp(-\frac{1}{2}x - \frac{1}{4}\mathrm{i}t)}{t^2+x^2+1}\Big\{x^4 - t^4 - 2t^2x + 2x^3 - 2t^2 + 4x^2 - \tilde{c_4}x - 7 - \tilde{c_4} \\ +\mathrm{i}(2t^3x + 2tx^3 + 4tx^2 + 10tx + 6t + \tilde{c_4}t)\Big\}. \tag{3.43}$$

When Lax pair work has been completed on the NLS equation to retrieve solutions ψ_n and ϕ_n, the first integration constant is found by setting the leading order coefficient of x to 1 as has been done here. The second constant is then found by considering $|\psi_n|^2 + |\phi_n|^2$ and selecting the constant such that the odd order terms are 0 as mentioned in Chapter 2. Unfortunately the same method does not work with the Boussinesq equation.

Since here the terms being considered are those which share the same exponential factor, ψ_0 has become,

$$\psi_0 = ((x + \mathrm{i}t)c_3 + c_2)\exp\left(-\frac{x}{2} - \frac{\mathrm{i}t}{4}\right), \tag{3.44}$$

Taking the square of the modulus of (3.44) and setting one constant such that numerator is a monic polynomial gives,

$$\frac{t^2 + x^2 + 2c_2x + c_2^2}{\mathrm{e}^x}. \tag{3.45}$$

As can be seen the only option of c_2 that will remove any odd order terms is 0 but

this may not be the best decision since if $c_2 = 1$ then $|\psi_0|^2 = (F_1 - 2x)\mathrm{e}^{-x}$ but if $c_2 = 0$ then $|\psi_0|^2 = (F_1 - 1)\mathrm{e}^{-x}$. It is a matter of selecting either the correct constant term or the correct coefficient of the odd order x term but it cannot be both.

We still need to find the recursive function in terms of u, F and ψ in order to move up the hierarchy. This is not appearing to give an easy to compute solution. Either the method in terms of the selection of constants needs to be altered in order to work, or the whole method needs to be adjusted to accommodate the Boussinesq equation. It is assumed in this that such a method for finding new solutions is possible, but given the high structure of the polynomial solutions and the behaviour of other soliton equations this is reasonable to do.

3.4 Limit of Travelling Wave Solution

In a paper by Ablowitz and Satsuma [6], rational solutions of the KdV, KP-I and the Boussinesq equation were achieved by taking the long wave limit of the travelling wave solution.

Starting with,

$$u_{tt} + u_{xx} - 2u_x^2 - 2uu_{xx} - \frac{1}{3}u_{xxxx} = 0, \tag{3.46}$$

we consider $u(x,t) = w(z)$ again with $z = x - ct$. After this substitution the equation is transformed into,

$$c^2\frac{\mathrm{d}^2w}{\mathrm{d}z^2} + \frac{\mathrm{d}^2w}{\mathrm{d}z^2} - 2\left(\frac{\mathrm{d}w}{\mathrm{d}z}\right)^2 - 2w\frac{\mathrm{d}^2w}{\mathrm{d}z^2} - \frac{1}{3}\frac{\mathrm{d}^4w}{\mathrm{d}z^4} = 0. \tag{3.47}$$

Following the same procedure as that for the KdV we integrate through the equation in order to simplify it, bearing in mind that we are looking for bounded

solutions.

$$c^2\frac{\mathrm{d}w}{\mathrm{d}z}+\frac{\mathrm{d}w}{\mathrm{d}z}-2\left(w\frac{\mathrm{d}w}{\mathrm{d}z}\right)-\frac{1}{3}\frac{\mathrm{d}^3w}{\mathrm{d}z^3}=a_1, \tag{3.48}$$

but $a_1 = 0$ since we require w and its differentials to tend to 0 as z tends to infinity.

Integrating again,

$$c^2w+w-w^2-\frac{1}{3}\frac{\mathrm{d}^2w}{\mathrm{d}z^2}=a_2, \tag{3.49}$$

but again $a_2 = 0$. We cannot integrate this equation straight away but we can multiply through by $\dfrac{\mathrm{d}w}{\mathrm{d}z}$ to give us,

$$\frac{\mathrm{d}^2w}{\mathrm{d}z^2}\frac{\mathrm{d}w}{\mathrm{d}z}=3c^2w\frac{\mathrm{d}w}{\mathrm{d}z}+3w\frac{\mathrm{d}w}{\mathrm{d}z}-3w^2\frac{\mathrm{d}w}{\mathrm{d}z}. \tag{3.50}$$

Integrating gives us,

$$\frac{1}{2}\left(\frac{\mathrm{d}w}{\mathrm{d}z}\right)^2=\frac{3}{2}c^2w^2+\frac{3}{2}w^2-w^3, \tag{3.51}$$

$$\frac{\mathrm{d}w}{\mathrm{d}z}=\pm w\sqrt{3(c^2+1)-2w}. \tag{3.52}$$

Separation of variables gives us the following travelling wave solution,

$$w(z)=\frac{3}{2}(c^2+1)\operatorname{sech}^2\left(\frac{\sqrt{3}}{2}\sqrt{c^2+1}(a_3+z)\right), \tag{3.53}$$

$$u(x,t)=\frac{3}{2}(c^2+1)\operatorname{sech}^2\left(\frac{\sqrt{3}}{2}\sqrt{c^2+1}(a_3+x-ct)\right). \tag{3.54}$$

Now let $\eta_1=\sqrt{3c^2+3}(x-ct)+a_1$, with a_1 some arbitrary constant, and we can rewrite $u(x,t)$ as,

$$u(x,t)=\frac{6(c^2+1)\mathrm{e}^{\eta_1}}{(\mathrm{e}^{\eta_1}+1)^2}. \tag{3.55}$$

In order to replicate the procedure used for the KdV equation we need the

solution of the bilinear equation such that the second logarithmic derivative of it gives the above function. It transpires that the same form of function works, at least for $N = 1$, that is,

$$F_1(x,t) = 1 + \mathrm{e}^{\eta_1}, \tag{3.56}$$

Performing a Bäcklund transformation on this should retrieve the two-soliton solution though one would hope that this follows the same expansion as that of the KdV.

The current problem which was fixed in the KdV situation and is yet to be fixed in the Boussinesq is that the arbitrary constant could be selected so that there was a term of order 1. In the Boussinesq, a series expansion of our solution $u(x,t)$ already has a term of order 1. Also, we have not determined the value of c as had been done in the KdV case. Determining the value of c could fix both of these issues.

It is possible to verify that the constant k can be expressed as $k^2 = c^2 + 1$. Considering (3.56) and setting $k^2 = c^2 + 1$ gives

$$F_1(x,t) = 1 + \exp\left\{\sqrt{3}k(x \pm \sqrt{k^2 - 1}t) + a_1\right\}. \tag{3.57}$$

Now consider a series expansion of $F_1(x,t)$ in terms of k up to order 1 to have

$$1 + \mathrm{e}^{a_1} + \mathcal{O}(k). \tag{3.58}$$

and thus set $\mathrm{e}^{a_1} = -1$. Substituting this into the (3.57) results in

$$F_1(x,t) = 1 - \exp\left\{\sqrt{3}k(x \pm \sqrt{k^2 - 1}t)\right\}. \tag{3.59}$$

Taking a series expansion in terms of k gives,

$$F_1(x,t) = \sqrt{3}(\mathrm{i}t \pm x)k + \mathcal{O}(k^2). \tag{3.60}$$

The second logarithmic derivative of $F_1(x,t)$ is then

$$u(x,t) = -\frac{2}{(x \pm \mathrm{i}t)^2} + \mathcal{O}(k). \tag{3.61}$$

Using the same format as in [6] consider $u_n(x,t) = [2\ln\{F_n(x,t)\}]_{xx}$ and take,

$$F_n(x,t) = \exp\left(\sum_{i=1}^{n} \mu_i \eta_i\right) + \sum_{j=1}^{n}\left(\sum_{i=1}^{j-1} \ln(A_{i,j})\mu_i\mu_j\right), \tag{3.62}$$

where

$$\eta_i = \sqrt{3}k_i(x + \epsilon_i\sqrt{k_i^2 - 1}t) + d_i, \tag{3.63}$$

with $\epsilon_i = \pm 1$ and the μ's are either 1 or 0.

To calculate $A_{1,2}$ substitute $u_n(x,t) = 2\{\ln(F_n(x,t))\}_{xx}$ into the Boussinesq equation and solve. The values of d_1 and d_2 are not required in order to solve this, however it is necessary to solve for both $\epsilon_1\epsilon_2 = 1$ and $\epsilon_1\epsilon_2 = -1$ since Maple requires that these be substituted in to simplify the equation.

$$A_{1,2} = \frac{3(k_1 - k_2)^2 + (\epsilon_1\sqrt{k_1^2 - 1} - \epsilon_2\sqrt{k_2^2 - 1})^2}{3(k_1 + k_2)^2 + (\epsilon_1\sqrt{k_1^2 - 1} - \epsilon_2\sqrt{k_2^2 - 1})^2}. \tag{3.64}$$

Moving on to $n = 3$ verifies that $A_{1,3}$ and $A_{2,3}$ follow the conjectured format from [6]. Again let $\mathrm{e}^{d_0} = \alpha_1$ and $\xi_1 = \sqrt{3}k_1(x + \epsilon_1\sqrt{k_1^2 - 1}t)$, thus,

$$F_1 = 1 + \alpha_1\mathrm{e}^{\xi_1}, \tag{3.65}$$

so $\mathcal{O}(1) = 1 + \alpha_1$ resulting in $\alpha_1 = -1$ as before. For the two-soliton solution

there is

$$F_2 = 1 + \alpha_1 e^{\xi_1} + \alpha_2 e^{\xi_2} + A_{1,2}\alpha_1\alpha_2 e^{\xi_1+\xi_2}. \tag{3.66}$$

Where now consider things of order 1 and of order $\mathbf{k}$.

$$\mathcal{O}(1) : 1 + \alpha_1 + \alpha_2 + \alpha_1\alpha_2 A_{1,2}, \tag{3.67}$$

$$\mathcal{O}(\mathbf{k}) : k_1\alpha_1 + k_2\alpha_2 + (k_1 + k_2)A_{1,2}\alpha_1\alpha_2. \tag{3.68}$$

Solving these two equations simultaneously does not give a nice result for α_1 and α_2. What [6] seems to have done with their equation is to determine some series expansion of $A_{1,2}$ dependant on the choice of what $\epsilon_1\epsilon_2$ is equal to and uses this to find an answer for α_1 and α_2.

The choice of how to compute the asymptotic expansions was somewhat confusing when dealing with higher order polynomials and as such the method is not one that can be replicated with a full explanation. Regardless, this type of generating function is not a closed form as is desired.

3.5 Shape and Structure of the Solutions

In order to better understand these rogue wave solutions, it is worthwhile considering their physical behaviour. The waves reach maximums at different values of x, though uniformly for $t = 0$. This can be seen in Figure 3.2. An investigation into whether the number of waves affects the height is productive as well, this would relate to the force involved.

3.5.1 Contour Graphs

Considering contour plots of the solutions u_2 up to u_5 as shown in Figure 3.3, it is possible to clearly see height and positional behaviour of the waves. One of

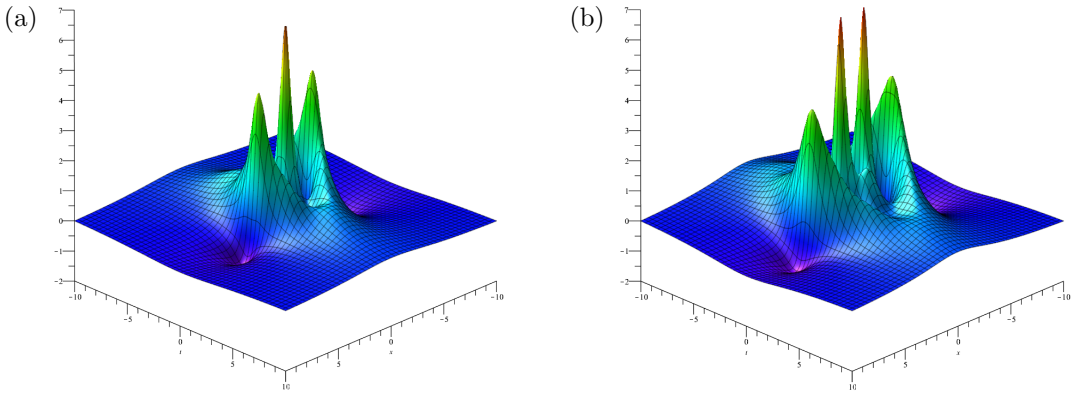

Figure 3.2: 3D plots of u_3 and u_4

the most integral points being that the waves closest to the origin are always the highest with the paired waves decreasing in height as we move farther away.

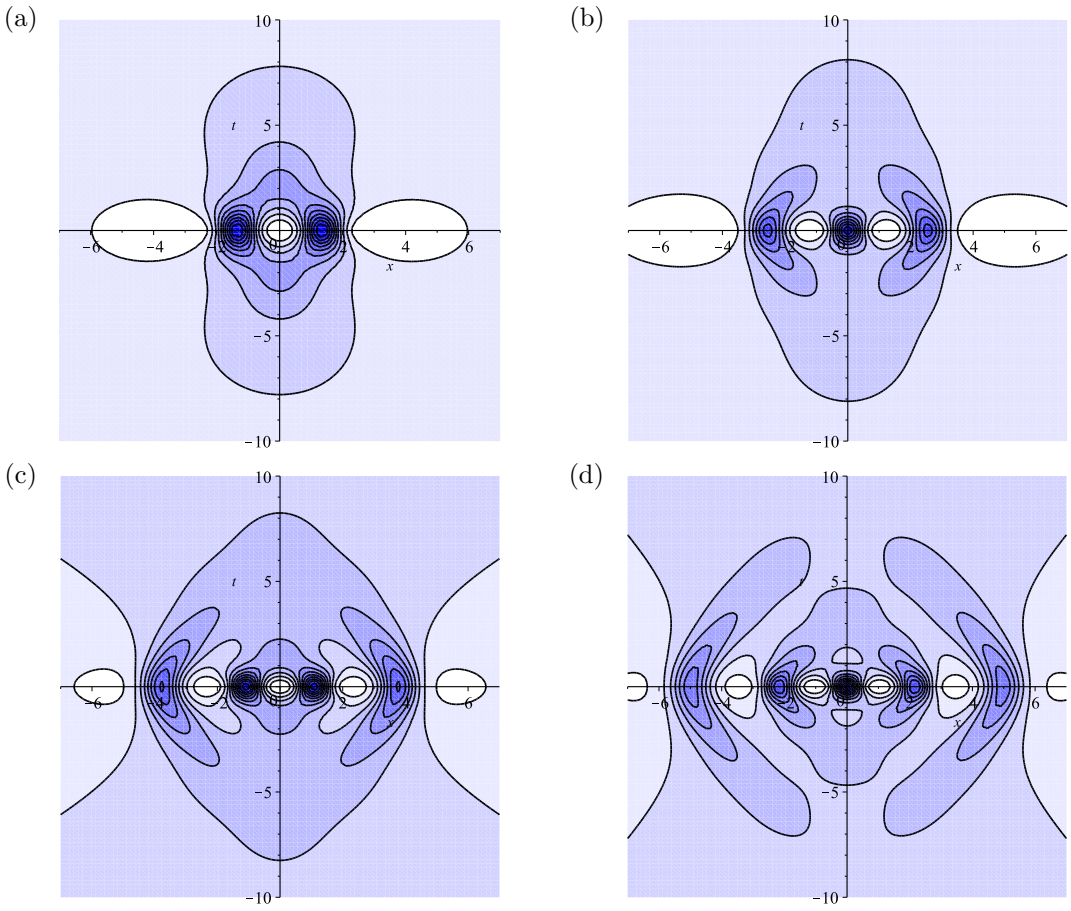

Figure 3.3: Contour plots of u_2, u_3, u_4 and u_5 respectively.

It can also be seen that there are occasionally troughs or peaks that occur in a

non-standard formation. For instance with u_5 there are two waves orthogonal to the standard peaks but of an almost insignificant height. Altering the number of contours can greatly alter the graphs shown but it is worth noting that while the majority of behaviour is fixed in the neighbourhood of $t = 0$, there are subsequent excited behaviours in other regions nearby. This behaviour will be of great interest in Chapter 4.

3.5.2 Position of Maximal Wave Height

Given that u_n has n peaks located around the origin, the highest peak for odd n is always at the origin. For u_3 the additional peaks are located at approximately $(\pm 2.55, 0)$. With u_5 they are located at approximately $(\pm 2.16, 0)$ and $(\pm 4.99, 0)$. With every peak there is also a trough to be considered. It seemed that the troughs of u_5 could be related to the peaks of u_4 but this is not directly the case. There is also the additional trough that occurs after the last peak which would not appear in u_4.

For even valued n there is no central peak but u_2 has peaks at $(\pm 2.89, 0)$ and u_4 has them at $(\pm 1.09, 0)$ and $(\pm 3.77, 0)$.

In addition to these main waves there are "half-waves" that occur perpendicular to the main waves. These waves are clearly distinct from the surface yet they do not reach the height of the full waves. They appear at instances where two or more full waves share the same vicinity and the combination results in a mass that rises from the surface but is not distinct from the full waves that create it. As the two waves nearest the origin join at the edge, these waves form.

Given its formation, u_1 has no "half-waves". They are located at approximately $(\pm 2.08, 0)$ for u_2, $(\pm 4.01, 0)$ for u_3, $(\pm 1.41, 0)$ for u_4 and $(\pm 2.94, 0)$ for u_5. Analytically there are "half-waves" on the outer perimeters according to the numerical calculations but this is regarded as numerical error from the code given

that the heights of these supposed waves are negligible.

3.6 Roots of the Bilinear Form Solutions

After investigation of the roots of F_1 to F_5 in terms of x, it is possible to vary t and view the behaviour as time progresses. This analysis has led to an interesting occurrence that all the roots follow very regimented trajectories. There are two lines of symmetry for each function, one being the real axis and the other the imaginary axis. These symmetries are maintained throughout the variation of t.

At large positive or negative t the roots appear in an equilateral triangular form with the apex on the imaginary axis. This sort of triangular structure has been noted in the Vorob'ev-Yablonski polynomials, but the roots of (3.1) are rotated 90° when compared with the Vorob'ev-Yablonski roots [22]. These polynomials are rational solutions of the Painlevé II equation. The number of roots on each side of the triangle F_n is n for the functions. Since (3.31) is invariant under the transformation $x \to -x$ then any complex root that exists in the first quadrant will have a partner root in the third quadrant. Since we establish the roots x as functions of t, we only consider real values of t. One can use the complex conjugate root theorem, with this specification of t and the form of the solutions, to establish that the roots exist in complex conjugate pairs. The combination of these two points leads to the two lines of symmetry.

The deformation that occurs around $t = 0$ is not replicated in the polynomials of Vorob'ev and Yablonski. As t tends towards 0 the roots deform into an oval with the height greater than the width. Prior to this there are situations where two roots share the same vicinity, in these cases they seem to abide by collision dynamics and repel away from each other. The structure at $t = -10$ and $t = 0$ are shown in Figure 3.4(a) and 3.4(b) respectively.

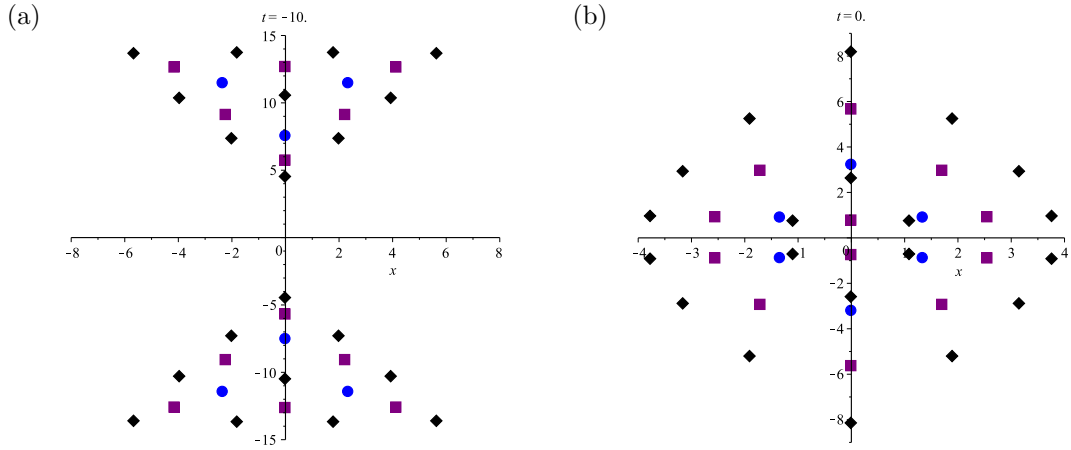

Figure 3.4: Complex Roots of F_2 (circle), F_3 (square) and F_4 (diamond).

One can see that the number of ovals of a particular function at $t = 0$ is exactly that of the number of triangles at $t = \pm 10$.

The roots also form a bowed square structure at certain times t which is shown in Figure 3.5.

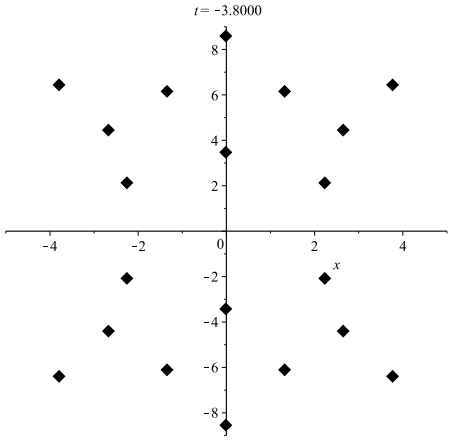

Figure 3.5: Complex Roots of F_4 showing a bowed square structure.

This structure seems similar to the structure of the generalised Hermite polynomials [22] with the addition of the roots on the imaginary axis. The generalised Hermite polynomials are rational solutions of the Painlevé IV equation. Thus the roots of the polynomials for the Boussinesq equation look like a rotated version of the Vorob'ev-Yablonski polynomials at large t but then move into something

like the generalised Hermite polynomials before the state at $t = 0$ with their oval structure. This gives a link between the roots of the Boussinesq bilinear form solutions and the Painlevé equations.

In order to understand the system more we will begin by investigating when a function's roots repel with other roots of the same function and then progress on to see what happens when roots of two different polynomials share the same point.

An interesting fact to note, if we consider the grouping the even number wave solutions and the odd number wave solutions separately, is that as the the degree of the polynomial increases the apex of the root triangle moves closer to 0. Since the root can never be 0 this could suggest that the functions will be of a finite number, but it would be natural given other equations with rogue wave solutions to assume that there are an infinite number.

3.6.1 Shared Roots

It transpires that no function F ever shares roots within the same polynomial, the roots only coalesce with other functions since it transpires that the multiplicity of any root is 1. It appears that when roots of the same polynomial come within a given distance of each other that they seem to repel and alter both their speed and direction so as not to collide.

The polynomials F_1 and F_2 have a pair of roots that coalesce above the real axis at two separate times (this is replicated below the real axis) but none of the other roots do so. The times at which this happens are $t = \pm\frac{1}{3}\sqrt{15 + 6\sqrt{19}}$. F_1 and F_3 have a pair of roots that do so above the real axis but at four separate times, again replicated below the real axis. F_1 and F_4 have a pair of roots but they only share the same point at two times again like with F_1 and F_2. F_1 and F_5 have two sets of shared points, the root closest to 0 from F_5 coalesces four times

and the root from F_5 that is neither the closest nor the farthest from 0 coalesces with the F_1 root twice.

In terms of when the roots share the same space, the following is observed:

- F_2 and F_3 only have two points that coalesce at 4 times .
- F_2 and F_4 have a pair that coalesce 4 times.
- F_2 and F_5 have a pair of points that coalesce 6 times, however at the first and last collision they seem to share the same root over a period of time rather than at a distinct time.
- F_3 and F_4 have a pair of roots that coalesce 6 times (the roots nearest 0) and a pair that coalesce twice.
- F_3 and F_5 have no roots that coalesce.
- F_4 and F_5 have the roots closest to 0 coalesce 8 times and 4 times for another pair of roots (farthest root for on imaginary axis for F_4 and the middle root for F_5).

At present it is unclear what can be deduced from this but it seems like a pattern is forming whereby we can establish some behaviour common to the different functions. An in depth numerical analysis has not yet been completed for this.

3.6.2 Colliding Roots and Number of Collision Events

When two roots from the same polynomial come close to each they abide by some collision dynamics and are propelled away from the interaction with an increase in the speed of their movement. This speed increase is observed but has not been numerically verified.

Define a collision event as a situation where two roots come within the neighbourhood of each other and then alter their linear or quadratic trajectory nearing

and leaving this neighbourhood. Counting the number of these events for each polynomial, F_1 obviously has no collisions or interactions with its two roots. Considering only negative time t since the positive time will just replicate the same number of collisions again. Bearing this in mind, consider rotational symmetry in all the counting so the whole solution will have 4-times the number of collision listed.

- F_2 has only one collision event with roots on the imaginary axis.
- F_3 has only one collision event, again with roots only on the imaginary axis.
- F_4 has 4 collisions; 3 interactions with roots on the imaginary axis but there is also an interaction with two roots that do not sit on the axis in each quadrant.
- F_5 behaves in the same way as F_4 and again the top row of complex roots do not add any number of interactions, so it is the F_4 structure that determines the collisions.

There seems to be some pairing occurring with the polynomials such that for each even n, F_n and F_{n+1} have the same number of collisions with their roots. This may have something to do with whether the function $u(x,t)$ has a central wave or not which may explain how the collision dynamics of the roots affects the overall solution.

The reason for these roots seemingly repelling each other has not been explained. It is known that the solutions have roots of multiplicity 1 and therefore roots of the same polynomial are not expected to share the same space, however the fact that they avoid a perimeter around other roots and change their behaviour is not justified by this fact. This behaviour is most likely a result of the interesting dynamics that occur in integrable equations.

3.6.3 Root Trajectories

There seems to be a correlation in the even wave root trajectories and the odd wave trajectories. The even wave roots have a circular zone about the origin that they follow the circumference of but never enter. The odd trajectories on the other hand seem to have an exponential decay around this circular zone. An interesting fact to note is that the zone for F_4 is smaller than that of F_2 and contained completely within it, so we assume that F_6 will be smaller still and as $n \to \infty$ in F_n the circle approaches the origin. From previous work we know that the roots of the polynomials can never be the origin as this would result in $u(x,t)$ tending to infinity.

The trajectories that each function's roots take are shown in Figure 3.6. The coding of these figures is given in Appendix E.2. The blue dots represent the initial position of the root at $t = 0$ and the red dots are the points at $t = 10$. Due to the symmetry we have only considered positive t as the behaviour is reflected for negative t. The line connecting the two dots represents the path of the root and it is graded from blue to red to highlight when the root moves quickly and when its speed slows.

The behaviour at F_2 and F_3 is interesting but still fairly simple. The complex roots do not move in a linear or even quadratic way but can be seen to repel if they come in the vicinity of a neighbouring root as has been mentioned previously. The most interesting behaviour is observed for F_3 and F_5 where the interaction between the greater number of roots obstructs the paths greatly. Some roots succeed in maintaining a linear path but this is not the standard behaviour. It is worth noting that roots never cross or share the same space so when the trajectory lines cross it indicates that the roots are obtaining that space at two distinct times. The behaviour relating to the roots moving closer to the origin can also be observed in these figures. The axes were removed for clarity.

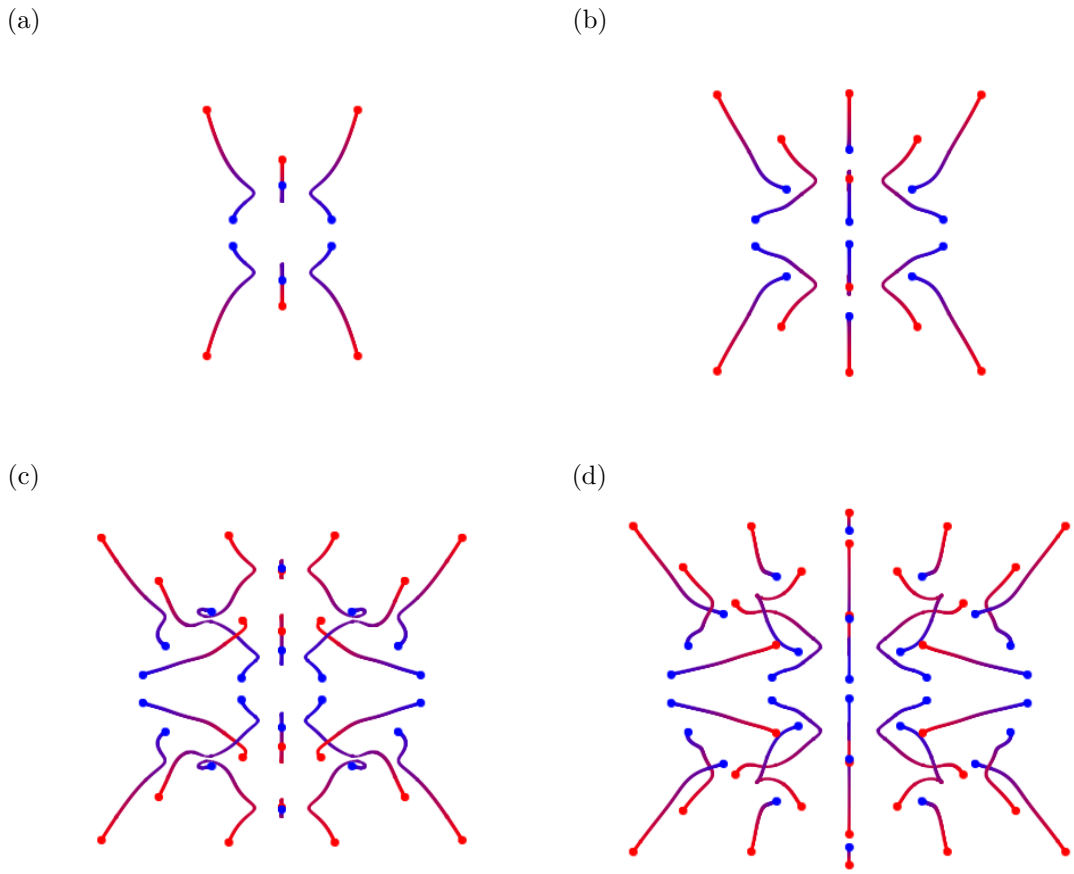

Figure 3.6: Complex Root Trajectories of F_2, F_3, F_4 and F_5 respectively where blue represents $t = 0$ and red $t = -7$.

3.6.4 Root and Wave Solution Behaviour

At $t = 0$ the horizontal line of complex roots that is closest to the real line determines where the peaks of the waves occur as shown in Figure 3.7. This behaviour is expected since nearing an asymptote of the equation will result in peaks with the highest peaks relating to the roots closest to the asymptote. From the graphs it seems that the roots are central to where the wave maximum is. It is possible however, that the outer waves instead of being symmetrical may be tilted slightly towards to origin. This has not been analytically explored however it would be an interesting extension.

All polynomials except F_2 give at least two roots that sit exactly on the imag-

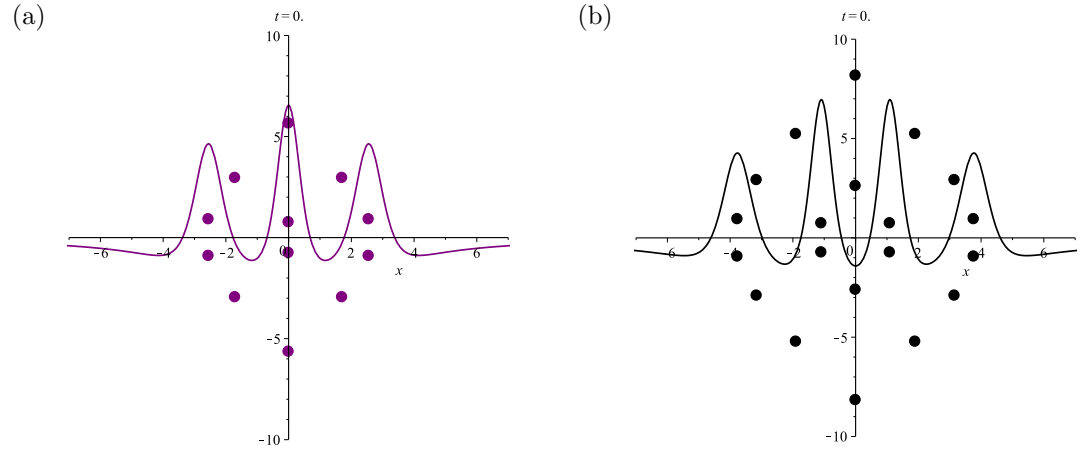

Figure 3.7: Complex Roots of $F_3(x,0)$ and $F_4(x,0)$ with their corresponding solutions $u(x,0)$.

inary line. The closest root for F_2 has a real part that diminishes as the accuracy is increased so it is reasonable to assume that this is a numerical error.

If we first consider only functions with an odd number of waves then the error, that is the difference between the location of the complex root and the maxima of $u(x,t)$, increases as the complex roots move further away from the origin. The same goes for the even number of waves functions. A problem does arise when considering the combination of the two. As the roots of all polynomials move further away from the origin the error increase until the farthest two roots, that from F_4 and then from F_5 show that the error for F_5 is slightly less than that of F_4. This is not as anticipated but may be due to the fact that there are an even number of waves for F_4 and since currently we only have F_2 to compare it with this does not give a lot of data for comparison.

Let us assume that uniformly the error increases as the roots move away from the origin, this begs the question of what the limit of this error can be as well as if the roots ever move outside of a waves and instead sit over a minima or a point where $u(x,t) = 0$.

3.7 Discussion

As mentioned in §3.2 the denominator of any rational coefficients is believed to be a multiple of 3 given the form of the equation and the coefficient of u_{xxxx}, it will be interesting to see what happens to the solutions if we change the coefficient of u_{xxxx} via a transformation.

In terms of the behaviour of the waves there is much that can be done. Currently it has not been ascertained whether the maximum height of the main wave is related to the number of waves present. It could be that the average height of the waves is uniform across all functions or that there is some equation which details the maximum height of the wave given the number of other waves present. This seems intuitive given that mass is preserved in the solutions.

It has not been investigated whether there are pivotal times at which the waves merge and separate either. As will be seen in Chapter 7, there are times when wave separation seems to be at critical times that can be expressed in surd form.

Similarly, as mentioned in §3.6.1 there could be a numerical analysis of complex root crossings and also of how close roots must come together before their trajectory is altered.

It still remains to find a generating function in a wronskian form for the Boussinesq along with the other analysis listed that could enlighten us as to why the solutions behave in such a way.

Chapter 4

Generalised Solutions of the Boussinesq Equation

This chapter will explore the generalised Boussinesq equation where the parameters α and β are introduced into the equation. To begin, the full equation will be given as well as some interesting nonlinear superposition occurrences. The parameters are introduced as coefficients of some other functions that are required in order to keep the function solving the Boussinesq bilinear form. The behaviour of these additional functions will also be considered.

Moving on, there will be an exploration into the physical behaviour that these parameters influence. This will be completed for both the solutions which give an even number of waves and those that give an odd number of waves as the behaviour can be somewhat different. The even or oddness of the function will be determined at the state $\alpha = \beta = 0$. There will also be some work regarding limits of these parameters and the effect on the solutions along with proofs.

There will be a brief consideration of additional symmetries that relate the parameters and the variables before moving to conclude the chapter.

Given that the solutions discussed in this chapter are a combination of F_n^{BE}

then superscript notation will be used where F_n^{GBE} denotes the generalised Boussinesq polynomial solutions.

4.1 The Equation

Interestingly for a nonlinear differential equation, it is possible to find solutions which are a linear combination of the original functions with specific coefficients and the addition of two more polynomials P_n and Q_n. This work is published in [23]. These solutions still solve the original equation

$$u_{tt} + u_{xx} - (u^2)_{xx} - \tfrac{1}{3}u_{xxxx} = 0, \tag{4.1}$$

and its bilinear form

$$\mathrm{B}(F, F) = FF_{tt} - F_t^2 + FF_{xx} - F_x^2 - \frac{1}{3}FF_{xxxx} + \frac{4}{3}F_xF_{xxx} - F_{xx}^2 = 0. \tag{4.2}$$

Theorem 4.1. *It is possible to construct a solution of the bilinear form* (4.2) *comprised of* 2 *solutions of the bilinear form along with* 2 *polynomials* P *and* Q*. The following equation gives the construct*

$$\begin{aligned} F_n^{GBE}(x,t;\alpha,\beta) =& F_n^{BE}(x,t) + 2\alpha t P_{n-1}(x,t) + 2\beta x Q_{n-1}(x,t) \\ &+ (\alpha^2+\beta^2)F_{n-2}^{BE}(x,t), \end{aligned} \tag{4.3}$$

for n *from* 2 *to* 5, $F_0^{BE} = 1$, $P_0 = Q_0 = 0$, P *and* Q *functions of* x *and* t *and with* α *and* β *parameters.*

Currently this has only been verified for n from 2 to 5 but the assumption is that this will be true for all n subject to finding the polynomials P_n and Q_n. The polynomials P_n and Q_n can be found in Appendix C.1.

It is still possible to solve the polynomials and determine their complex roots but there will now be 3 variables in them. In Chapter 3 the roots were solved for x in terms of t and with (4.3) there will also be an α and β involved.

Let

$$\Phi_n^{\pm}(x,t) = xP_n(x,t) \pm \mathrm{i}tQ_n(x,t), \tag{4.4}$$

where P_n and Q_n are the same polynomials as in (4.3) such that F_n^{GBE} satisfies (4.2).

Conjecture 4.1. *The polynomials $\Phi_n^{\pm}(x,t)$ given in* (4.4) *satisfy the bilinear form* (4.2).

Conjecture 4.1 and Theorem 4.1 combined, result in the following lemma.

Lemma 4.1. *Taking $\Phi_n^{\pm}(x,t)$ as given in* (4.4)*, then the function $F_n^{GBE}(x,t;\alpha,\beta)$ from* (4.3) *can be written as*

$$\begin{aligned} F_n^{GBE}(x,t;\alpha,\beta) =& F_n^{BE}(x,t) + (\alpha + \mathrm{i}\beta)\Phi_{n-1}^{+}(x,t) + (\alpha - \mathrm{i}\beta)\Phi_{n-1}^{-}(x,t) && (4.5)\\ &+ (\alpha^2 + \beta^2)F_{n-2}^{BE}(x,t), && (4.6) \end{aligned}$$

for $n < 6$, which is a linear combination of four functions $F_n^{BE}, \Phi_n^{\pm}$ and F_{n-2}^{BE} that solve (4.2)*. The proof is computational by entering these functions into the bilinear form and showing that the form equates to* 0*. We conjecture that the same will happen for the functions of $n > 6$.*

4.2 Methods for Calculating P and Q Functions

Since there are fewer coefficients to calculate in the P_n and Q_n functions than their F_n^{BE} counterparts, perhaps there is a way to utilise this in order reduce calculation time. If it were possible to establish some equalities between the

functions $F_n^{BE}, F_{n-2}^{BE}, P_n$ and Q_n then it may be that F_n^{BE} can be calculated quicker using these equalities than the ansatz in the original (4.2).

Given that the operator B, as given in (4.2) is bilinear, and from [23] we know that $tP_{n-1} \pm \mathrm{i}xQ_{n-1}$ satisfies the bilinear form, we can establish that,

$$\mathrm{B}(tP_n, tP_n) = \mathrm{B}(xQ_n, xQ_n), \tag{4.7}$$

$$\mathrm{B}(xQ_n, tP_n) = -\mathrm{B}(tP_n, xQ_n), \tag{4.8}$$

by equating real and imaginary parts.

Since $\mathrm{B}(F_n^{GBE}, F_n^{GBE}) = 0$ for all α and β and $\mathrm{B}(F^{BE}, F^{BE}) = 0$ for any F^{BE} we can also establish that

$$\mathrm{B}(F_n^{BE}, tP_{n-1}) = -\mathrm{B}(tP_{n-1}, F_n^{BE}), \tag{4.9a}$$

$$\mathrm{B}(F_{n-2}^{BE}, tP_{n-1}) = -\mathrm{B}(tP_{n-1}, F_{n-2}^{BE}), \tag{4.9b}$$

$$\mathrm{B}(F_n^{BE}, xQ_{n-1}) = -\mathrm{B}(xQ_{n-1}, F_n^{BE}), \tag{4.9c}$$

$$\mathrm{B}(F_{n-2}^{BE}, xQ_{n-1}) = -\mathrm{B}(xQ_{n-1}, F_{n-2}^{BE}), \tag{4.9d}$$

$$\mathrm{B}(F_n^{BE}, F_{n-2}^{BE}) + \mathrm{B}(F_{n-2}^{BE}, F_n^{BE}) = -4\mathrm{B}(tP_{n-1}, tP_{n-1}). \tag{4.9e}$$

Note that with equations (4.9a) and (4.9b) as well as (4.9c) and (4.9d) that we can replace F_n^{BE} with F_{n-2}^{BE} and the same equality holds, the reason for which is not trivial. It may be that there is some underlying symmetry here that has not been evaluated. The equalities from (4.7) and (4.8) are also retrieved once more.

It transpires that the modulus of the sum of the leading order coefficients of P_n and Q_n are always $2^{\frac{n(n+1)}{2}}$. The functions share some other patterns and can

be written as,

$$P_n = (2n+1)x^{n(n+1)} + \sum_{\substack{i+j\leq(N-2)\\ i,j\geq 0}} a_{ij}x^{2i}t^{2j} + (-1)^n t^{n(n+1)}$$

$$Q_n = x^{n(n+1)} + \sum_{\substack{i+j\leq(N-2)\\ i,j\geq 0}} b_{ij}x^{2i}t^{2j} + (-1)^n(2n+1)t^{n(n+1)}.$$

The leading order terms are mirrored between P_n and Q_n, that is if the coefficient of a leading order term say x^4t^2 of P_2 is 5 then the coefficient of t^4x^2 in Q_2 is $(-1)^2 5$.

4.3 Behaviour of the New Functions

Since there are now parameters introduced into the solutions there is more that can be investigated regarding their impact. One such thing to consider is how the α and β alter the solutions or the solutions' complex roots. It is necessary to consider not just one solution but to investigate if their are any differences between the even and odd solutions regarding this as well. It transpires that it is possible to also complete some proofs regarding limiting behaviour with α and β also.

4.3.1 Behaviour of $F_2^{GBE}(x,t,\alpha,\beta)$

The behaviour found in this section will likely be mirrored for many of the even n generalised functions. There will be additional behaviour from the additional roots but the behaviour near the origin should be the same or very similar.

As an introductory step, first examine the behaviour of each of these new parameters individually. Setting $\beta = 0$ and varying α for F_2^{GBE} it is possible to compare the standard root behaviour to that of the generalized root behaviour

around $t = -10$ and $t = 0$. These values of t were chosen in particular as they show the most distinct behaviour within the polynomial.

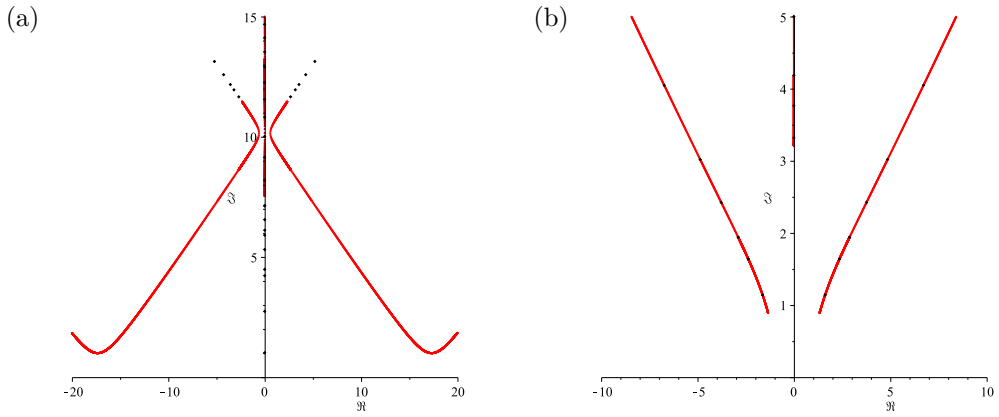

Figure 4.1: Complex root paths of $F_2^{GBE}(x, -10, \alpha, 0)$ and $F_2^{GBE}(x, 0, \alpha, 0)$ respectively. The red lines are for positive α and black is negative.

Firstly we notice that the sign of alpha does not matter when $t = \beta = 0$ which can be verified by looking at the full equation of F_2^{GBE} where this combination of values for t and β reduces the equation to $F_2 + \alpha^2$. As $t \to 0$ all roots move towards the real axis at the same speed and so result in the formation seen in Figure 4.1(b).

In Figure 4.1(a), the triangular formation of the roots is maintained as α goes from $-20,000$ to $20,000$ but the orientation of the triangle changes. It transpires that this change occurs between $\alpha = 19$ and $\alpha = 20$ where the roots have come steadily closer together until they interact much as they did previously with what appear to be collision dynamics. Once this collision occurs the roots then expand out. At some point the roots come close to the real axis but since there can never be real roots they propel themselves away once more. The second turning point occurs when $6,800 \leq \alpha \leq 10,200$ where the roots come close to the real axis then move off. The natural question now is what occurs in the 3D plots around these values of α. It transpires that some odd behaviour occurs as the roots come very close to the real axis, the waves seem to oscillate within themselves with a

greater trough and grow and shrink repeatedly until the roots move away from the axis once more when the waves stabilise. Looking at the behaviour of the 3D plot around the $\alpha = 20$ point suggests that the alteration in the root behaviour mirrors the change in the waves direction. Initially the waves move away from each other on the t-axis but after the root collision they seem to move away from each other on the x-axis.

The behaviour with $\alpha = 0$ and β varying has a slightly more interesting result where at $t = -10$ the roots curve in a clockwise way before tending off in a straight line. The apex of the original triangular formation will obviously come close to the real axis and then move off at roughly 90° from its original trajectory. This behaviour is show in Figure 4.2(a). Again as $t \to 0$ the roots move down at the same speed and result in the structure observed in Figure 4.2(b).

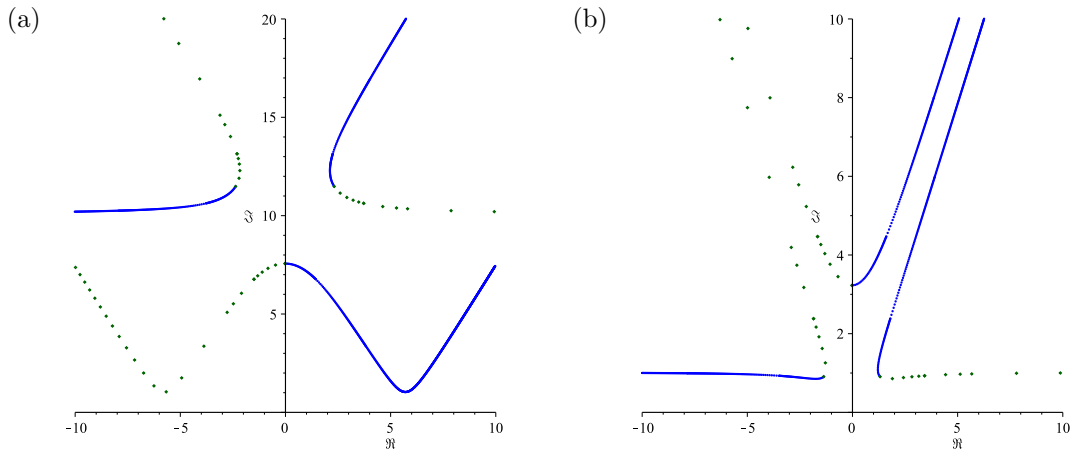

Figure 4.2: Complex root paths of $F_2^{GBE}(x, -10, 0, \beta)$ and $F_2^{GBE}(x, 0, 0, \beta)$ respectively. The blue lines are for positive β and green is negative.

It would be reasonable to assume that when both α and β vary the effect is that of the rotation from α at $t = -10$ (considering roots defined in terms of t) and the shift away from the origin from β. When $t = 0$ all roots are pushed away from the origin but the trajectory of each would be determined by the size of β in relation to α as to which line the root is more likely to follow. Under experimentation it is seen that the roots of a function where both α and β vary

does not precisely change by the ratio of α and β, when looking at the function F_n^{GBE} it becomes clear why.

The larger α and β in the F_n^{GBE} function, the more the input from F_{n-1}^{BE} will have an effect.

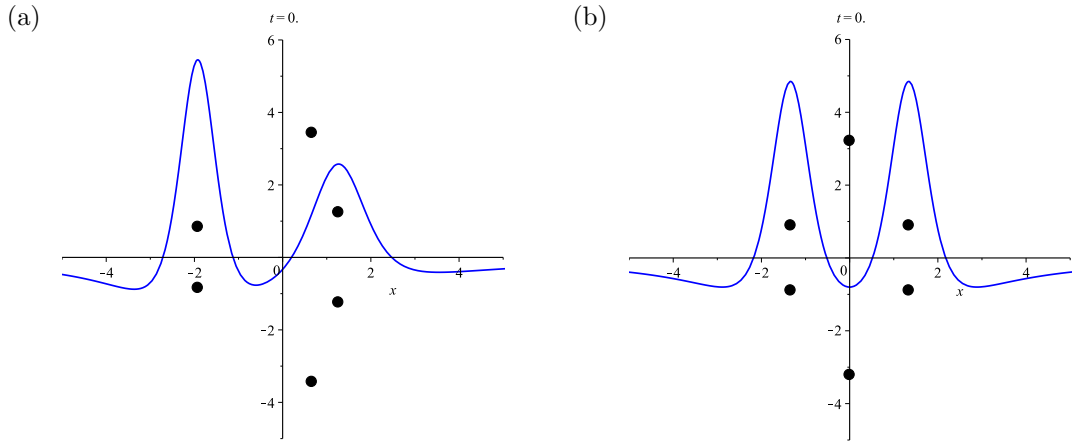

Figure 4.3: Complex roots of F_2^{GBE} and the corresponding solutions $u_2(x, 0)$ with $\alpha = t = 0$ and $\beta = 10$ in Figure 4.3(a) and $\alpha = t = \beta = 0$ in Figure 4.3(b).

By comparing Figures 4.3(a) and 4.3(b) we can see that one of the waves increases in size while the other reduces if we alter β in comparison to when $\beta = 0$. Interestingly this does not result in the net height of both waves being maintained though, with Figure 4.3(a) still being lower overall than Figure 4.3(b). This transference of energy may well have gone into the width of the waves as we see that the lower wave in Figure 4.3(a) is much wider than its counterpart when $\beta = 0$. Waves still appear as a coupling of roots come close to the real axis, as has been observed before, but when there are 4 roots within the vicinity of a wave, the width of this wave increases and the symmetry is lost. The highest wave is retrieved with the two roots that come closest to the real axis where the lowest waves roots never come as near.

When we vary α instead of β the waves no longer reach their maximum at $t = 0$ but instead for positive α the maximum is reached at negative t (a lower value of t for higher α) and the waves move further away from each other as

the roots that near the real axis move further apart. This behaviour is shown in Figure 4.4.

By considering (4.3) with the knowledge that the functions P_{n-1} and Q_{n-1} are functions of even powers of x and t, one can see that symmetry in the imaginary axis is maintained when we set $\beta = 0$ and vary α since sending $x \to -x$ does not change the equation. However, since β is multiplied by x, if we set $\alpha = 0$ and vary β then the symmetry is lost.

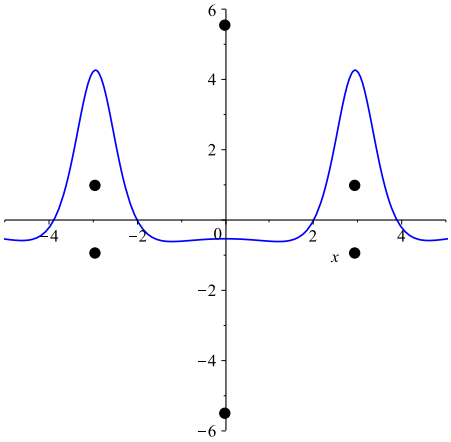

Figure 4.4: Complex roots of $F_2^{GBE}(x, -1.5, 50, 0)$ with $u_2^{GBE}(x, -1.5, 50, 0)$.

4.3.2 Behaviour of $F_3^{GBE}(x, t, \alpha, \beta)$

As in §4.3.1, this behaviour will likely be extrapolated to the odd n generalised functions. Once more, additional roots will clearly have additional behaviours but the behaviour at the origin should be similar if not the same. Figure 4.5 shows the behaviour of the maximums for both α and β changing. It should be noted that large values of the parameters are needed in order to see a change in the 3D graphs.

Now α is fixed as 0 and β varied as well as the converse. The complex roots of the solution F_3^{GBE} are shown in Figures 4.6 and 4.7. The symmetries that were observed in F_2^{GBE} are no longer present for most of the graphs. Instead the full

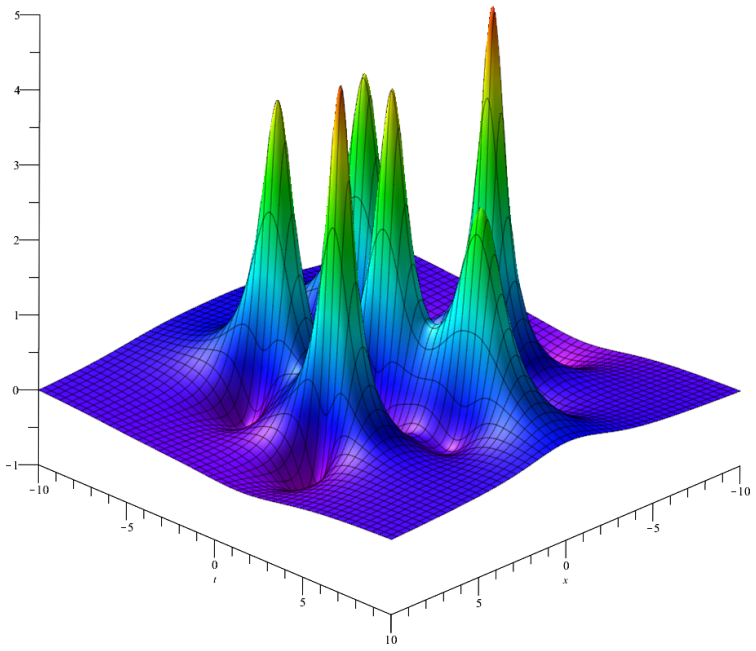

Figure 4.5: 3D plot of ${F_3}^{GBE}$ for $\alpha = -4000$ and $\beta = 1000$.

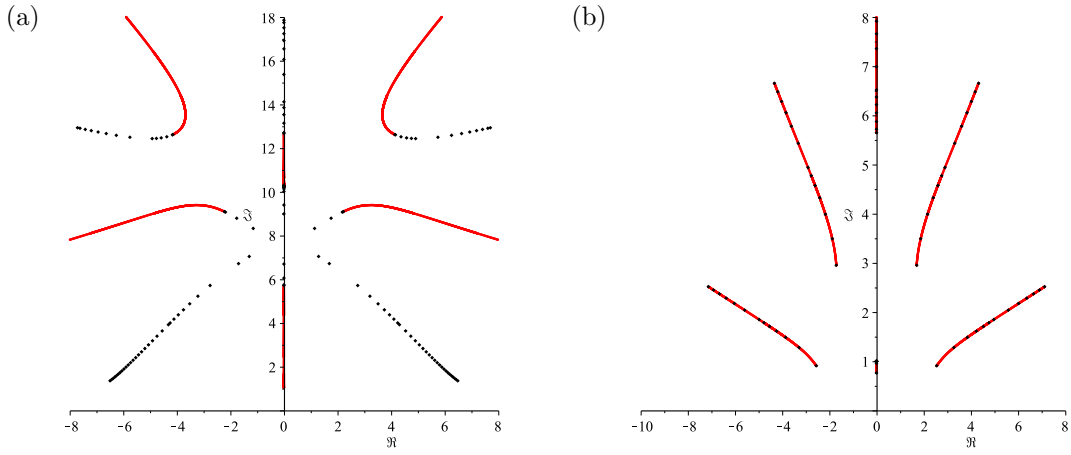

Figure 4.6: Complex root paths of $F_3^{GBE}(x, -10, \alpha, 0)$ and $F_3^{GBE}(x, 0, \alpha, 0)$ respectively. The red lines are for positive α and black is negative.

graphs with both negative and positive values of the parameter have symmetry but it is not necessarily that the negative value of the parameter is the mirror of the positive parameter. Indeed, Figure 4.6(a) has some very interesting behaviour. The information shown in Figure 4.6(b) will not be explored as the varying of the parameter only takes the roots back on the same root that they travelled when the sign of $|\alpha|$ is changed.

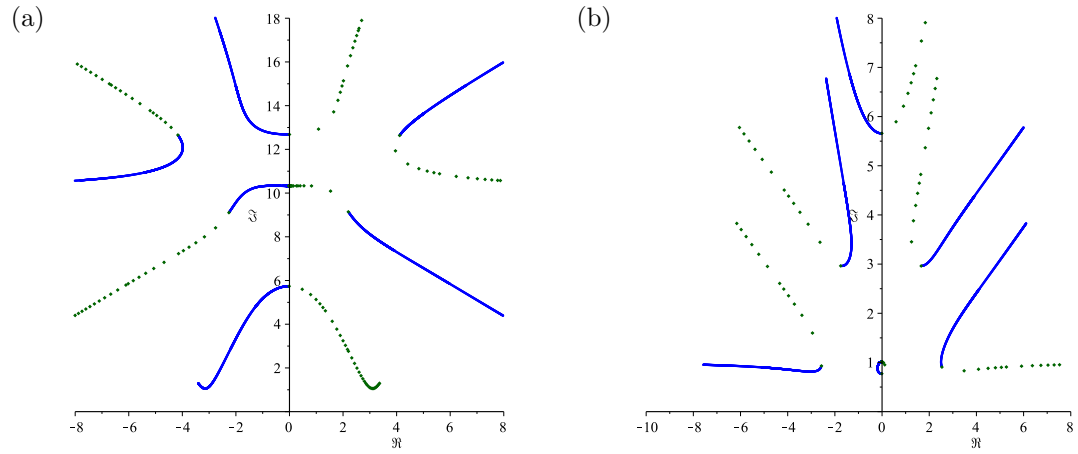

Figure 4.7: Complex root paths of $F_3^{GBE}(x, -10, 0, \beta)$ and $F_3^{GBE}(x, 0, 0, \beta)$ respectively. The blue lines are for positive β and green is negative.

Very large values of $|\alpha|$ and $|\beta|$ are used in the figures and it is clear that there are certain turning points. It may be that these turning points pertain to a distinct change in the behaviour of the solutions since they are not always related to the alteration from a positive value of the parameter to a negative one. Numerically these turning points are as follows. For $t = 10$ values of α at turning points are between $\alpha = 1185.18$ and $\alpha = 1185.16$ and between $\alpha = 1938.81$ and $\alpha = 1938.83$. For t $= 10$ values of β at turning points are between $\beta = 834.53$ and $\beta = 834.55$ which is one of the ellipses, between $\beta = 834.55$ and $\beta = 834.53$ which is the other of the ellipses, between $\beta = 140079.73$ and $\beta = 140079.75$ and between $\beta = 140079.75$ and $\beta = 140079.73$. As is seen, it is occasionally very large values of the parameters until these turning points occur.

4.3.3 Limiting Behaviour

One can look at the trajectory graphs and deduce that the difference between positive and negative β is merely a reflection in the imaginary axis. However, when considering α this cannot be true else the symmetry would be broken. Indeed varying α, symmetry is maintained throughout but the roots follow parabolic-like

paths providing that they are not the roots that reside on the axis. Should the roots then come close to the imaginary axis they change direction once again at approximately 90° which is the only break of the curve.

As β increases from 0 some of the waves split to increase the total number of waves for each function. This phenomena is discussed further in §4.3.4. It seems at first that altering β splits waves apart until there is a central wave and a circular group of waves. Once this separation and formation period has passed, the waves that surround the central waves then seem to rotate round as they move farther away from the origin.

For $x = 0$ we find that the peak develops as $\alpha = t^3$ and in the limit and as $|\alpha| \to \infty$ the maximum is 4. For $\alpha = 0$ there are 3 peaks one of which sits on $t = 0$. This develops as $\beta = t^3$ and in the limit the maximum is 4. These behaviours can be seen for all functions in the Figures 4.10 and 4.11 respectively.

Figure 4.8 shows graphs of the maximums that occur along $x = 0$ for $\alpha = 0$ and $t = 0$ for $\beta = 0$. In Figure 4.8(a) the positive α values occur on the positive t axis and the negative values on the negative t axis. The opposing occurs for Figure 4.9(a) where the positive β values occur on the negative t axis and vice versa for the negative β values. Positive and negative values of α and β have been plotted in different colour sets for clarity.

The images shown in Figures 4.10 and 4.11 look somewhat simplistic as Maple did not have a way of creating a heat map. As such, these graphs were created using a similar code to that found in Appendix E.5.

Lemma 4.2. *The functions u_2^{GBE} up to u_5^{GBE} have one maximum that moves along a line in x when we consider $\beta = 0$ and vary α, or t with $\alpha = 0$ and varying β. These maximums tend to a limit as α or β respectively tend to $\pm\infty$. The limit is* 4.

Proof of u_2^{GBE}, u_3^{GBE}, u_4^{GBE} and u_5^{GBE} as $\alpha \to \infty$.

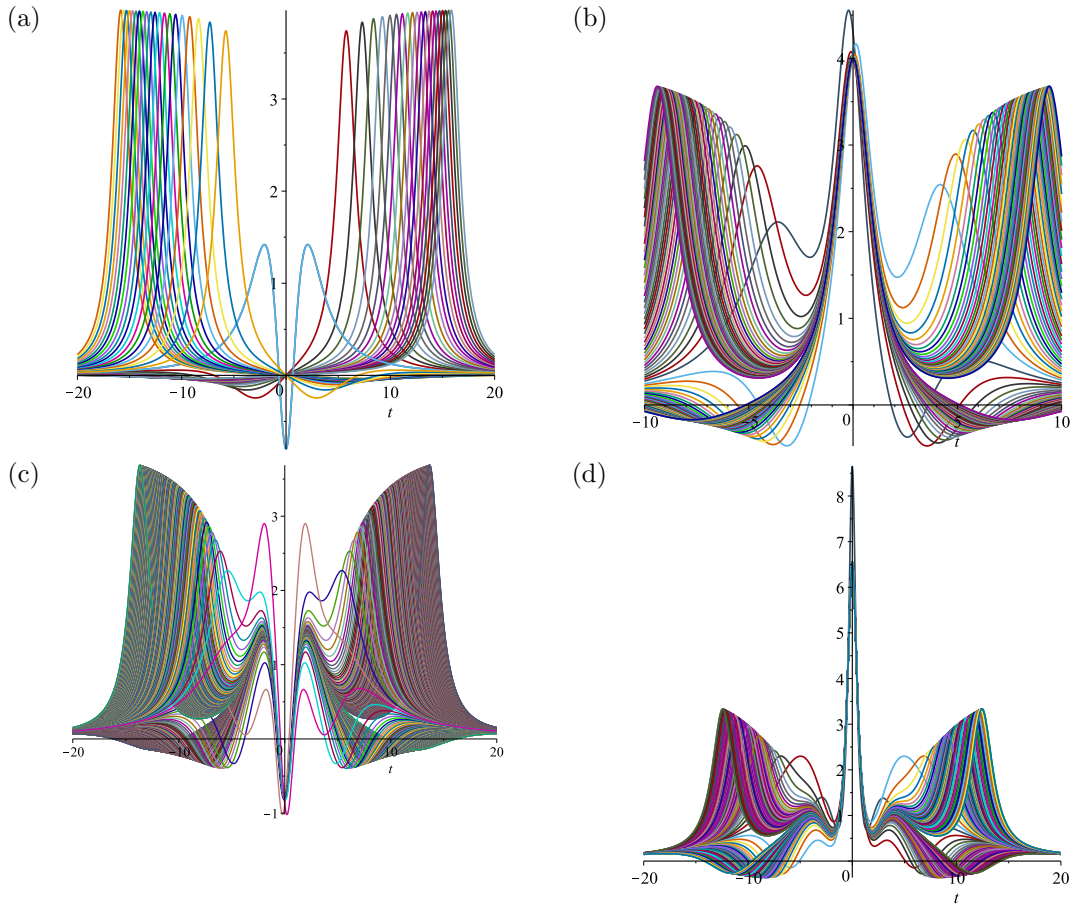

Figure 4.8: Time evolution plots of the maximums of u_2, u_3, u_4 and u_5 for $\beta = 0, x = 0$ and α positive for the blue/yellow colour scheme and negative for the purple/grey colour scheme.

Consider the limit as $\alpha \to \infty$ when $\beta = 0$ in which a maximum of the functions u_2^{GBE}, u_3^{GBE}, u_4^{GBE} and u_5^{GBE} all occur on $x = 0$ for α both positive and negative.

Let $x = 0$ since the maximums always occur on these, and $t = c_2\alpha^{1/3} + t_2, t = c_3\alpha^{1/5} + t_3, t = c_4\alpha^{1/7} + t_4$ and $t = c_5\alpha^{1/9} + t_0$ respectively for $u_2^{GBE}, u_3^{GBE}, u_4^{GBE}$ and u_5^{GBE}. These powers of α represent how the waves develop in the limit. These have Taylor series in the limit as

$$u_2^{GBE}(0, c_2\alpha^{1/3} + t_2, \alpha, 0) \sim 4\,\frac{27\,{c_2}^4 + 54\,c_2}{(9\,{c_2}^6 - 18\,{c_2}^3 + 9)\,\alpha^{2/3}} + \mathcal{O}\left(\frac{1}{\alpha}\right), \tag{4.10a}$$

$$u_3^{GBE}(0, c_3\alpha^{1/5} + t_3, \alpha, 0) \sim 4\,\frac{6\,{c_3}^{10} - 18\,{c_3}^5 + 1}{{c_3}^2\,(c_3 + 1)^2\,({c_3}^4 - {c_3}^3 + {c_3}^2 - c_3 + 1)^2\,\alpha^{2/5}}$$

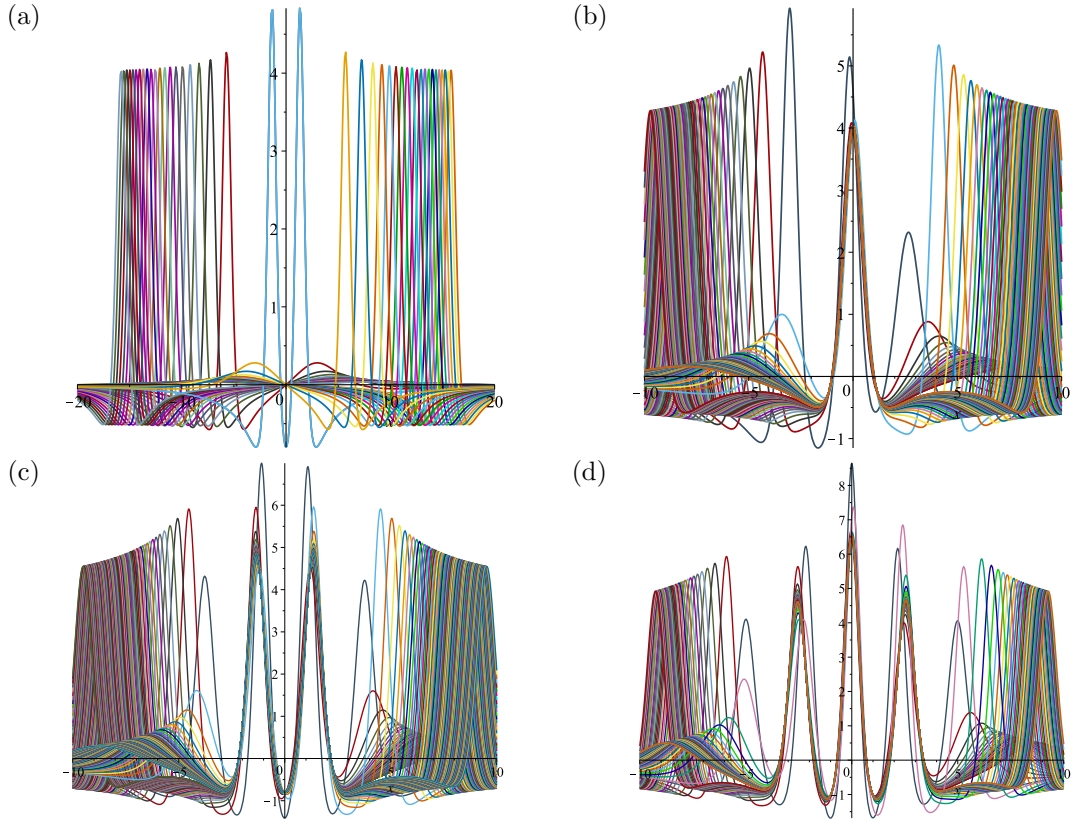

Figure 4.9: Time evolution plots of the maximums of u_2, u_3, u_4 and u_5 for $\alpha = 0, t = 0$ and β positive for the blue/yellow colour scheme and negative for the purple/grey colour scheme.

$$+\mathcal{O}\left(\frac{1}{\alpha^{3/5}}\right), \tag{4.10b}$$

$$u_4^{GBE}(0, c_4\alpha^{1/7} + t_4, \alpha, 0) \sim \frac{4(10\,{c_4}^{14} + 36\,{c_4}^7 + 3)}{{c_4}^2\left(c_4 - 1\right)^2\left({c_4}^6 + {c_4}^5 + {c_4}^4 + {c_4}^3 + {c_4}^2 + c + 1\right)^2\alpha^{2/7}}$$

$$+\mathcal{O}\left(\frac{1}{\alpha^{3/7}}\right), \tag{4.10c}$$

$$u_5^{GBE}(0, c_5\alpha^{1/9} + t_5, \alpha, 0) \sim 12\,\frac{5\,{c_5}^{18} - 20\,{c_5}^9 + 2}{{c_5}^2\left(1 + c_5\right)^2\left({c_5}^2 - c_5 + 1\right)^2\left({c_5}^6 - {c_5}^3 + 1\right)^2\alpha^{2/9}}$$

$$+\mathcal{O}\left(\frac{1}{\alpha^{3/9}}\right). \tag{4.10d}$$

Given that the first term is required to be to independent of α and only real values of c are considered, try the following substitutions $c_2 = 1, c_3 = -1, c_4 = 1$ and $c_5 = -1$. For the time being, disregard when $c_i = 0$ as these are the waves

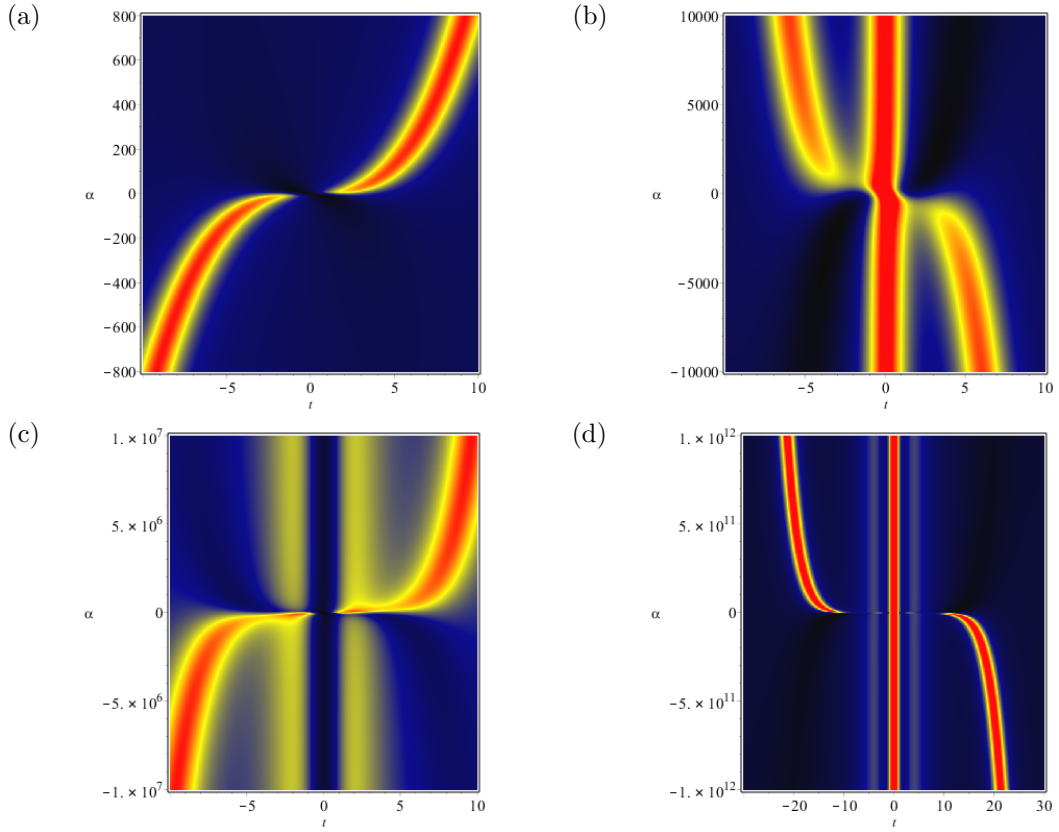

Figure 4.10: Heat map of $u_2^{GBE}, u_3^{GBE}, u_4^{GBE}$ and u_5^{GBE} when $x = 0, \beta = 0$ and $|\alpha|$ is increased.

that move linearly and they will be proven later. These values of the c_i's can also be verified numerically. Now the series is recalculated.

$$u_2^{GBE}(0, \alpha^{1/3} + t_2, \alpha, 0) \sim \frac{4}{t_2^2 + 1} + \mathcal{O}\left(\frac{1}{\alpha^{1/3}}\right) \tag{4.11}$$

$$u_3^{GBE}(0, -\alpha^{1/5} + t_3, \alpha, 0) \sim \frac{4}{t_3^2 + 1} + \mathcal{O}\left(\frac{1}{\alpha^{1/5}}\right) \tag{4.12}$$

$$u_4^{GBE}(0, \alpha^{1/7} + t_4, \alpha, 0) \sim \frac{4}{t_4^2 + 1} + \mathcal{O}\left(\frac{1}{\alpha^{1/7}}\right) \tag{4.13}$$

$$u_5^{GBE}(0, -\alpha^{1/9} + t_5, \alpha, 0) \sim \frac{4}{t_5^2 + 1} + \mathcal{O}\left(\frac{1}{\alpha^{1/9}}\right) \tag{4.14}$$

where the leading terms are maximal when $t_i = 0$ and the maximums are 4.

Returning to the linear waves that occur when $c_3 = c_4 = c_5 = 0$, it transpires that only u_3^{GBE} gives a maximum of 4 and the others have different heights. This

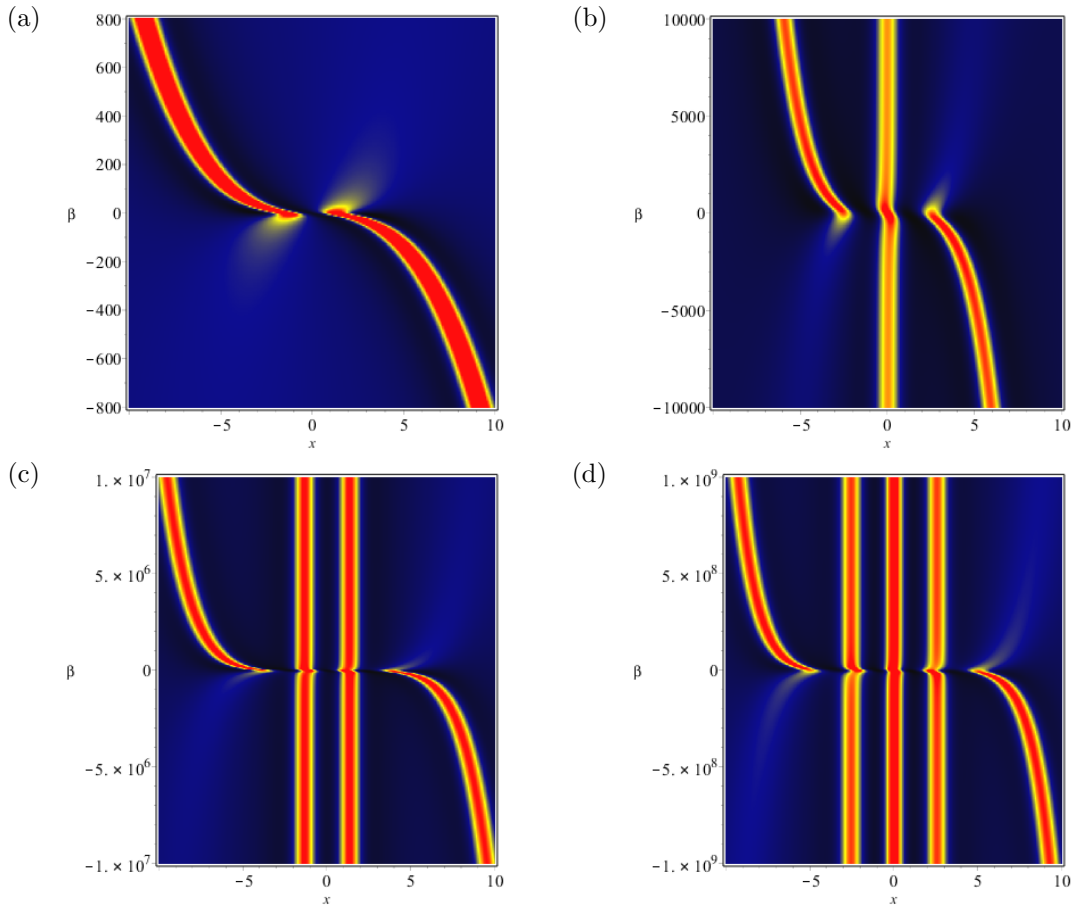

Figure 4.11: Heat map of u_2, u_3, u_4 and u_5 when $t = 0, \alpha = 0$ and $|\beta|$ is increased.

is discussed later in §4.5. For u_3^{GBE} there is the series

$$u_3^{GBE}(0, t_3, \alpha, 0) \sim \frac{4}{t_3^2 + 1} + \mathcal{O}\left(\frac{1}{\alpha}\right), \tag{4.15a}$$

which is maximal for $t_3 = 0$ and the maximum value is 4. □

Proof of u_2^{GBE}, u_3^{GBE}, u_4^{GBE} and u_5^{GBE} as $\beta \to \infty$.

Consider the limit as $\beta \to \infty$ when $\alpha = 0$ in which a maximum of the functions u_2^{GBE}, u_3^{GBE}, u_4^{GBE} and u_5^{GBE} all occur on $t = 0$ for β both positive and negative.

Let $t = 0$ since the maximums always occur on these, and $x = d_2\beta^{1/3} + x_2, x = d_3\beta^{1/5} + x_3, x = d_4\beta^{1/7} + x_4$ and $x = d_5\beta^{1/9} + x_5$ respectively for $u_2^{GBE}, u_3^{GBE}, u_4^{GBE}$ and u_5^{GBE}. These powers of β represent how the waves develop in the limit. These

have Taylor series in the limit as

$$u_2^{GBE}(d_2\beta^{1/3}+x_2,0,0,\beta) \sim -\frac{12d_2(d_2^3-2)}{(d_2+1)^2(d_2^2-d_2+1)^2\beta^{2/3}} + \mathcal{O}\left(\frac{1}{\beta}\right) \tag{4.16a}$$

$$u_3^{GBE}(d_3\beta^{1/5}+x_3,0,0,\beta) \sim -\frac{-4(6d_3^{10}-18d_3^5+1)}{d_3^2(d_3+1)^2(d_3^4-d_3^3+d_3^2-d_3+1)^2\beta^{2/5}} + \mathcal{O}\left(\frac{1}{\beta^{3/5}}\right), \tag{4.16b}$$

$$u_4^{GBE}(d_4\beta^{1/7}+x_4,0,0,\beta) \sim -\frac{4(10d_4^{14}-36d_4^7+3)}{d_4^2(d_4+1)^2(d_4^6-d_4^5+d_4^4-d_4^3+d_4^2-d_4+1)^2\beta^{2/7}} + \mathcal{O}\left(\frac{1}{\beta^{3/7}}\right), \tag{4.16c}$$

$$u_5^{GBE}(d_5\beta^{1/9}+x_5,0,0,\beta) \sim -\frac{12(5d_5^{18}-20d_5^9+2)}{d_5^2(d_5+1)^2(d_5^2-d_5+1)^2(d_5^6-d_5^3+1)^2\beta^{2/9}} + \mathcal{O}\left(\frac{1}{\beta^{3/9}}\right). \tag{4.16d}$$

Given that the first term is required to be to independent of β and only real values of d are considered, try the following substitution $d_i = -1$ for $2 \leq i \leq 5$. For the time being, disregard when $d_i = 0$ as these are the waves that move linearly and they will be proven later. These values of the d_i's can also be verified numerically. Now the series is recalculated.

$$u_2^{GBE}(-\beta^{1/3}+x_2,0,0,\beta) \sim -\frac{4(x_2-1)(x_2+1)}{(x_2^2+1)^2} + \mathcal{O}\left(\frac{1}{\beta^{1/3}}\right) \tag{4.17a}$$

$$u_3^{GBE}(-\beta^{1/5}+x_3,0,0,\beta) \sim -\frac{4(x_3-1)(x_3+1)}{(x_3^2+1)^2} + \mathcal{O}\left(\frac{1}{\beta^{1/5}}\right) \tag{4.17b}$$

$$u_4^{GBE}(-\beta^{1/7}+x_4,0,0,\beta) \sim -\frac{4(x_4-1)(x_4+1)}{(x_4^2+1)^2} + \mathcal{O}\left(\frac{1}{\beta^{1/7}}\right) \tag{4.17c}$$

$$u_5^{GBE}(-\beta^{1/9}+x_5,0,0,\beta) \sim -\frac{4(x_5-1)(x_5+1)}{(x_5^2+1)^2} + \mathcal{O}\left(\frac{1}{\beta^{1/9}}\right) \tag{4.17d}$$

where the leading terms are maximal when $x_i = 0$ and the maximums are 4.

Returning to the linear waves that occur when $d_3 = d_4 = d_5 = 0$, it transpires that only u_3^{GBE} gives a maximum of 4 and the others have different heights as

before. For u_3^{GBE} has the same series when $x = d_3$ as when $\beta \neq 0$ and the same limit of 4 when $d_3 = 0$, which is maximal for $t_3 = 0$ and the maximum value is 4. □

It does not seem to be the case that all waves tend to the same limit however. In Figure 4.9(c), the central two waves have a limit of just under 5 rather than 4. This would need to be verified to establish whether the limits differ for different waves.

4.3.4 Maximum Number of Waves in F_n^{GBE}

Unlike in Chapter 3, using the generalised Boussinesq equation and varying α and β can result in an increase in the number of waves in the solution. This arises as the "half-waves" combine to make new, full rogue waves.

Assessing all of the functions informs that F_2^{GBE} can reach 3 waves, F_3^{GBE} has 6, F_4^{GBE} has 9 plus two "half waves" and F_5^{GBE} has 12. In terms of how many additional waves are attained this means that an order 2 solution gains 1 wave, order 6 gains 2, order 12 gains 3, order 20 gains 4 and order 30 gains 5 from F_n.

Conjecture 4.2. *Varying parameters in F_n^{GBE} can increase the number of waves that exist for F_n^{BE} up to $n-1$ additional waves.*

Considering only the peaks of the waves, in all bar the second image of Figure 4.12 with which we shall refer to as the transition phase, all waves appear to sit on a circle with the origin as their centre. Given the symmetries that are involved with these solutions, this is not surprising for u_2^{GBE}. Instead let us consider u_3^{GBE}. As can be seen in Figure 4.13, once more it seems that the waves reside on a circle as we increase the value of β and a similar behaviour is observed for $\beta = 0$ and α varying. These figures also act to detail how the waves separate, and the appearance is that they separate on the positive x range first until it reaches the

origin where this wave splits. The wave that originated in negative x maintains its structure which would explain the $n-1$ additional waves as in Conjecture 4.2.

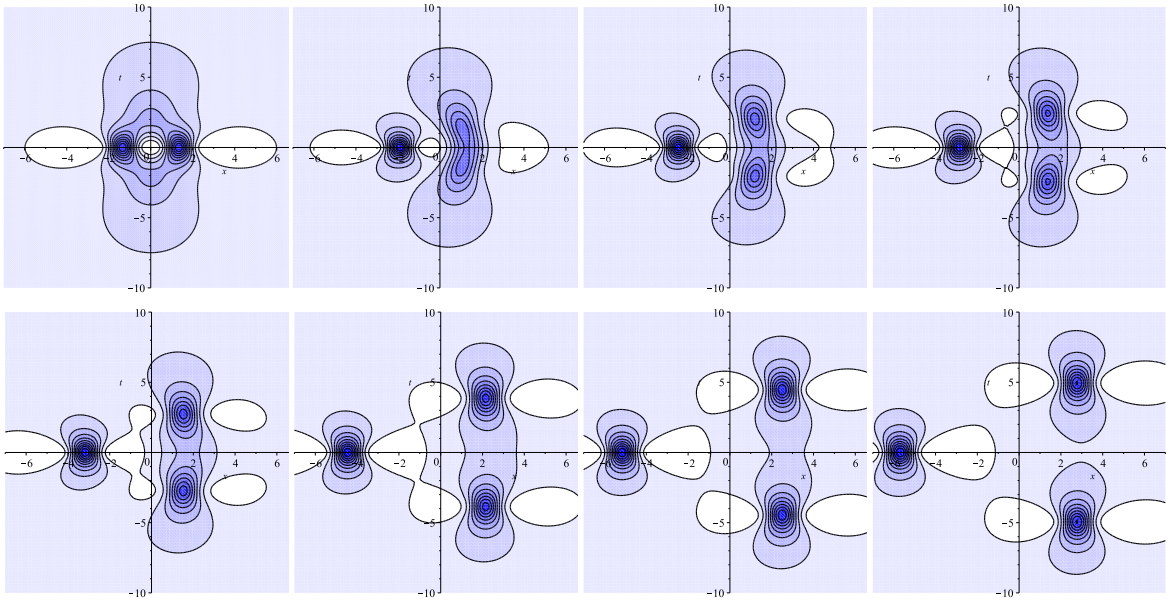

Figure 4.12: Contour plots of u_2^{GBE} with $\alpha = 0$ and $\beta = 0, 10, 20, 30, 40, 100,\ 150$ and 200 respectively.

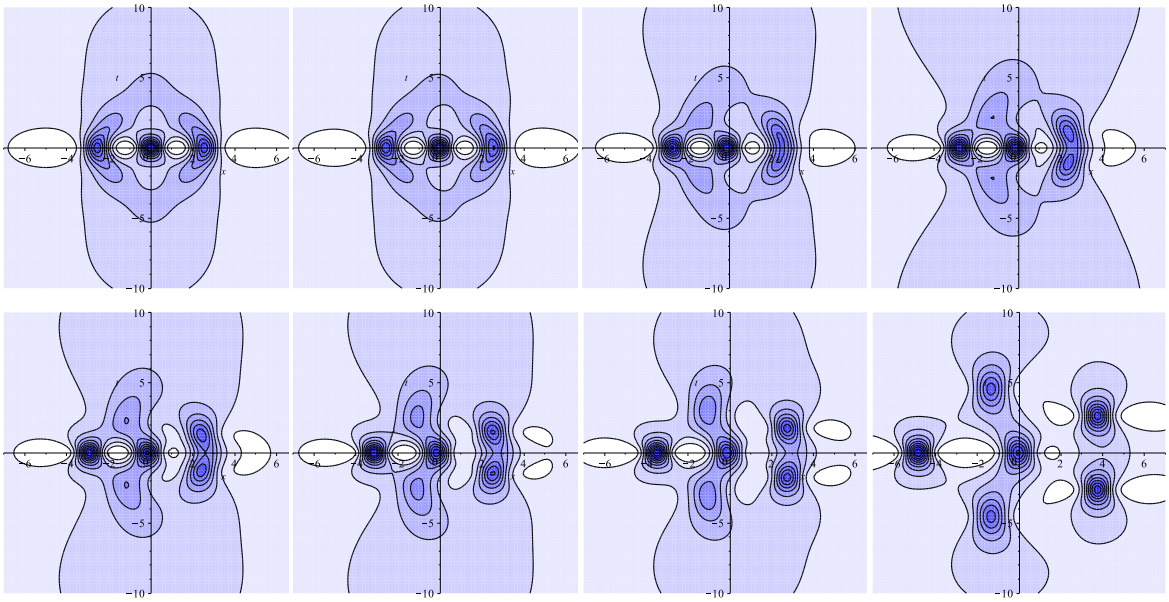

Figure 4.13: Contour plots of u_3^{GBE} with $\alpha = 0$ and $\beta = 0, 50, 200, 300, 400, 600,$ 1000 and 4000 respectively.

4.4 Wave Formations

All waves seem to dissipate away from the origin in the (x,t)-plane in a circular formation. Around the centre the formation is dictated by F_{n-2}^{BE} where we take $F_0^{BE}=0$. It was hoped that calculating u^{GBE} in terms of F^{BE} would allow for the explicit extraction of F_{n-2}^{BE} but this was not resolved.

For u_2^{GBE} and u_3^{GBE} the waves form circularly around the origin (or central wave located at the origin when there is one) and dissipate out. However, for u_4^{GBE} and u_5^{GBE} there is no longer a single central wave but the other behaviour is observed. Indeed for u_4^{GBE} the central formation is two waves and two half-waves, such as u_2^{BE} is and for u_5^{GBE} the central formation is that of u_3^{BE}. This structure can be seen in the final graphs of Figures 4.12 and 4.13. Based on the equation for F_n^{GBE} and its relation to F_{n-1}^{BE}, it seems that the central formation in u_n^{GBE} is the same as u_{n-1}^{BE}. This satisfies the formation for u_3^{GBE} as well and explains why u_2^{GBE} has no central pivot since we consider $F_0=1$. Despite the fact that F_{n-2}^{BE} has a much lower order than F_n this central behaviour is present throughout the range of α and β.

The central formations do move slightly just not as fast as the outer formations and they seem to be moving slower as $|t|$ increases. At present there has been no analytical analysis as to why this occurs, however the same thing seems to happen in the Schrödinger equation [33].

4.5 Discussion

This chapter has considered a parametrised version of the Boussinesq equation which allows for a great deal of freedom. The limiting behaviour that has been completed only provide proofs for waves that reside on certain linear lines rather than the waves that move outside of this. An open question is to find a proof that

gives the limits for all waves which may require the expression of α and β in terms of x and t. This would also solve the explicit scaling and rotation influenced by increasing $|\alpha|$ or $|\beta|$. This should also aid in the proof that the waves reside on a circle which still remains to be found.

The limits found for negative α and β were not consistent with the hypothesis as they seemed to tend to 72/11. This could be further researched to see if there is an error in the methodology or if there is different behaviour occurring in the negative infinite limit.

The heights of the waves were seen to vary given the alterations of the parameters, but it was not identified for which values of the parameters that the heights were drastically combined. There was also most analysis completed only on the varying of one parameter with the other fixed at 0 but this greatly reduces the ability to generalise the behaviour found.

Subsequent to the work on this, F_6^{BE} was found and so it remains to find P_5 and Q_5 in order to establish F_6^{GBE}. Given the degree of the polynomials involved this will take a reasonable amount of computing time and memory so some streamlining of the process would also be beneficial where possible.

Chapter 5

Conservation Laws for the Boussinesq Equation

This chapter focusses on the conversation laws and integral relations of the Boussinesq equation in the form

$$u_{tt} + u_{xx} - 2(u_x)^2 - 2uu_{xx} - \tfrac{1}{3}u_{xxxx} = 0. \tag{5.1}$$

The solutions are rational solutions that decay algebraically as mentioned in Chapter 3, with

$$u_n = 2\frac{\partial^2}{\partial x^2} \ln F_n, \tag{5.2}$$

where F_n is given by

$$F_n(x,t) = \sum_{m=0}^{n(n+1)/2} \sum_{j=0}^{m} a_{j,m} x^{2j} t^{2(m-j)}, \tag{5.3}$$

for specific constants $a_{j,m}$.

First the equalities in the bilinear form are investigated, followed by consideration of the conservation laws and the chapter closes with the main work on

integral relations.

The work in this chapter has been published in [8].

5.1 Equalities of the Bilinear Form

Lemma 5.1. *Consider functions F that satisfy the bilinear form*

$$FF_{tt} - F_t^2 + FF_{xx} - F_x^2 - \frac{1}{3}FF_{xxxx} + \frac{4}{3}F_xF_{xxx} - F_{xx}^2 = 0, \tag{5.4}$$

then they also satisfy

$$\int_{-\infty}^{\infty} \left(\frac{F_t}{F}\right)_t \mathrm{d}x = \int_{-\infty}^{\infty} \left(\frac{F_{xx}^2}{F^2} - \frac{F_xF_{xxx}}{F^2}\right) \mathrm{d}x. \tag{5.5}$$

Proof. Consider the Boussinesq bilinear form as in (5.4) and divide through by F^2 to retrieve

$$\left(\frac{F_t}{F}\right)_t + \left(\frac{F_x}{F}\right)_x - \frac{1}{3}\frac{F_{xxxx}}{F} + \frac{4}{3}\frac{F_xF_{xxx}}{F^2} - \frac{F_{xx}^2}{F^2} = 0. \tag{5.6}$$

Rewriting the left hand side of this as,

$$\left(\frac{F_t}{F}\right)_t + \left(\frac{F_x}{F}\right)_x - \frac{1}{3}\left(\frac{F_{xxxx}}{F} - \frac{F_xF_{xxx}}{F^2}\right) + \frac{F_xF_{xxx}}{F^2} - \frac{F_{xx}^2}{F^2} \tag{5.7}$$

$$= \left(\frac{F_t}{F}\right)_t + \left(\frac{F_x}{F}\right)_x - \frac{1}{3}\left(\frac{F_{xxx}}{F}\right)_x + \frac{F_xF_{xxx}}{F^2} - \frac{F_{xx}^2}{F^2}, \tag{5.8}$$

to result in

$$\left(\frac{F_t}{F}\right)_t + \frac{F_xF_{xxx}}{F^2} - \frac{F_{xx}^2}{F^2} = -\left(\frac{F_x}{F}\right)_x + \frac{1}{3}\left(\frac{F_{xxx}}{F}\right)_x. \tag{5.9}$$

Integrating through with respect to x from $-\infty$ to ∞ gives,

$$\int_{-\infty}^{\infty}\left(\left(\frac{F_t}{F}\right)_t+\frac{F_xF_{xxx}}{F^2}-\frac{F_{xx}^2}{F^2}\right)\mathrm{d}x=-\left[\frac{F_x}{F}\right]_{-\infty}^{\infty}+\frac{1}{3}\left[\frac{F_{xxx}}{F}\right]_{-\infty}^{\infty}. \tag{5.10}$$

Given that the polynomials F that will be considered are of even power in x and t then the rational solution u_n of the form (5.2) has a denominator of higher order than the numerator and therefore between the limits $-\infty$ and ∞ gives 0. As such the bilinear form can be simplified further to,

$$\int_{-\infty}^{\infty}\left(\frac{F_t}{F}\right)_t\mathrm{d}x=\int_{-\infty}^{\infty}\left(\frac{F_{xx}^2}{F^2}-\frac{F_xF_{xxx}}{F^2}\right)\mathrm{d}x. \tag{5.11}$$

However, it is not possible to remove the integral from this equation as the equality only holds with the limits. □

5.2 Conservation Laws

Definition 5.1. *A conservation law is comprised of a conserved density $T(x,t)$ and an associated flux $X(x,t)$ and satisfies the equation,*

$$\frac{\partial T}{\partial t}+\frac{\partial X}{\partial x}=0. \tag{5.12}$$

Integrating both sides of the (5.12) with respect to t then x gives

$$\int_{-\infty}^{\infty}T(x,t)\mathrm{d}x+\int_{-\infty}^{\infty}X(x,t)\mathrm{d}t=0, \tag{5.13}$$

where the order of integration has been interchanged since it is assumed that the integrals exist.

More simply

$$\int_{-\infty}^{\infty}T(x,t)\mathrm{d}x=-\int_{-\infty}^{\infty}X(x,t)\mathrm{d}t. \tag{5.14}$$

Consider (5.14) and differentiate with respect to t so that

$$\frac{\mathrm{d}}{\mathrm{d}t}\int_{-\infty}^{\infty} T\mathrm{d}x = \int_{-\infty}^{\infty} \frac{\partial T}{\partial t}\mathrm{d}x \tag{5.15}$$

$$= -\int_{-\infty}^{\infty} \frac{\partial X}{\partial x}\mathrm{d}x \tag{5.16}$$

$$= -\big[X\big]_{-\infty}^{\infty}, \tag{5.17}$$

by Leibniz's rule, thus it is required that $\lim_{|x|\to\infty} X = 0$ so that the integral exists and is finite. Subsequently

$$\frac{\mathrm{d}}{\mathrm{d}t}\int_{-\infty}^{\infty} T\mathrm{d}x = 0, \tag{5.18}$$

giving that the integral of T with respect to x must be equal to some constant c_1. It follows that the integral of X with respect to t is equal to $-c_1$.

Now consider the integral

$$\int_{-\infty}^{\infty} T(x,t)\mathrm{d}x = c_1, \tag{5.19}$$

as the conserved density with x a spatial coordinate and

$$\int_{-\infty}^{\infty} X(x,t)\mathrm{d}t = -c_1, \tag{5.20}$$

as the constant of motion with t a time coordinate.

By rewriting the (5.1) as a system it is possible to examine the conserved quantities. The system is

$$u_t + v_x = 0, \tag{5.21a}$$

$$v_t + 2uu_x - u_x + \tfrac{1}{3}u_{xxx} = 0, \tag{5.21b}$$

where

$$u = 2\frac{\partial^2}{\partial x^2}\ln F, \tag{5.22}$$

$$v = -2\frac{\partial^2}{\partial x \partial t}\ln F, \tag{5.23}$$

i.e $v_x = -u_t$.

The first few conserved quantities for the Boussinesq equation [36, pp.19–78] are as follows

$$T_1 = u, \qquad X_1 = v, \tag{5.24}$$

$$T_2 = v, \qquad X_2 = u^2 - u + \tfrac{1}{3}u_{xx}, \tag{5.25}$$

$$T_3 = uv, \qquad X_3 = \tfrac{2}{3}u^3 + \tfrac{1}{2}(v^2 - u^2) - \tfrac{1}{6}u_x^2 + \tfrac{1}{3}uu_{xx}, \tag{5.26}$$

$$T_4 = \tfrac{2}{3}u^3 + v^2 - u^2 - \tfrac{1}{3}u_x^2, \qquad X_4 = 2u^2v - 2uv + \tfrac{2}{3}vu_{xx} - \tfrac{2}{3}u_xv_x. \tag{5.27}$$

Graphs of T_2 and X_2 for differing values of u_n can also be seen in Figures 5.1 and 5.2. As expected, there remains a large amount of structure to these waves and exploration of the behaviour of the T_i and X_i functions is another avenue for further research.

It is easy to calculate that for the solutions found and detailed in Chapter 3 that the integrals of T_i and X_i for $i = 1, .., 4$ are all constant and furthermore are 0.

The conserved density T_3, is considered as the total energy conservation and X_3 as the power conservation law [37]. Plotting the functions v_2 and v_3 for one fixed parameter and one varying, it seems that the waves reside on a circle with centre $(0, 0)$. In Figure 5.3 these plots are shown with a circle superimposed on top calculated by using the location of the roots. As can be seen, even when α and β vary the roots still seem to be positioned on a circle with the origin at its

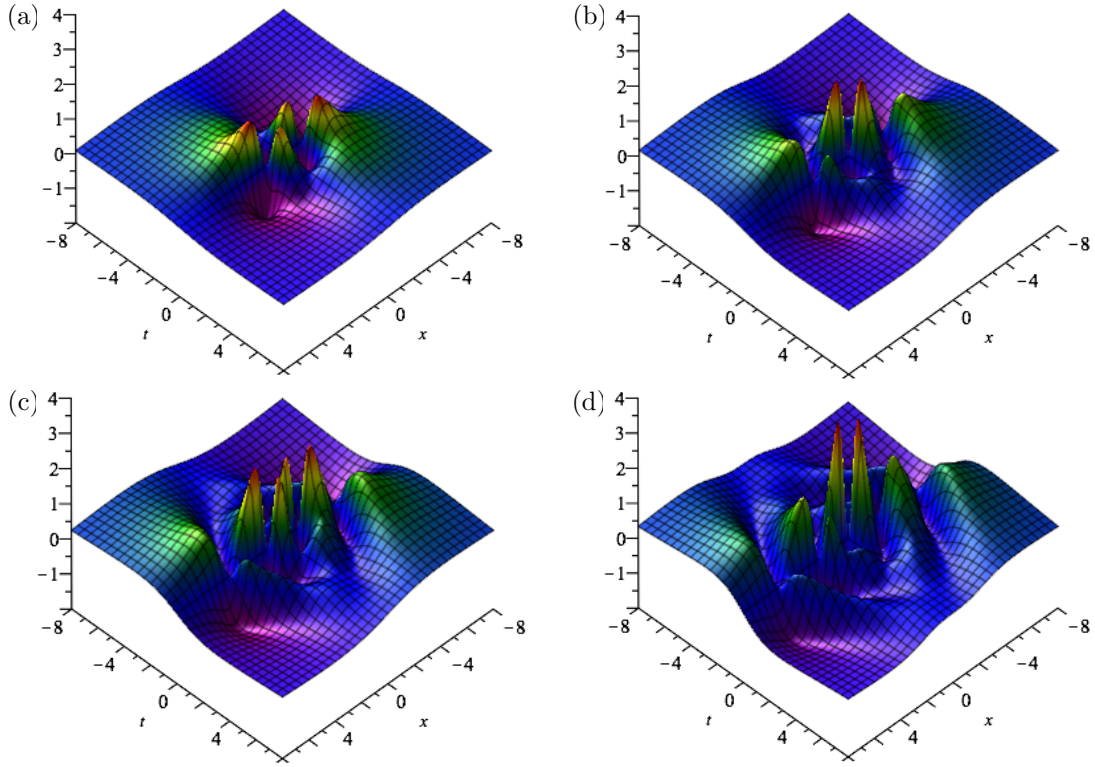

Figure 5.1: T_2 for u_2, u_3, u_4 and u_5.

centre. What is also interesting is that in the choices made for α and β, there is always at least one root (not at the origin) which resides on one of the axes. Further work would be to determine the angle of rotation and the influence that α and β have on this.

5.3 Integral Relations

This section will be concerned with proving the following result:

Theorem 5.1. *Let $u_n(x,t;\alpha,\beta)$ be a rational solution of the Boussinesq equation* (5.1) *in the form*

$$u_n(x,t;\alpha,\beta) = 2\frac{\partial^2}{\partial x^2}\ln F_n(x,t;\alpha,\beta),$$

with F_n satisfying the bilinear form (5.4)*, then*

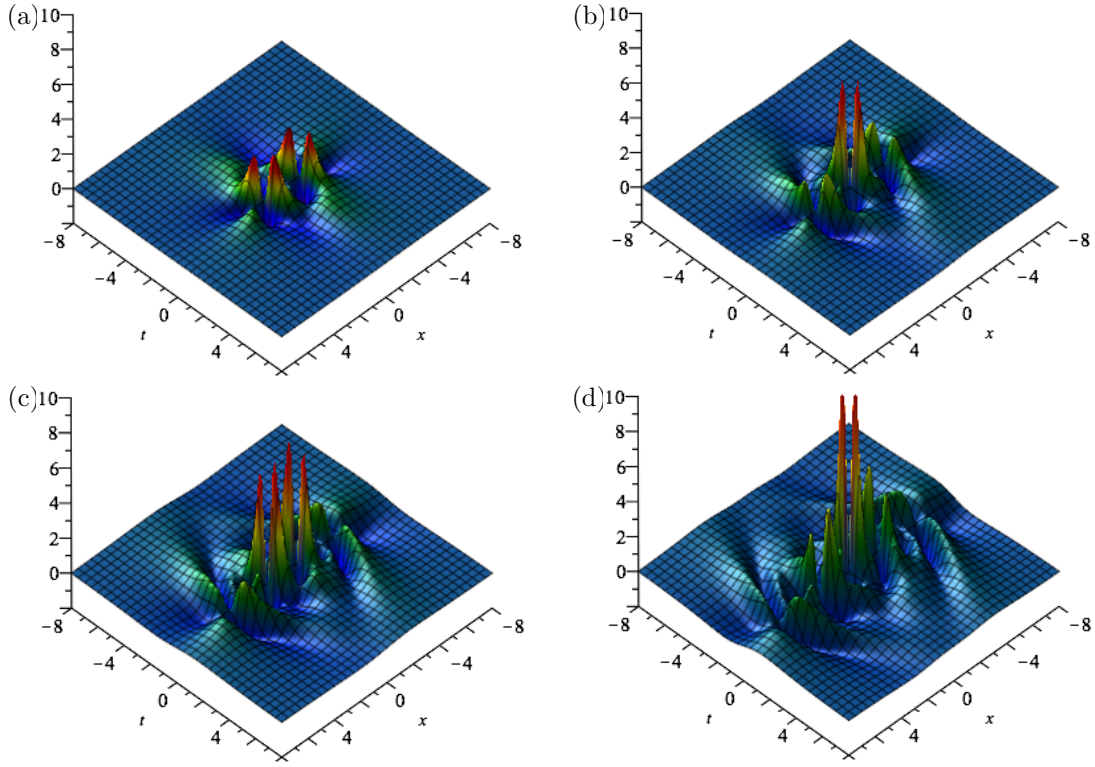

Figure 5.2: X_2 for u_2, u_3, u_4 and u_5.

$$\frac{1}{8\pi}\int_{-\infty}^{\infty}\int_{-\infty}^{\infty} u_n^2(x,t;\alpha,\beta)\mathrm{d}x\mathrm{d}t = \tfrac{1}{2}n(n+1), \tag{5.28}$$

$$\frac{1}{8\pi}\int_{-\infty}^{\infty}\int_{-\infty}^{\infty} u_n^3(x,t;\alpha,\beta)\mathrm{d}x\mathrm{d}t = n(n+1). \tag{5.29}$$

Given that n is directly related to the degree of the polynomial F_n then the following theorem gives a relation between this and the integrals given.

In [7] numerical result were published regarding rogue wave solutions of the NLS equation that show a similar behaviour. These are mentioned in Chapter 2. There has not been an analytical proof of this for the NLS equation, unlike what my collaborators and I have found for the Boussinesq equation[8].

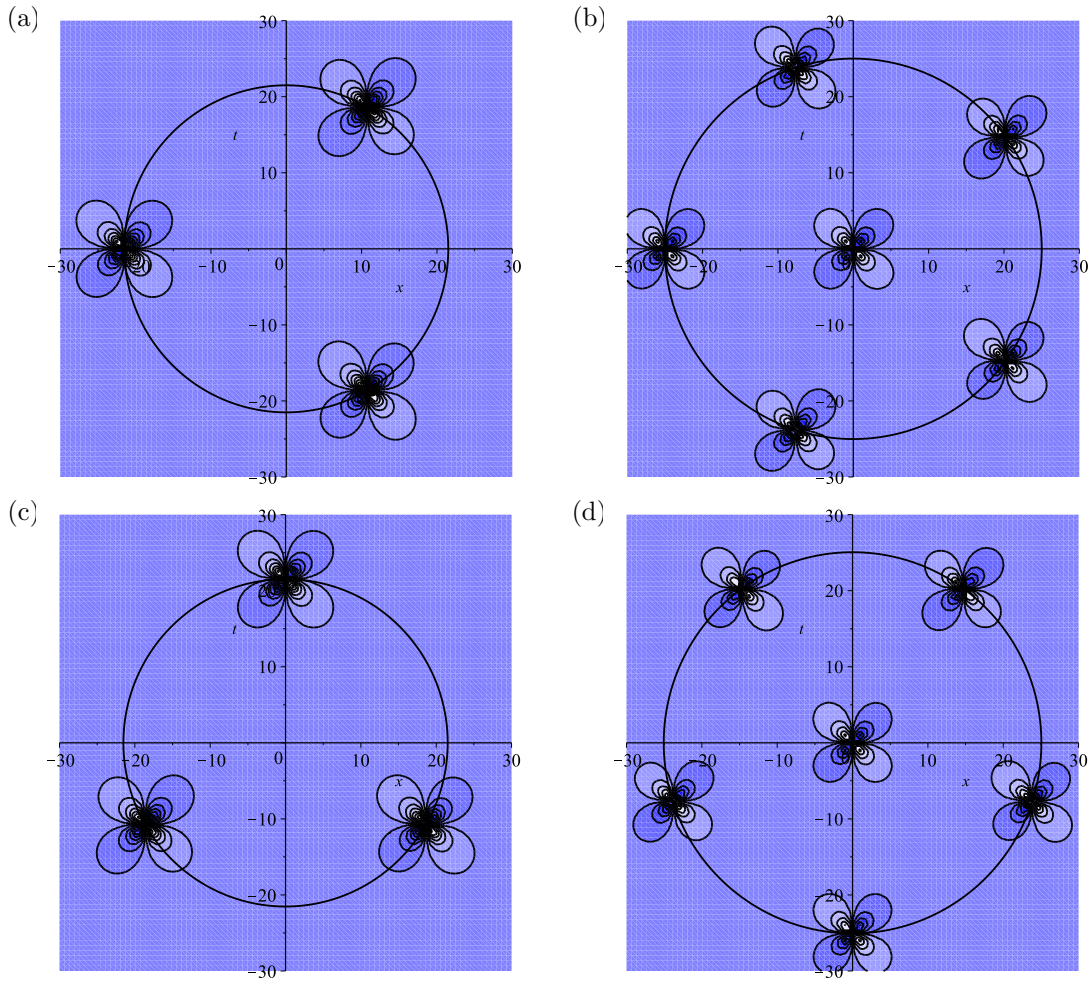

Figure 5.3: v_2 and v_3 for (α, β) being $(0, 10^4)$, $(0, 10^7)$, $(10^4, 0)$ and $(10^7, 0)$ respectively and the circular perimeter added.

5.3.1 Integrals of u_n^2

Lemma 5.2. *Let u solve the Boussinesq equation (5.1) and set $u = U_{xx}$. Then*

$$U_{xx} \notin L^1(\mathbb{R}^2),$$

$$U_{tt} \notin L^1(\mathbb{R}^2),$$

$$(U_{xx} + U_{tt}) \in L^1(\mathbb{R}^2),$$

where $L^1(\mathbb{R}^2)$ is the space of functions where the modulus of the function is Lesbesgue integrable in $\mathbb{R}^2$.

Sketch of Proof. The sketch of this proof is given for u_1 and we expect u_n to behave in a similar way. The case U_{xx} is given as the working is almost identical to that for U_{tt}. Given that $u = U_{xx}$ then

$$U_{xx} = 2\frac{t^2 - x^2 + 1}{(x^2 + t^2 + 1)^2}. \tag{5.30}$$

For a function to be in L^1 means

$$\int_{\mathbb{R}^2} |U_{xx}| \mathrm{d}x\mathrm{d}t < \infty, \tag{5.31}$$

so for $U_{xx} \notin L^1$ this means the integral is infinite. Take the modulus of U_{xx} and converting to polar coordinates gives,

$$|U_{xx}| = 2\frac{|r^2\cos(2\theta) - 1|}{(1 + r^2)^2} > 2\frac{r^2|\cos(2\theta)|}{(1 + r^2)^2} - \frac{2}{(1 + r^2)^2}, \tag{5.32}$$

where we have used the triangle inequality.

As such we have

$$\int_{\mathbb{R}^2} |U_{xx}| \mathrm{d}x\mathrm{d}t = 2\lim_{R\to\infty}\int_{r=0}^{R}\int_{\theta=0}^{2\pi} \frac{r^3|\cos(2\theta)|}{(1 + r^2)^2} - \frac{r}{(1 + r^2)^2}\mathrm{d}\theta\mathrm{d}r. \tag{5.33}$$

The first term in the integrand is then

$$\lim_{R\to\infty}\int_{r=0}^{R}\int_{\theta=0}^{2\pi} \frac{r^3|\cos(2\theta)|}{(1 + r^2)^2}\mathrm{d}\theta\mathrm{d}r = \lim_{R\to\infty}(2\ln(1 + R^2) - \frac{2R^2}{1 + R^2} = \infty. \tag{5.34}$$

The second term of the integrand is

$$\lim_{R\to\infty}\int_{r=0}^{R}\int_{\theta=0}^{2\pi} \frac{r}{(1 + r^2)^2}\mathrm{d}\theta\mathrm{d}r = \lim_{R\to\infty}\frac{\pi R^2}{1 + R^2} = \pi. \tag{5.35}$$

As such we have shown that

$$\int_{\mathbb{R}^2} |U_{xx}| \mathrm{d}x\mathrm{d}t \to \infty \tag{5.36}$$

and U_{xx} is therefore not in L^1. Similarly $U_{tt} \notin L^1$.

Consider

$$U_{xx} + U_{tt} = \frac{4}{(x^2+t^2+1)^2} = \frac{4}{(r^2+1)^2}, \tag{5.37}$$

when changing the coordinates to polar coordinates. Using (5.36) we can show that

$$\int_{\mathbb{R}^2} |U_{xx} + U_{tt}| \mathrm{d}x\mathrm{d}t = 4\pi, \tag{5.38}$$

and so $(U_{xx} + U_{tt}) \in L^1$. □

Proof of (5.28) ***from Theorem 5.1.*** One can work directly from the Boussinesq equation,

$$u_{tt} + u_{xx} - (u^2)_{xx} - \tfrac{1}{3}u_{xxxx} = 0, \tag{5.39}$$

so that,

$$u^2 = u + \partial_x^{-2} u_{tt} - \tfrac{1}{3}u_{xx}, \tag{5.40}$$

assuming $|u| \to 0$ as $|x| \to \infty$.

Now let $u = U_{xx}$ so that $U = 2\ln F$ to retrieve,

$$u^2 = U_{xx} + U_{tt} - \tfrac{1}{3}U_{xxxx}, \tag{5.41}$$

and

$$\int_{-\infty}^{\infty} u^2 \mathrm{d}x = \int_{-\infty}^{\infty} (U_{xx} + U_{tt} - \tfrac{1}{3}U_{xxxx}) \mathrm{d}x \tag{5.42}$$

$$= [-\tfrac{1}{3}U_{xxx}]_{-\infty}^{\infty} + \int_{-\infty}^{\infty} (U_{xx} + U_{tt}) \mathrm{d}x. \tag{5.43}$$

Given the form of U, it is know that its derivatives will vanish as $|x| \to \infty$ so the equation simplifies to,

$$\int_{-\infty}^{\infty} u^2 \mathrm{d}x = \int_{-\infty}^{\infty} (U_{xx} + U_{tt}) \mathrm{d}x. \tag{5.44}$$

Therefore the conservation law is

$$\widetilde{C}_1 = \frac{1}{8\pi} \int_{-\infty}^{\infty} \int_{-\infty}^{\infty} (U_{xx} + U_{tt}) \mathrm{d}x\mathrm{d}t. \tag{5.45}$$

Consider now $(x,t) \in [-R,R] \times [-R,R]$ where R is very large but finite in order to compute the integrals. By doing this, it is possible to integrate U_{xx} and U_{tt} seperately and compute these finite integrals by interchanging the order of integration, then take the limit as $R \to \infty$. Without changing to a finite integral, it would seem that the integrands become 0 after integrating once due to the lack of Lesbegue integrability of U_{xx} and U_{tt} individually (see Lemma 5.2), however this is not actually the case.

Now consider F_n in the form

$$F_n(x,t) = (x^2 + t^2)^{n(n+1)/2} + G_n, \tag{5.46}$$

where G_n is a function of x and t of degree $(n+2)(n-1)$ in x and t. As such, and recalling that $U_x = 2F_x/F$ and $U_t = 2F_t/F$, the following holds

$$\begin{aligned}
\frac{1}{8\pi} \int_{-R}^{R} \int_{-R}^{R} (U_{xx} + U_{tt}) \mathrm{d}x\mathrm{d}t &= \frac{1}{4\pi} \int_{-R}^{R} \int_{-R}^{R} \left(\left(\frac{F_{n,x}(x,t)}{F_n(x,t)} \right)_x + \left(\frac{F_{n,t}(x,t)}{F_n(x,t)} \right)_t \right) \mathrm{d}x\mathrm{d}t \\
&= \frac{1}{4\pi} \int_{-R}^{R} \int_{-R}^{R} \left(\frac{F_{n,x}(x,t)}{F_n(x,t)} \right)_x \mathrm{d}x\mathrm{d}t \\
&\quad + \frac{1}{4\pi} \int_{-R}^{R} \int_{-R}^{R} \left(\frac{F_{n,t}(x,t)}{F_n(x,t)} \right)_t \mathrm{d}t\mathrm{d}x \\
&= \frac{1}{4\pi} \int_{-R}^{R} \left(\frac{F_{n,x}(R,t)}{F_n(R,t)} - \frac{F_{n,x}(-R,t)}{F_n(-R,t)} \right) \mathrm{d}t
\end{aligned}$$

$$+\frac{1}{4\pi}\int_{-R}^{R}\left(\frac{F_{n,t}(x,R)}{F_n(x,R)}-\frac{F_{n,t}(x,-R)}{F_n(x,-R)}\right)\mathrm{d}x. \quad (5.47)$$

Now consider the asymptotics of $F_{n,x}/F_n$ and $F_{n,t}/F_n$ in order to simplify the integral further. Given that

$$F_{n,x}=n(n+1)x(x^2+t^2)^{n(n+1)/2-1}+G_{n,x}(x,t),$$

and similarly for $F_{n,t}$ then it is possible to use the form of F_n as given in (5.46) to retrieve

$$\begin{aligned}
\frac{F_{n,x}(R,t)}{F_n(R,t)} &= \frac{n(n+1)R(R^2+t^2)^{n(n+1)/2-1}+G_{n,x}(R,t)}{(R^2+t^2)^{n(n+1)/2}+G_n(R,t)}\\
&= \frac{n(n+1)R(R^2+t^2)^{n(n+1)/2-1}}{(R^2+t^2)^{n(n+1)/2}+G_n(R,t)}+\frac{G_{n,x}(R,t)}{(R^2+t^2)^{n(n+1)/2}+G_n(R,t)}\\
&= \frac{n(n+1)R}{(R^2+t^2)+G_n(R,t)(R^2+t^2)^{1-n(n+1)/2}}\\
&\quad +\frac{G_{n,x}(R,t)}{(R^2+t^2)^{n(n+1)/2}+G_n(R,t)}\\
&= \frac{n(n+1)R}{R^2+t^2}\left(\frac{1}{1+G_n(R,t)(R^2+t^2)^{-n(n+1)/2}}\right)\\
&\quad +\frac{G_{n,x}(R,t)}{(R^2+t^2)^{n(n+1)/2}+G_n(R,t)}\\
&= \frac{n(n+1)R}{R^2+t^2}\left(\frac{(R^2+t^2)^{n(n+1)/2}}{(R^2+t^2)^{n(n+1)/2}+G_n(R,t)}\right)\\
&\quad +\frac{G_{n,x}(R,t)}{(R^2+t^2)^{n(n+1)/2}+G_n(R,t)}\\
&= \frac{n(n+1)R}{R^2+t^2}\left(\frac{(R^2+t^2)^{n(n+1)/2}+G_n(R,t)}{(R^2+t^2)^{n(n+1)/2}}\right)^{-1}\\
&\quad \frac{G_{n,x}(R,t)}{(R^2+t^2)^{n(n+1)/2}+G_n(R,t)}\\
&= \frac{n(n+1)R}{R^2+t^2}\left(1+\frac{G_n(R,t)}{(R^2+t^2)^{n(n+1)/2}}\right)^{-1}\\
&\quad +\frac{G_{n,x}(R,t)}{(R^2+t^2)^{n(n+1)/2}+G_n(R,t)}. \quad (5.48)
\end{aligned}$$

Given that x and t are of the same order, make the transformation $t = \tau R$ where τ is of order 1 in the limit as $R \to \infty$ which makes t infinite with $\tau = \mathcal{O}(1)$. This gives

$$\begin{aligned}\frac{F_{n,x}(R,\tau R)}{F_n(R,\tau R)} =& \frac{n(n+1)R}{R^2(1+\tau^2)}\left(1+\frac{G_n(R,\tau R)}{(R^2(1+\tau^2))^{n(n+1)/2}}\right)^{-1} \\ &+ \frac{G_{n,x}(R,\tau R)}{(R^2(1+\tau^2))^{n(n+1)/2}+G_n(R,\tau R)}.\end{aligned}$$

Given

$$\begin{aligned}G_n(R,\tau R) &= \mathcal{O}(R^{(n+2)(n-1)}),\\ G_{n,x}(R,\tau R) &= \mathcal{O}(R^{n^2+n-3}),\end{aligned}$$

then

$$\begin{aligned}\frac{G_{n,x}(R,\tau R)}{(R^2(1+\tau^2))^{n(n+1)/2}+G_n(R,\tau R)} &= \mathcal{O}(R^{-3}),\\ \frac{G_n(R,\tau R)}{(R^2(1+\tau^2))^{n(n+1)/2}} &= \mathcal{O}(R^{-2}).\end{aligned}$$

As such,

$$\frac{F_{n,x}(R,\tau R)}{F_n(R,\tau R)} = \frac{n(n+1)R}{R^2(1+\tau^2)}\left(1+\mathcal{O}(R^{-2})\right).$$

Similarly, it can be shown that

$$\frac{F_{n,x}(-R,t)}{F_n(-R,t)} = \frac{F_{n,x}(-R,\tau R)}{F_n(-R,\tau R)} = -\frac{n(n+1)R}{R^2(1+\tau^2)}\left(1+\mathcal{O}(R^{-2})\right).$$

Now compute

$$\frac{1}{4\pi}\int_{-R}^{R}\left(\frac{F_{n,x}(R,t)}{F_n(R,t)}-\frac{F_{n,x}(-R,t)}{F_n(-R,t)}\right)\mathrm{d}t=\frac{1}{4\pi}\int_{-1}^{1}\frac{2n(n+1)R^2}{R^2(1+\tau^2)}(1+\mathcal{O}(R^{-2}))\mathrm{d}\tau$$
$$=\frac{n(n+1)}{2\pi}(1+\mathcal{O}(R^{-2}))\int_{-1}^{1}\frac{1}{1+\tau^2}\mathrm{d}\tau$$

$$=\frac{n(n+1)}{2\pi}(1+\mathcal{O}(R^{-2}))\left[\arctan(\tau)\right]_{-1}^{1}$$
$$=\frac{n(n+1)}{2\pi}(1+\mathcal{O}(R^{-2}))\frac{\pi}{2}$$
$$=\frac{n(n+1)}{4}(1+\mathcal{O}(R^{-2})),\tag{5.49}$$

using that $\mathrm{d}t=R\mathrm{d}\tau$ and that the transformation $t=R\tau$ changes the limits from $-R$ to R when integrating with respect to t, to -1 to 1 when integrating with respect to τ.

Using (5.48) and interchanging x with t gives

$$\frac{F_{n,t}(x,R)}{F_n(x,R)}=\frac{n(n+1)R}{x^2+R^2}\left(1+\frac{G_n(x,R)}{(x^2+R^2)^{n(n+1)/2}}\right)^{-1}$$
$$+\frac{G_{n,t}(x,R)}{(x^2+R^2)^{n(n+1)/2}+G_n(x,R)},\tag{5.50}$$

and let $x=\xi R$ with ξ of order 1 to get

$$\frac{F_{n,t}(\xi R,R)}{F_n(\xi R,R)}=\frac{n(n+1)R}{R^2(\xi^2+1)}\left(1+\frac{G_n(\xi R,R)}{(R^2(\xi^2+1))^{n(n+1)/2}}\right)^{-1}$$
$$+\frac{G_{n,t}(\xi R,R)}{(R^2(\xi^2+1))^{n(n+1)/2}+G_n(\xi R,R)}$$
$$=\frac{n(n+1)R}{R^2(\xi^2+1)}(1+\mathcal{O}(R^{-2})).$$

So

$$\frac{1}{4\pi}\int_{-R}^{R}\left(\frac{F_{n,t}(x,R)}{F_n(x,R)}-\frac{F_{n,t}(x,-R)}{F_n(x,-R)}\right)\mathrm{d}x = \frac{1}{4\pi}\int_{-1}^{1}\frac{2n(n+1)R^2}{R^2(\xi^2+1)}(1+\mathcal{O}(R^{-2}))\mathrm{d}\xi$$
$$= \frac{n(n+1)}{2\pi}(1+\mathcal{O}(R^{-2}))\int_{-1}^{1}\frac{1}{\xi^2+1}\mathrm{d}\xi$$
$$= \frac{n(n+1)}{4}(1+\mathcal{O}(R^{-2})). \tag{5.51}$$

Using (5.49) and (5.51) in (5.47) gives

$$\frac{1}{8\pi}\int_{-R}^{R}\int_{-R}^{R}(U_{xx}+U_{tt})\mathrm{d}x\mathrm{d}t = \frac{n(n+1)}{2}(1+\mathcal{O}(R^{-2})), \tag{5.52}$$

which, in the limit $R\to\infty$ results in

$$\frac{1}{8\pi}\int_{-\infty}^{\infty}\int_{-\infty}^{\infty}(U_{xx}+U_{tt})\mathrm{d}x\mathrm{d}t = \frac{n(n+1)}{2}, \tag{5.53}$$

as stated in (5.28) from Theorem 5.1. □

5.3.2 Integrals of u_n^3

This proof is more complex than that for u_n^2 and requires the use of two of the Boussinesq conservation laws; (5.26) and (5.27).

Proof of (5.29) ***from Theorem 5.1.*** Take

$$u^2 = u + U_{tt} - \tfrac{1}{3}u_{xx}, \tag{5.54}$$

and multiply through by u to retrieve an expression for u^3;

$$\int_{-\infty}^{\infty}\int_{-\infty}^{\infty}u^3\mathrm{d}x\mathrm{d}t = \int_{-\infty}^{\infty}\int_{-\infty}^{\infty}(u^2+uU_{tt}-\tfrac{1}{3}uu_{xx})\mathrm{d}x\mathrm{d}t$$

$$
\begin{aligned}
&= \int_{-\infty}^{\infty} \left(\int_{-\infty}^{\infty} (u^2 + uU_{tt}) \mathrm{d}x - \frac{1}{3} \int_{-\infty}^{\infty} u u_{xx} \mathrm{d}x \right) \mathrm{d}t \\
&= \int_{-\infty}^{\infty} \left(\int_{-\infty}^{\infty} (u^2 + uU_{tt}) \mathrm{d}x - \frac{1}{3} \left([u u_x]_{-\infty}^{\infty} - \int_{-\infty}^{\infty} u_x^2 \mathrm{d}x \right) \right) \mathrm{d}t \\
&= \int_{-\infty}^{\infty} \int_{-\infty}^{\infty} \left(u^2 + uU_{tt} + \frac{1}{3} u_x^2 \right) \mathrm{d}x \mathrm{d}t. \qquad (5.55)
\end{aligned}
$$

It is still not possible to integrate this directly and using the previous expression for the double integral of u^2 here will not help cancel the u_x^2 or the uU_{tt} that need to be resolved. Consider (5.26) and (5.27) however, it is possible to get an expression for u^3 in terms of some of these functions.

From (5.20) with $c_1 = 0$ and (5.26) the following holds

$$
\int_{-\infty}^{\infty} (\tfrac{2}{3} u^3 + \tfrac{1}{2}(v^2 - u^2) - \tfrac{1}{6} u_x^2 + \tfrac{1}{3} u u_{xx}) \mathrm{d}t = 0, \qquad (5.56)
$$

which can be integrated with respect to x to give

$$
\int_{-\infty}^{\infty} \int_{-\infty}^{\infty} \left(\tfrac{2}{3} u^3 \right) \mathrm{d}t \mathrm{d}x = \int_{-\infty}^{\infty} \int_{-\infty}^{\infty} \left(\tfrac{1}{2}(u^2 - v^2) + \tfrac{1}{6} u_x^2 - \tfrac{1}{3} u u_{xx} \right) \mathrm{d}t \mathrm{d}x.
$$

Again change the order of integration and then integrate once with respect to x to give

$$
\begin{aligned}
\int_{-\infty}^{\infty} \int_{-\infty}^{\infty} u^3 \mathrm{d}x \mathrm{d}t &= \int_{-\infty}^{\infty} \int_{-\infty}^{\infty} \left(\tfrac{3}{4}(u^2 - v^2) + \tfrac{1}{4} u_x^2 - \tfrac{1}{2} u u_{xx} \right) \mathrm{d}x \mathrm{d}t \\
&= \int_{-\infty}^{\infty} \int_{-\infty}^{\infty} \left(\tfrac{3}{4}(u^2 - v^2) + \tfrac{1}{4} u_x^2 \right) \mathrm{d}x \mathrm{d}t \\
&\quad - \tfrac{1}{2} \left([u u_x]_{-\infty}^{\infty} - \int_{-\infty}^{\infty} \int_{-\infty}^{\infty} u_x^2 \mathrm{d}x \mathrm{d}t \right) \\
&= \tfrac{3}{4} \int_{-\infty}^{\infty} \int_{-\infty}^{\infty} \left(u^2 - v^2 + u_x^2 \right) \mathrm{d}x \mathrm{d}t. \qquad (5.57)
\end{aligned}
$$

Now from (5.19) with $c_1 = 0$ and (5.27) gives

$$\int_{-\infty}^{\infty} \tfrac{2}{3}u^3 + v^2 - u^2 - \tfrac{1}{3}u_x^2 \mathrm{d}x = 0, \tag{5.58}$$

and integrating this with respect to t gives

$$\int_{-\infty}^{\infty}\int_{-\infty}^{\infty} u^3 \mathrm{d}x\mathrm{d}t = \tfrac{3}{2}\int_{-\infty}^{\infty}\int_{-\infty}^{\infty}(u^2 - v^2 + \tfrac{1}{3}u_x^2)\mathrm{d}x\mathrm{d}t. \tag{5.59}$$

Consider equating (5.57) and (5.59) in order to remove u_x^2 and then $u^2 - v^2$ respectively gives

$$\int_{-\infty}^{\infty}\int_{-\infty}^{\infty} u^3 \mathrm{d}x\mathrm{d}t = 3\int_{-\infty}^{\infty}\int_{-\infty}^{\infty}(u^2 - v^2)\mathrm{d}x\mathrm{d}t, \tag{5.60a}$$

$$\int_{-\infty}^{\infty}\int_{-\infty}^{\infty} u^3 \mathrm{d}x\mathrm{d}t = \int_{-\infty}^{\infty}\int_{-\infty}^{\infty} u_x^2 \mathrm{d}x\mathrm{d}t. \tag{5.60b}$$

Returning to (5.55) and using both equations from (5.60) simultaneously results in

$$\int_{-\infty}^{\infty}\int_{-\infty}^{\infty} u^3 \mathrm{d}x\mathrm{d}t = 3\int_{-\infty}^{\infty}\int_{-\infty}^{\infty}(v^2 + uU_{tt})\mathrm{d}x\mathrm{d}t, \tag{5.61a}$$

and

$$\int_{-\infty}^{\infty}\int_{-\infty}^{\infty} u^3 \mathrm{d}x\mathrm{d}t = \tfrac{3}{2}\int_{-\infty}^{\infty}\int_{-\infty}^{\infty}(u^2 + uU_{tt})\mathrm{d}x\mathrm{d}t. \tag{5.61b}$$

Since there is an expression for u^2 but not a comparable one for uU_{tt}, it is necessary to find an equality that removes this from the equation. It transpires (see Lemma 5.3) that uU_{tt} can be expressed only in terms of v^2.

Lemma 5.3. *Consider $u(x,t)$ and $v(x,t)$ that are solutions of* (5.21) *whereby*

$u(x,t) = U_{xx}(x,t)$ *and* $v(x,t) = -U_{xt}(x,t)$ *and*

$$\lim_{|x|\to\infty} U_x(x,t) = 0, \qquad \lim_{|t|\to\infty} U_x(x,t) = 0, \tag{5.62}$$

then

$$\int_{-\infty}^{\infty}\int_{-\infty}^{\infty} v^2(x,t)\mathrm{d}x\mathrm{d}t = \int_{-\infty}^{\infty}\int_{-\infty}^{\infty} u(x,t)U_{tt}(x,t)\mathrm{d}x\mathrm{d}t. \tag{5.63}$$

Proof. Given the form of $v^2(x,t)$ it is possible to interchange the order of integration and state that

$$\begin{aligned}
\int_{-\infty}^{\infty}\int_{-\infty}^{\infty} v^2(x,t)\mathrm{d}x\mathrm{d}t &= \int_{-\infty}^{\infty}\int_{-\infty}^{\infty} U_{xt}^2\mathrm{d}t\mathrm{d}x \\
&= \int_{-\infty}^{\infty}\left([U_{xt}U_x]_{-\infty}^{\infty} - \int_{-\infty}^{\infty} U_xU_{xtt}\mathrm{d}t\right)\mathrm{d}x \\
&= -\int_{-\infty}^{\infty}\int_{-\infty}^{\infty} U_xU_{xtt}\mathrm{d}t\mathrm{d}x.
\end{aligned}$$

Equally one can consider

$$\begin{aligned}
\int_{-\infty}^{\infty}\int_{-\infty}^{\infty} u(x,t)U_{tt}(x,t)\mathrm{d}x\mathrm{d}t &= \int_{-\infty}^{\infty}\left(\int_{-\infty}^{\infty} U_{xx}U_{tt}\mathrm{d}x\right)\mathrm{d}t \\
&= \int_{-\infty}^{\infty}\left([U_{tt}U_x]_{-\infty}^{\infty} - \int_{-\infty}^{\infty} U_xU_{xtt}\mathrm{d}x\right)\mathrm{d}t \\
&= -\int_{-\infty}^{\infty}\int_{-\infty}^{\infty} U_xU_{xtt}\mathrm{d}x\mathrm{d}t \\
&= -\int_{-\infty}^{\infty}\int_{-\infty}^{\infty} U_xU_{xtt}\mathrm{d}t\mathrm{d}x \\
&= \int_{-\infty}^{\infty}\int_{-\infty}^{\infty} v^2(x,t)\mathrm{d}x\mathrm{d}t.
\end{aligned}$$

□

Using the equality from Lemma 5.3 it is possible to write (5.61) as

$$\int_{-\infty}^{\infty}\int_{-\infty}^{\infty} u^3 \mathrm{d}x\mathrm{d}t = \tfrac{3}{2}\int_{-\infty}^{\infty}(u^2+v^2)\mathrm{d}x\mathrm{d}t,$$

and (5.64a)

$$\int_{-\infty}^{\infty}\int_{-\infty}^{\infty} u^3 \mathrm{d}x\mathrm{d}t = 6\int_{-\infty}^{\infty} v^2\mathrm{d}x\mathrm{d}t. \tag{5.64b}$$

Now substitute in (5.60a) into either of these and deduce that

$$\int_{-\infty}^{\infty}\int_{-\infty}^{\infty} u^3 \mathrm{d}x\mathrm{d}t = 2\int_{-\infty}^{\infty}\int_{-\infty}^{\infty} u^2\mathrm{d}x\mathrm{d}t. \tag{5.65}$$

Consequently

$$\frac{1}{8\pi}\int_{-\infty}^{\infty}\int_{-\infty}^{\infty} u^3 \mathrm{d}x\mathrm{d}t = n(n+1), \tag{5.66}$$

from (5.28).

□

Corollary 5.1. *Take $v_n(x,t)$ as an algebraically decaying solution of* (5.21) *then*

$$\frac{1}{8\pi}\int_{-\infty}^{\infty}\int_{-\infty}^{\infty} v^2 \mathrm{d}x\mathrm{d}t = \frac{n(n+1)}{6}. \tag{5.67}$$

Proof. The proof follows from (5.29) and (5.64b). □

5.3.3 Integrals of u_1^m

It is possible to explicitly calculate the integrals for u_1 since $F_1 = x^2+t^2+1$. It transpires that the integral can be expressed as

$$\frac{1}{8\pi}\int_{-\infty}^{\infty} u_1^m \mathrm{d}x = \frac{c_m}{(t^2+1)^{m-1/2}}. \tag{5.68}$$

Choosing just to consider the expressions c_m then these appear in sequence as

$$0, \frac{1}{2}, \frac{3}{2}, \frac{21}{4}, \frac{75}{4}, \frac{1095}{16}, \frac{4053}{16}, \frac{30317}{32}, \frac{114291}{32}, \frac{3468555}{256}, \frac{13225025}{256}, \frac{101272611}{512}, ... \tag{5.69}$$

This can also be written as

$$\frac{(1)}{(2)}, \frac{(3)}{(2)}, \frac{(3)(7)}{((2))^2}, \frac{(3)((5))^2}{((2))^2}, \frac{(3)(5)(73)}{((2))^4}, \frac{(3)(7)(193)}{((2))^4}, \frac{(7)(61)(71)}{((2))^5},$$
$$\frac{((3))^4(17)(83)}{((2))^5}, \frac{((3))^3(5)(25693)}{((2))^8}, \frac{((5))^2(11)(48091)}{((2))^8},$$
$$\frac{(3)(11)(23)(29)(43)(107)}{((2))^9}, ...$$

One can see that the pattern on the denominator is highly structured and that the difference between every other power of 2 is

$$1, 2, 1, 3, 1, ... \tag{5.70}$$

This sequence is in fact $a(n)$ [58, A001511] such that

$$a(2n+1) = 1, \tag{5.71}$$
$$a(2n) = 1 + a(n), \tag{5.72}$$
$$a(0) = 1. \tag{5.73}$$

Further from this, one can calculate the integral in terms of the power m via the following theorem.

Theorem 5.2. *Taking the first rational solution of the Boussinesq equation as*

$$u_1(x,t) = 2\frac{\partial^2}{\partial x^2}\ln(x^2+t^2+1) = \frac{4(1-x^2+t^2)}{(1+x^2+t^2)^2}, \tag{5.74}$$

then

$$\frac{1}{8\pi}\int_{-\infty}^{\infty}\int_{-\infty}^{\infty} u_1^m(x,t)\mathrm{d}x\mathrm{d}t = \frac{m!}{(2m-1)!}\sum_{l=0}^{\lfloor m/2\rfloor}\frac{(2l)!(2m-2l-2)!}{2^{2l-2m-3}(l!)^2(m-2l)!}, \tag{5.75}$$

with $\lfloor x\rfloor$ *being the largest integer less than or equal to* x *and* m *is an integer greater than or equal to* 2*.*

Proof. Consider

$$\int_{-\infty}^{\infty}\int_{-\infty}^{\infty} u_1^m\mathrm{d}x\mathrm{d}t = 2^{2m}\int_{-\infty}^{\infty}\int_{-\infty}^{\infty}\frac{(1-x^2+t^2)^m}{(1+x^2+t^2)^{2m}}, \tag{5.76}$$

and make a change of variables to polar coordinates of $x = r\cos(\theta)$ and $t = r\sin(\theta)$. This gives

$$\begin{aligned}
\int_{-\infty}^{\infty}\int_{-\infty}^{\infty} u_1^m\mathrm{d}x\mathrm{d}t &= 2^{2m}\int_0^{\infty}\int_0^{2\pi}\frac{r\left(1-r^2(\cos^2(\theta)-\sin^2(\theta))\right)^m}{(1+r^2)^{2m}}\mathrm{d}\theta\mathrm{d}r \\
&= 2^{2m}\int_0^{\infty}\int_0^{2\pi}\frac{r\left(1-r^2\cos(2\theta)\right)^m}{(1+r^2)^{2m}}\mathrm{d}\theta\mathrm{d}r \\
&= 2^{2m}\int_0^{\infty}\frac{r}{(1+r^2)^{2m}}\left(\int_0^{2\pi}\left(1-r^2\cos(2\theta)\right)^m\mathrm{d}\theta\right)\mathrm{d}r \\
&= 2^{2m}\int_0^{\infty}\frac{r}{(1+r^2)^{2m}}\left(\int_0^{2\pi}\sum_{k=0}^{m}\binom{m}{k}(-1)^k r^{2k}\cos^k(2\theta)\mathrm{d}\theta\right)\mathrm{d}r \\
&= 2^{2m}\int_0^{\infty}\frac{r}{(1+r^2)^{2m}}\left(\int_0^{2\pi}\sum_{k=0}^{m}\binom{m}{k}(-1)^k r^{2k}\cos^k(2\theta)\mathrm{d}\theta\right)\mathrm{d}r.
\end{aligned} \tag{5.77}$$

Since this involves integrating powers of $\cos(2\theta)$ between 0 and 2π, the integral is 0 if the power is odd. If the power is even then

$$\int_0^{2\pi}\cos^{2l}(2\theta)\mathrm{d}\theta = \frac{\pi}{2^{2l-1}}\frac{(2l)!}{(l!)^2}. \tag{5.78}$$

In order to accommodate this difference between odd and even powers, let $k = 2l$ for l an integer in (5.77) to get

$$
\begin{aligned}
&2^{2m}\int_0^\infty \frac{r}{(1+r^2)^{2m}}\left(\int_0^{2\pi}\sum_{l=0}^{\lfloor m/2\rfloor}\binom{m}{2l}(-1)^{2l}r^{4l}\cos^{2l}(2\theta)\mathrm{d}\theta\right)\mathrm{d}r\\
=&2^{2m}\int_0^\infty \frac{r}{(1+r^2)^{2m}}\left(\int_0^{2\pi}\sum_{l=0}^{\lfloor m/2\rfloor}\binom{m}{2l}r^{4l}\cos^{2l}(2\theta)\mathrm{d}\theta\right)\mathrm{d}r\\
=&2^{2m}\int_0^\infty \frac{r}{(1+r^2)^{2m}}\left(\sum_{l=0}^{\lfloor m/2\rfloor}\binom{m}{2l}r^{4l}\left(\int_0^{2\pi}\cos^{2l}(2\theta)\mathrm{d}\theta\right)\right)\mathrm{d}r\\
=&2^{2m}\int_0^\infty \frac{r}{(1+r^2)^{2m}}\left(\sum_{l=0}^{\lfloor m/2\rfloor}\binom{m}{2l}r^{4l}\frac{\pi}{2^{2l-1}}\frac{(2l)!}{(l!)^2}\right)\mathrm{d}r\\
=&2^{2m}\left(\sum_{l=0}^{\lfloor m/2\rfloor}\binom{m}{2l}\frac{\pi}{2^{2l-1}}\frac{(2l)!}{(l!)^2}\int_0^\infty\frac{r^{4l+1}}{(1+r^2)^{2m}}\mathrm{d}r\right)\\
=&\sum_{l=0}^{\lfloor m/2\rfloor}\frac{m!}{(2l)!(m-2l)!}\frac{\pi}{2^{2l-2m-1}}\frac{(2l)!}{(l!)^2}\int_0^\infty\frac{r^{4l+1}}{(1+r^2)^{2m}}\mathrm{d}r\\
=&\sum_{l=0}^{\lfloor m/2\rfloor}\frac{m!\pi}{(m-2l)!2^{2l-2m-1}(l!)^2}\int_0^\infty\frac{r^{4l+1}}{(1+r^2)^{2m}}\mathrm{d}r.
\end{aligned}
$$

Now make a change of variables of $\rho = r^2$ so that

$$
\begin{aligned}
\int_{-\infty}^\infty\int_{-\infty}^\infty u_1^m\mathrm{d}x\mathrm{d}t &= \sum_{l=0}^{\lfloor m/2\rfloor}\frac{m!\pi}{(m-2l)!2^{2l-2m-1}(l!)^2}\frac{1}{2}\int_0^\infty\frac{\rho^{2l}}{(1+\rho)^{2m}}\mathrm{d}\rho\\
&= \sum_{l=0}^{\lfloor m/2\rfloor}\frac{m!\pi}{(m-2l)!2^{2l-2m}(l!)^2}\frac{(2l)!(2m-2l-2)!}{(2m-1)!}\\
&= \frac{m!\pi}{(2m-1)!}\sum_{l=0}^{\lfloor m/2\rfloor}\frac{(2l)!(2m-2l-2)!}{2^{2l-2m}(l!)^2(m-2l)!},
\end{aligned}
$$

where it has been used that

$$
\int_0^\infty\frac{\rho^k}{(1+\rho)^{2m}}\mathrm{d}\rho = \frac{k!(2m-k-2)!}{(2m-1)!}. \tag{5.79}
$$

As such the following equality holds

$$\frac{1}{8\pi}\int_{-\infty}^{\infty}\int_{-\infty}^{\infty} u_1^m \mathrm{d}x\mathrm{d}t = \frac{m!}{(2m-1)!}\sum_{l=0}^{\lfloor m/2\rfloor}\frac{(2l)!(2m-2l-2)!}{2^{2l-2m+3}(l!)^2(m-2l)!}. \tag{5.80}$$

□

Consider now using (5.80) to verify Theorem 5.1 for $n = 1$. When $m = 2$, (5.80) gives

$$\begin{aligned}
\frac{1}{8\pi}\int_{-\infty}^{\infty}\int_{-\infty}^{\infty} u_1^2 \mathrm{d}x\mathrm{d}t &= \frac{1}{3}\sum_{l=0}^{1}\frac{(2l)!(2-2l)!}{2^{2l-1}(l!)^2(2-2l)!} && (5.81)\\
&= \frac{1}{3}\sum_{l=0}^{1}\frac{(2l)!2}{2^{2l}(l!)^2} && (5.82)\\
&= \frac{1}{3}(2+1) && (5.83)\\
&= 1, && (5.84)
\end{aligned}$$

as expected. When $m = 3$, (5.80) gives

$$\begin{aligned}
\frac{1}{8\pi}\int_{-\infty}^{\infty}\int_{-\infty}^{\infty} u_1^3 \mathrm{d}x\mathrm{d}t &= \frac{6}{5!}\sum_{l=0}^{\lfloor 3/2\rfloor}\frac{(2l)!(4-2l)!}{2^{2l-3}(l!)^2(3-2l)!} && (5.85)\\
&= \frac{1}{20}\sum_{l=0}^{1}\frac{(2l)!(4-2l)!}{2^{2l-3}(l!)^2(3-2l)!} && (5.86)\\
&= \frac{2^3}{20}\left(\frac{4!}{3!}+\frac{2!(2!)}{4}\right) && (5.87)\\
&= 2, && (5.88)
\end{aligned}$$

again, as expected from Theorem 5.1.

5.4 Discussion

It may be that there are similar results for higher powers of u, however this was not supported by any of the numerical work done by Ankiewicz[1]. The results that came from this were non-rational, however this could be down to numerical error given the complexity of the problem at this level. Given the nature of soliton equations and their inherent properties, it could be hypothesised that there is some similar equation and this is something that we would consider when furthering the research. Investigating this will require knowledge of further conservation laws if the same method was to be utilised.

Given Corollary 5.1 it may also be that there are similar equations relating to powers of v but this is not something that has been considered in this thesis.

Having such simple solutions for the integrals of u^2 and u^3 is logical with regard to the conservation laws being 0 as cancellation of more complex functions would be much less likely.

As mentioned in §5.2, it would be interesting to see what happens to the roots of v_2 and v_3 in terms of their rotation expressed as a function of α and β. From Figure 5.3 there seems to be some interesting behaviour discovered but there is certainly more that can be done with this. Firstly solving the rotation problem when one of the variables is 0 and then extending this to both α and β non-zero. Similarly it would be interesting to identify at what values of α and β there will always be one of the roots, not including any at the origin, which lie on an axis.

[1]Private communication, Oct 2016

Chapter 6

The KP-I Equation

The Kadomtsev-Petviashvili (KP) equation is a soliton equation but it can also be shown to have rogue waves solutions. These solutions are bounded for real x and t and form a hierarchy.

As previously, the chapter will begin with an introduction to the equation and some history and properties that it contains. There will also be a discussion of the bilinear form as this is the main equation that will be worked from.

Moving to the generating functions as defined by [1], both functions used in this paper; the summation generating function and the matrix generating function, will be detailed with the main work pertaining to the matrix function. The next few subsections contain work pertaining to the combinatorics of the matrix function regarding a number of different areas.

There follows a detailed explanation of the physical wave behaviour for the matrix function solutions. The analysis is separated between the cases when half the degree is even and when it is odd. The different matrix ranks are also considered separately. A number of solutions have been considered in order to give a good range of behaviours.

The limiting behaviour of KP solutions in the 1×1 matrix case are then

discovered and proven with heat maps as in Chapter 3.

The final two sections cover the relation between the Boussinesq and the KP-I equation and the parametrised KP-I equation whereby an infinite number of parameters are introduced. These are both only considered briefly prior to the conclusion.

6.1 Introduction

The KP equation is a $2+1$-dimensional equation as follows:

$$u_{tx} + 6u_x^2 + 6uu_{xx} + u_{xxxx} + 3\sigma^2 u_{yy} = 0, \tag{6.1}$$

where $\sigma^2 = \pm 1$. The KP-I equation which has rational solutions that have no singularities for real x, y and t is (6.1) with $\sigma^2 = -1$. KP-II is when $\sigma^2 = 1$ in (6.1), however the rational solutions found for this are singular.

6.1.1 Background

The equation (6.1) was found in 1970 by Boris Kadomtsev and Vladimir Petviashvili [40]. Originally this was to model ion-acoustic waves as an extension of the Korteweg-de Vries which includes transverse movement. The applications were extended to include water waves from the work of Ablowitz and Segur [4].

As with the other equations investigated, (6.1) is solvable by inverse scattering [2].

6.1.2 Invariants and Symmetries

Unlike in the previous two equations, now there are 3 variables to consider and as such the invariants and symmetries are slightly more complicated to check.

6.1.2.1 Invariants

Now the substitution for invariants becomes

$$u \to \alpha u^* + \beta, \quad x \to \gamma x^* + \delta, \quad t \to \xi t^* + \epsilon, \quad y \to \chi y^* + \omega. \tag{6.2}$$

Substitution of these into (6.1) results in

$$\tfrac{\alpha}{\gamma\xi} u^*_{x^*t^*} + 6\tfrac{\alpha^2}{\gamma^2}\{(u^*_{x^*})^2 + u^*_{x^*x^*}u^*\} + 6\tfrac{\alpha\beta}{\gamma^2} + \tfrac{\alpha}{\gamma^4} u^*_{x^*x^*x^*x^*} - 3\tfrac{\alpha}{\chi^2} = 0. \tag{6.3}$$

This equation can be multiplied by $\gamma\xi/\alpha$ since α is non-zero in order to keep required terms, leaving

$$u^*_{x^*t^*} + 6\tfrac{\alpha\xi}{\gamma}\{(u^*_{x^*})^2 + u^*_{x^*x^*}u^*\} + 6\tfrac{\xi\beta}{\gamma} + \tfrac{\xi}{\gamma^3} u^*_{x^*x^*x^*x^*} - 3\tfrac{\gamma\xi}{\chi^2} = 0. \tag{6.4}$$

In order for the equation to remain invariant under the transformation, the following must hold

$$\alpha\xi = \gamma, \quad \xi\beta = 0, \quad \xi = \gamma^3, \quad \gamma\xi = \chi^2. \tag{6.5}$$

This occurs when $\beta = 0, \xi = \gamma^3, \alpha = 1/\gamma^2$ and $\chi = \pm\gamma^2$.

The invariants of the KP-I equation in terms of the free variables γ, δ, ϵ and ω are thus

$$u \to \tfrac{1}{\gamma^2} u^*, \quad x \to \gamma x^* + \delta, \quad t \to \gamma^3 t^* + \epsilon, \quad y \to \pm\gamma^2 y^* + \omega. \tag{6.6}$$

These invariants show some relations between the scalings of x, y and t but once again there are no translations in the dependant variable u that can leave the equation invariant.

6.1.2.2 Symmetries

Given that the KP-I equation is a $2+1$-dimensional equation, there are 3 main symmetries.

1. The t-independent symmetries where the equation deforms to that of the Boussinesq equation with the time parameter being defined by y.

2. The y-independent symmetries where the equation is equivalent to the KdV equation subject to differentiation.

3. The x-independent symmetries where the equation is of lower order.

The solutions found in this thesis are still different from those that can be obtained from these symmetries.

6.2 Bilinear Form

Making the substitution $u = v_{xx}$ in (6.1) and integrate twice, setting any constant of integration to 0, retrieves the potential KP equation,

$$v_{xt} + 3v_{xx}^2 + v_{xxxx} + 3\sigma^2 v_{yy} = 0. \tag{6.7}$$

Letting $v = 2\ln(F)$ and $\sigma^2 = -1$ gives the bilinear form,

$$FF_{xt} - F_xF_t + FF_{xxxx} - 4F_xF_{xxx} + 3F_{xx}^2 - 3FF_{yy} + 3F_y^2 = 0. \tag{6.8}$$

In addition to the bilinear form (6.8), it is also possible to write the KP equation using Hirota's bilinear form as,

$$(D_xD_t + D_x^4 - 3D_y^2)F \cdot F = 0. \tag{6.9}$$

6.3 Generating Rational Solutions

Ablowitz et al detailed a generating function for rational solutions of KPI in [1]. The simplest solutions are constructed by first considering the equation,

$$p_n = (\partial_k^n \mathrm{e}^{\mathrm{i}\phi}|_{k=-\mathrm{i}})\mathrm{e}^{-\mathrm{i}\phi}, \tag{6.10}$$

where, in the paper, it is stated that $\phi = kx - k^2y + 4k^3t$. It is necessary to also make the invariant transformation $x \to -x$ and $t \to -t$ in p_n so that our polynomials generated with this are solutions of the bilinear form of KP. As such the following will be used, $\phi = -kx - k^2y - 4k^3t$. Polynomial solutions of the bilinear form are constructed as

$$F_n = \sum_{j=0}^{2n} \frac{1}{(2b)^j} \partial_x^j |p_n|^2 \tag{6.11}$$

and thus rational solutions of KP-I are simply twice the second logarithmic differential.

There have only been some similarities between the solutions created via (6.11) and equations (18a) to (18c) from [1]. Namely (18b) and F_2 are exactly the same and (18a) is equal to F_1 after the linear transformation $x \to x + \frac{1}{2}$. It also transpires that equation (18c) as stated in the paper is not a solution of the bilinear form.

In order to simplify the problem, the paper discusses using moving frame coordinates. It is stated that the co-ordinates that are used are $x = x' + (a^2 + b^2)t$ and $y = y' + 12at$ where a and b are from $k = a - ib$. The transformation that seems to have been used, elicited by the behaviour of the graphs, is $x = x' + 12(a^2 + b^2)t$ and $y = y' + 12at$, this is also referred to in [61].

Work presented in Pelinovsky's papers [52] and [53] details a method for generating rational solutions via a Wronskian whose elements are solutions to the KP

Lax pair, up to scaling. These rational solutions are for KP-II however and they result in singularities so cannot be used to model rogue waves.

Using a transformation of $u \to -\frac{1}{3}, t \to \mathrm{i}\sqrt{3}x, y = 3t$ and $x = \mathrm{i}\sqrt{3}x$ in (6.1) one can retrieve (3.1). This shows that solutions of the Boussinesq equation exist, subject to some transformation, as solutions to KP-I. The converse is not true as one can move from a 2-dimensional equation up to a 3-dimensional equation but moving in the opposite direction would lose some solutions. With this information, techniques used to describe rational solutions of KP-I could be employed to find rational solutions of the Boussinesq equation.

6.3.1 Matrix Formulation

In [1], a matrix generating function was described that broadens the solution set to include a variety of functions of the same degree. The leading order behaviour of these polynomials is identical for the same degree but lower order coefficients change. Once more the form of ϕ must be altered from the paper to make the polynomials solutions of the KP bilinear form.

Taking

$$\phi(k) = -kx - k^2y - 4k^3t, \tag{6.12}$$

and

$$\psi_j = \partial_k^{m_j} \mathrm{e}^{\mathrm{i}\phi(k)}|_{k=-\mathrm{i}}, \tag{6.13}$$

then we can construct a square matrix M which has entries,

$$M_{l,j} = \int_{-\infty}^{x} \psi_l \overline{\psi_j} \mathrm{d}x'. \tag{6.14}$$

These functions have been slightly altered form [1] since $\Phi_j(k)$ has been taken to be 0 for simplicity, it will be reintroduced in §6.8. The polynomial solutions to

the bilinear form in terms of the variables m_j for $j \in [1, .., N]$ are

$$F_{[m_1,\ldots,m_N]} = -2|\mathbf{M}|\mathrm{e}^{2(-\mathrm{i}\phi(-\mathrm{i})+\mathrm{i}\phi(\mathrm{i}))}, \tag{6.15}$$

where N is the rank of the matrix $\mathbf{M}$.

Note that m_j must be used rather than j to retrieve all the solutions in the hierarchy, for instance in the 2×2 case if just j was used instead of m_j then one can get a polynomial of degree 4 with 1 and 2 as the two values but this restricts from retrieving the degree 6 polynomial by using $m_1 = 1$ and $m_2 = 3$. It is also not possible to have fractional values of m_j since it relates to the number of differentials taken and thus must be an integer to produce reasonable, bounded solutions. In order to have the matrix M formed of linearly independent rows, it is required that $m_j \neq m_l$ unless $j = l$. Were the flexibility to have $m_j \neq j$ not allowed then the solution set would be drastically reduced.

When $m_1 = 1$ in the 1×1 case, this retrieves the first solution in the hierarchy, $m_1 = 2$ the second and so on.

The leading order of the polynomial in the $N \times N$ case, which is the same for x, y and t is defined as,

$$\left(\sum_{i=1}^{N} 2m_i\right) - N(N-1). \tag{6.16}$$

Due to this structure and the fact that $m_i \neq m_j$ unless $i = j$ then if the rank of the matrix is N, it is possible to calculate polynomials of degree greater than,

$$\frac{(N-1)(N+2)}{2}. \tag{6.17}$$

It should be noted for each matrix size, the polynomials change even if they share a degree. The leading order behaviour is the same but anything of a lower degree has different coefficients.

The notation for the following chapter will be $u_{[m_1,m_2,\ldots,m_N]}$, where the number of m_N's will pertain to the rank of the matrix that is being used and the degree of the polynomial $F_{[m_1,m_2,\ldots,m_N]}$ used can be calculated from (6.16).

6.3.1.1 Simplification of the Matrix Formulation in the 1×1 Case

Some interesting simplifications of the matrix method occur when only considering the 1×1 case. In this there is

$$\psi_1(m_1) = \left(\frac{\partial}{\partial k} + \mathrm{i}\frac{\partial}{\partial k}\phi(k)\right)^{m_1} \exp(4t + \mathrm{i}y - x)\bigg|_{k=-\mathrm{i}}, \tag{6.18}$$

$$\overline{\psi_1(m_1)} = \left(\frac{\partial}{\partial k} - \mathrm{i}\frac{\partial}{\partial k}\phi(k)\right)^{m_1} \exp(4t - \mathrm{i}y - x)\bigg|_{k=\mathrm{i}}. \tag{6.19}$$

As such, this can be factorised as

$$M_{1,1} = \mathrm{e}^{8t}\int_{-\infty}^{x} \left(\frac{\partial}{\partial k} + \mathrm{i}\frac{\partial}{\partial k}\phi(k)\right)^{m_1} \mathrm{e}^{-x'}\bigg|_{k=-\mathrm{i}} \left(\frac{\partial}{\partial k} - \mathrm{i}\frac{\partial}{\partial k}\phi(k)\right)^{m_1} \mathrm{e}^{-x'}\bigg|_{k=\mathrm{i}} \mathrm{d}x', \tag{6.20}$$

where now the power of some operator is considered. The operator acts on the function e^{-x} in each case of (6.20). It is worth noting that any derivative of $\phi(k)$ of order 4 or higher will be 0.

6.3.1.2 Combinatorics of the Method

If we consider $(\partial_k^m \mathrm{e}^{f(k)})\mathrm{e}^{-f(k)}$, for $f(k)$ a polynomial in k, then the pattern of the results are highly structured. Indeed the first 5 iterations are shown below.

$$F_1, \tag{6.21a}$$

$$F_1^2 + F_2, \tag{6.21b}$$

$$F_1^3 + 3F_1F_2 + F_3, \tag{6.21c}$$

$$F_1^4 + 6F_1^2F_2 + 4F_1F_3 + 3F_2^2 + F_4, \tag{6.21d}$$

$$F_1^5 + 10F_1^3F_2 + 10F_1^2F_3 + 15F_1F_2^2 + 5F_1F_4 + 10F_2F_3 + F_5, \tag{6.21e}$$

where F_n denotes the n'th derivative of $f(k)$. These are complete Bell polynomials. The coefficients are all multinomial coefficients relating to the degree of differentiation and sometimes divided by some specific factor. For example when $m = 3$ we can write this as

$$\frac{1}{3!}\binom{3}{1,1,1}F_1 + \binom{3}{1,2}F_1F_2 + \binom{3}{3}F_3. \tag{6.22}$$

It is necessary to introduce $\frac{1}{3!}$ to the coefficient of F_1 since in the multinomial expression there are 3 repetitions of 1 which introduces 3! repeated terms and only unique terms are wanted.

If there was a way to express these as sums or products then there is hope for a mathematical proof as to why the patterns are the way they are.

It is possible to use the Faá di Bruno formula to express $\partial_k^m \mathrm{e}^{f(k)}$, for $f(k)$ a polynomial in k.

Theorem 6.1 (Faá di Bruno)**.** *[39] If g and f are functions with a sufficient number of derivatives, then*

$$\frac{\mathrm{d}^m}{\mathrm{d}t^m}g(f(t)) = \sum \frac{m!}{b_1!b_2!\cdots b_m!}g^{(k)}(f(t))\left(\frac{f'(t)}{1!}\right)^{b_1}\left(\frac{f''(t)}{2!}\right)^{b_2}\cdots\left(\frac{f^{(m)}(t)}{m!}\right)^{b_m}, \tag{6.23}$$

where the sum is over all different solutions in non-negative integers $b_1, \cdots, b_m$ of $b_1 + 2b_2 + \cdots + mb_m = m$, and $k := b_1 + \cdots + b_m$.

This in itself is not the easiest formula to work with when we are dealing with m as an unknown value. However there is an equivalent formula in determinant

form,

$$\frac{\mathrm{d}^m}{\mathrm{d}t^m}g(f(t)) = \begin{vmatrix} \binom{m-1}{0}f'g & \binom{m-1}{1}f''g & \binom{m-1}{2}f'''g & \dots & \binom{m-1}{m-2}f^{(m-1)}g & \binom{m-1}{m-1}f^{(m)}g \\ -1 & \binom{m-2}{0}f'g & \binom{m-2}{1}f''g & \dots & \binom{m-2}{m-3}f^{(m-2)}g & \binom{m-2}{m-2}f^{(m-1)}g \\ 0 & -1 & \binom{m-3}{0}f'g & \dots & \binom{m-3}{m-4}f^{(m-3)}g & \binom{m-3}{m-3}f^{(m-2)}g \\ \vdots & \vdots & \vdots & & \vdots & \vdots \\ 0 & 0 & 0 & \dots & \binom{1}{0}f'g & \binom{1}{1}f''g \\ 0 & 0 & 0 & \dots & -1 & \binom{0}{0}f'g \end{vmatrix}, \tag{6.24}$$

where powers of g after the determinant has been taken, should be considered as $g^{(k)}(f(t))$. Ordinarily this is quite an important factor, however, because in our case we are only using the exponential function as our function g, and the function appears at least once in every column, we can extract the function from the matrix and substitute it back in later. In essence, we use the fact that any derivative of the exponential function is just the function itself to remove the necessity to distinguish g from $g^{(2)}$. The following definitions and corollaries will be useful to explore the problem in this form.

Definition 6.1 (Upper Hessenberg Matrix)**.** *An Upper Hessenberg matrix is an upper triangular square matrix with an additional diagonal so that it appears as,*

$$\begin{bmatrix} a_{1,1} & a_{1,2} & \dots & a_{1,n-1} & a_{1,n} \\ a_{2,1} & a_{2,2} & \dots & a_{2,n-1} & a_{2,n} \\ 0 & a_{3,2} & \dots & a_{3,n-1} & a_{3,n} \\ \vdots & \ddots & \ddots & \vdots & \vdots \\ 0 & \dots & 0 & a_{n,n-1} & a_{n,n} \end{bmatrix}. \tag{6.25}$$

The matrix $\mathbf{M}$ is an upper Hessenberg matrix where the entries are defined as given in (6.14). There has been work conducted that expresses the determinant of an upper Hessenberg matrix as a recursive formula. One such formulation given in [17], taking A_n as the upper Hessenberg matrix, $\det(A_0) = 1$ and $\det(A_1) = a_{1,1}$, is

$$\det(A_n) = a_{n,n} \cdot \det(A_{n-1}) + \sum_{r=1}^{n-1} \left((-1)^{n-r} a_{n,r} \prod_{j=r}^{n-1} a_{j,j+1} \cdot \det(A_{r-1}) \right). \quad (6.26)$$

In our case, g is the exponential and f is the function ϕ from (6.12). Thus the matrix that will be used is,

$$\frac{\partial^m}{\partial k^m} \exp(\mathrm{i}\phi(k)) = \begin{vmatrix} \phi' & \binom{m-1}{1}\phi'' & \binom{m-1}{2}\phi''' & \dots & \binom{m-1}{m-2}\phi^{(m-1)} & \phi^{(m)} \\ -1 & \phi' & \binom{m-2}{1}\phi'' & \dots & \binom{m-2}{m-3}\phi^{(m-2)} & \phi^{(m-1)} \\ 0 & -1 & \phi' & \dots & \binom{m-3}{m-4}\phi^{(m-3)} & \phi^{(m-2)} \\ \vdots & \vdots & \vdots & & \vdots & \vdots \\ 0 & 0 & 0 & \dots & \phi' & \phi'' \\ 0 & 0 & 0 & \dots & -1 & \phi' \end{vmatrix} \mathrm{i}^m \exp(\mathrm{i}\phi). \quad (6.27)$$

There is not a trivial simplification of this matrix as the coefficients reduce to multinomial coefficients, even with the specific construction of -1 on the sub-diagonal and the exponential being taken out as a factor. Using the recursive formula (6.26) it may be possible to evaluate what the matrix is really doing. This will give the entries of ψ_i and then this needs to be used in $\mathbf{M}$ to find the true workings behind the generating function.

6.3.1.3 Number of m_i Variations by Matrix Rank

Clearly in the 1×1 case there is only 1 option per degree of polynomial for m_1. In the 2×2 case there are more options. We know that we are considering even power polynomials of degree 4 and up from (6.17). Let the degree of the polynomial be d, where $d = 2z_2$ and $z_2 \in \mathbb{Z} \setminus \{0, 1\}$. Then the number of combinations of $\{m_1, m_2\}$ is

$$\begin{cases} \dfrac{z_2}{2} & \text{for } z_2 \text{ even,} \\ \dfrac{z_2 - 1}{2} & \text{else.} \end{cases} \tag{6.28}$$

In the 3×3 case we are considering even power polynomials of degree 6 and up. Now let the degree d be $d = 2z_3$ and $z_3 \in \mathbb{Z} \setminus \{0, 1, 2\}$. Then the number of combinations of $\{m_1, m_2, m_3\}$ is

z_3	no. combinations	$m_1 + m_2 + m_3$
3	1	6
4	1	7
5	2	8
6	3	9
7	4	10
8	5	11
9	7	12
10	8	13
11	10	14
12	12	15
13	14	16
14	16	17
15	19	18
16	21	19

Consider a triangular lattice of size $z_3 + 4$. Bearing in mind that we require

that $m_i \in \mathbb{Z} \setminus \{0\}$, removing the perimeter which will always have at least one value of $m_i = 0$ and the lines of symmetry which will have some $m_i = m_j$ for $i \neq j$, the number of points left are the number of combinations of m_1, m_2 and m_3 including permutations. We remove all bar one segment from the diagram and the number of points is the number of combinations not including permutations. This is illustrated in Figure 6.1.

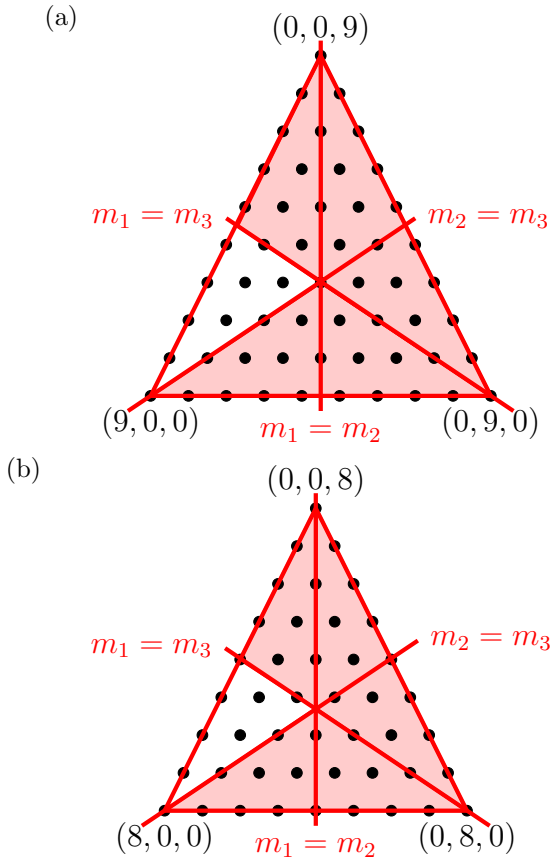

Figure 6.1: Lattice representation of the combinations of m_1, m_2 and m_3.

If $m_1 + m_2 + m_3$ is divisible by 3 then the intersection of the three lines of symmetry is a solution or node that is excluded. Since $m_1 + m_2 + m_3 = z_3 + 3$, the number of perimeter nodes that are removed is

$$3(z_3 + 3). \tag{6.29}$$

The number of nodes removed from each line of symmetry, not including the end points is

$$\begin{cases} \dfrac{z_3+1}{2} & \text{for } z_3 \text{ odd,} \\ \dfrac{z_3}{2}+1 & \text{else.} \end{cases} \tag{6.30}$$

There are always 3 lines of symmetry but if z_3 is divisible by 3 then the central intersection is triple counted. If z_3 is divisible by 2 then 3 points are double counted from the symmetry lines and the perimeter.

So the number of points to remove are

$$\left\{ \begin{array}{ll} 3(z_3+3)+3\dfrac{z_3+1}{2} & \text{for } z_3 \in [1]_6 \cup [5]_6, \\ 3(z_3+3)+3\dfrac{z_3+1}{2}-2 & \text{for } z_3 \in [3]_6, \\ 3(z_3+3)+3\left(\dfrac{z_3}{2}+1\right) & \text{for } z_3 \in [2]_6 \cup [4]_6, \\ 3(z_3+3)+3\left(\dfrac{z_3}{2}+1\right)-2 & \text{for } z_3 \in [0]_6. \end{array} \right\}, \tag{6.31}$$

where $[\mathbf{n}]_k$ represents $\mathbf{n}$ modulo k.

Given that the total number of points in a triangle for a given value of z_3 is

$$\sum_{i=1}^{z_3+1} i = \frac{(z_3+1)(z_3+2)}{2}, \tag{6.32}$$

then once permutations have been excluded the number of combinations of

$\{m_1, m_2, m_3\}$ is

$$\begin{cases} \frac{1}{12}(z_3^2 - 6z_3 - 19) & \text{for } z_3 \in [1]_6 \cup [5]_6, \\ \frac{1}{12}(z_3^2 - 6z_3 - 15) & \text{for } z_3 \in [3]_6, \\ \frac{1}{12}(z_3^2 - 6z_3 - 22) & \text{for } z_3 \in [2]_6 \cup [4]_6, \\ \frac{1}{12}(z_3^2 - 6z_3 - 18) & \text{for } z_3 \in [0]_6. \end{cases} \tag{6.33}$$

These methods have worked fine for small N, however, extending this to even the 4×4 case is problematic. As such there will be an alteration of the method and partitions of an integer shall be considered.

For the $N \times N$ case we are looking for a counting of partitions of $z_N + \frac{N(N-1)}{2}$ with distinct parts. The partitions need to be unordered, distinct and with a fixed number of parts. Consider the expression,

$$P(Z,k) = \partial_x^Z \left(x^k \prod_{i=1}^{k} \frac{1}{1-x^i} \right) \Bigg|_{x=0}, \tag{6.34}$$

which gives the number of partitions of an integer Z into k parts [20, p.374]. The differentiation and substitution merely extracts the coefficient of x^Z from the original polynomial. Comparing this equation with the 4×4 case with distinct parts and of length k, we conjecture that the equation for the partitions of an integer Z into k distinct parts is,

$$Q(Z,k) = \partial_x^Z \left(x^{2k+\binom{k}{2}} \prod_{i=1}^{k} \frac{1}{1-x^i} \right) \Bigg|_{x=0}. \tag{6.35}$$

Therefore in the $N \times N$ matrix case the number of combinations of m_i is,

$$Q\left(z_N + \frac{N(N-1)}{2}, k\right) = \partial_x^{z_N + \frac{N(N-1)}{2}} \left(x^{2k+\binom{k}{2}} \prod_{i=1}^{k} \frac{1}{1-x^i} \right) \Bigg|_{x=0}, \tag{6.36}$$

with z_N still being half the degree of the polynomial we are calculating. Using this method, solutions can be retrieved for $N = 1, 2$ and 3 as well.

This can also be related to Young diagrams.

6.4 Wave Behaviour

In order to classify the different groups of waves, and given that the solutions created by (6.11) are invariant under permutations of m_i, we will always consider $m_i < m_{i+k}$ where $k > 0$.

6.4.1 Fix $m_1 = 1$ in the 2×2 Case

It was interesting to investigate whether increasing m_2 may increase or decrease the height of the waves. This would need to be separated in order to compare even and odd wave cases but is most likely solved by considering an average of the wave height. Firstly we fix $m_1 = 1$ and vary m_2. Another issue however is that we have to consider positive time for the even m_2 case and negative time for the odd m_2 case due to where the waves lie and accurate calculations. With the data gained from considering $F_{[1,2]}$ against $F_{[1,4]}$ we would hypothesise that increasing the value of m_2 very slightly decreases the average height if we consider the waves at the same time. Again this needs to be extended to higher order functions to see if this still holds or if it is an isolated incident. If we consider the odd values of m_2 then it seems that increasing m_2 leads to an increase in the main maximum wave height. However we are considering negative time for these therefore it could

still tie in that in the positive time case the wave will in fact increase in height as it seemed to do for the even m_2 case.

6.4.1.1 Even m_2

When looking at the pattern of the waves for even m_2 at negative time, see Figure 6.2, it firstly appears that the waves travel on a fixed line in X but further inspection reveals that they are moving incrementally so there is not a fixed X for the maximums. The pattern is such that there are two waves moving in the $-X$ region towards $Y = 0$ and all remaining waves (if there are more) travel along $Y = 0$. In terms of these waves moving on $Y = 0$, the wave farthest back on $-X$ is the largest with the waves decreasing in height until you reach the one at the largest value of $+X$. The smaller waves split into two and the larger waves merge together and become wider. The two waves that were always travelling along some line in the $-X$ region merge together and the other waves form an arc around them.

Additionally, increasing the value of m_2 makes the pair of waves move closer together sooner and shifts the line in X that they travel on so that it is nearer to 0. It also appears that it increases the height of the waves.

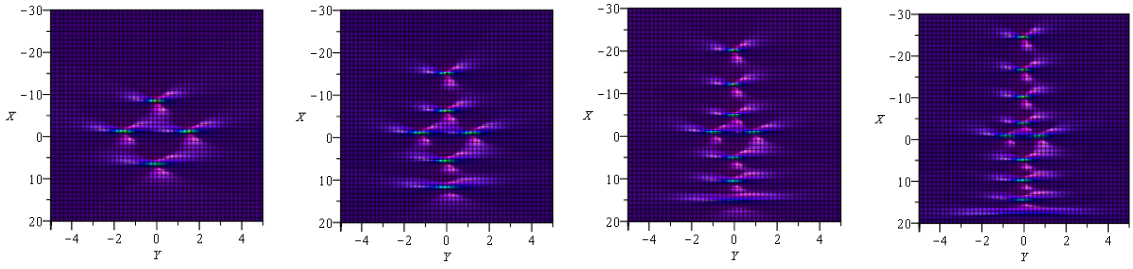

Figure 6.2: $u_{[1,m_2]}$ for $m_2 \in \{4, 6, 8, 10\}$ at $t = -1$.

As we move to positive time it again looks like the waves move away on fixed lines in X but again this is not quite the case. With the behaviour occurring around $t = 0$, we now have one central wave and an arc of waves around this

which can be seen in Figure 6.3, so we are dealing with far fewer waves than originally. The original number of waves is retrieved in positive time though as the tallest two waves stay combined as do the perpendicular waves and the remaining waves split into two in the $u_{[1,8]}$ case. This formation can be seen in Figure 6.4.

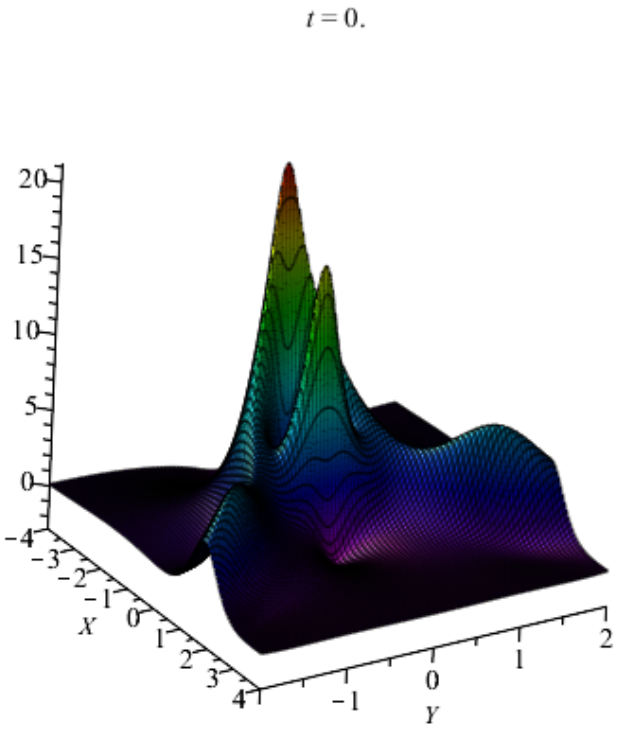

Figure 6.3: 3D graph of $u_{[1,5]}$ at $t = 0$

Starting from the maximum that resides at the highest value of positive X, the waves gradually split into two until the only waves left are those that sit on negative X.

6.4.1.2 Odd m_2

When we consider odd m_2 then the central structure changes as we have an additional wave. We have what looks like an isosceles triangle around the origin whose apex lies towards positive X. Nevertheless, for different values of t the

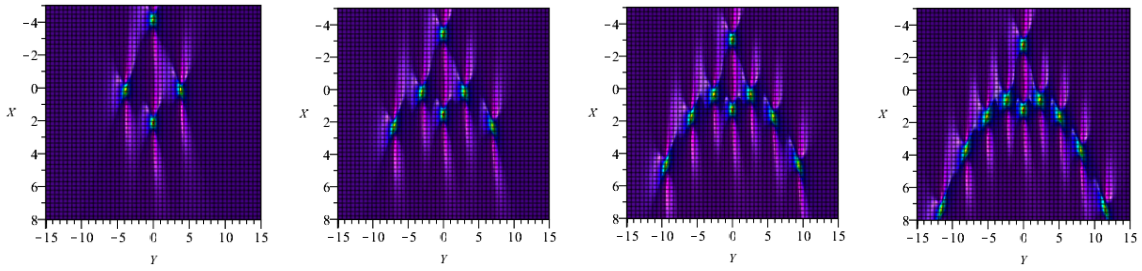

Figure 6.4: $u_{[1,m_2]}$ for $m_2 \in \{4, 6, 8, 10\}$ at $t = 1$.

scaling between the lengths of the sides do change. If we ignore this central structure then for negative time we still have the largest waves at the most negative X, decreasing in height until you reach the final wave in the positive X region as with the even m_2 case. However, considering the central 3 waves, these follow the opposite pattern with the largest wave being the apex in the positive X region and the shorter waves being the two that sit in the negative X region. The paired waves are the same height throughout this process. As time progresses from negative to positive the waves on positive X increase in height as those on negative X decrease.

Moving back to negative time, there are a pair of waves that move both closer together and towards the origin in negative X. Increasing the value of m_2 also moves the waves closer to the origin sooner, but the difference is not as pronounced as that which was observed when m_2 is even. It seems that the waves decrease in height as m_2 is increased as well, however, this may be related to things happening sooner, like there is some sort of a time shift, since the waves alter in height as time passes.

In terms of merging and separating behaviour, the triangle that occurs near $t = 0$ starts in positive X and gains the maximums until it has them all.

Figure 6.5 shows the behaviour around $t = 1$ where the central triangle can be clearly seen in each function and Figure 6.6 shows the behaviour at $t = -1$.

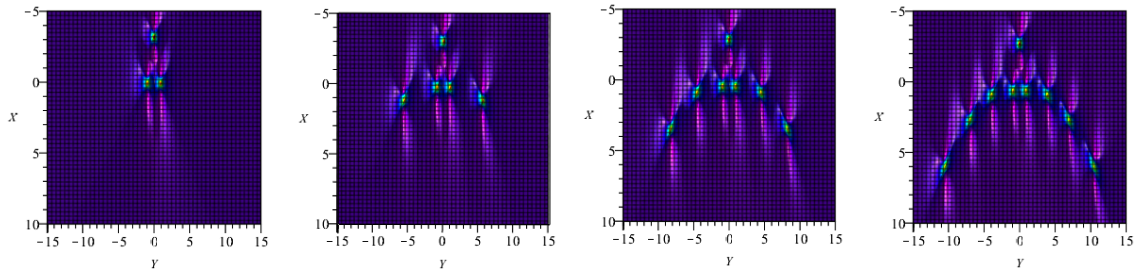

Figure 6.5: $u_{[1,m_2]}$ for $m_2 \in \{3,5,7,9\}$ at $t = 1$.

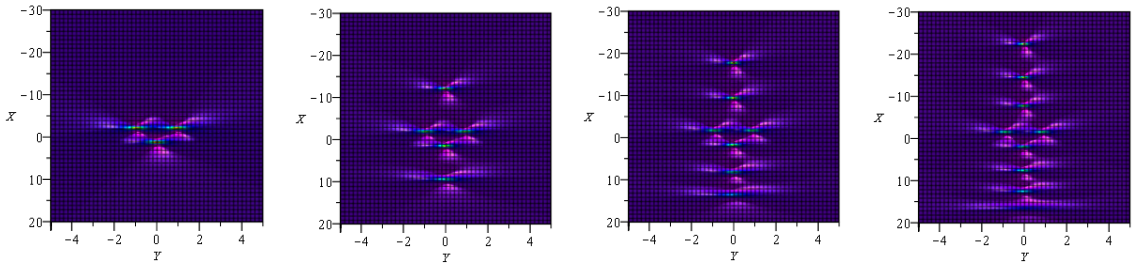

Figure 6.6: $u_{[1,m_2]}$ for $m_2 \in \{3,5,7,9\}$ at $t = -1$.

6.4.2 Fix m_2 as Even in the 2×2 Case

It seems that the value of m_1 in the 2×2 case determines the number of 'pairs' of waves that sit off $Y = 0$ for negative time. For positive time the behaviour is more complex so we shall examine this in the subsections below.

6.4.2.1 Even m_1

Considering $m_2 = 8$ and negative time, see Figure 6.7, the sequence of waves from negative X to positive for $u_{[2,8]}$ is $[1,1,2,1,2,1,1]$. For $u_{[4,8]}$ the sequence is $[1,2,2,1,2,2,1]$ and for $u_{[6,8]}$ it is $[2,2,2,1,2,2,2]$. So for even m_1 it seems that the central wave is 1 and there are m_1 number of paired waves that emanate out from the central wave and as soon as the value of m_1 has been reached they revert to singular waves until the total number of peaks for that solution are reached.

The sequence could be written as

$$[\overbrace{1,..,1}^{m_2/2-1},\overbrace{2,..,2}^{m_1/4},1,\overbrace{2,..,2}^{m_1/4},\overbrace{1,..,1}^{m_2/2-1}]. \tag{6.37}$$

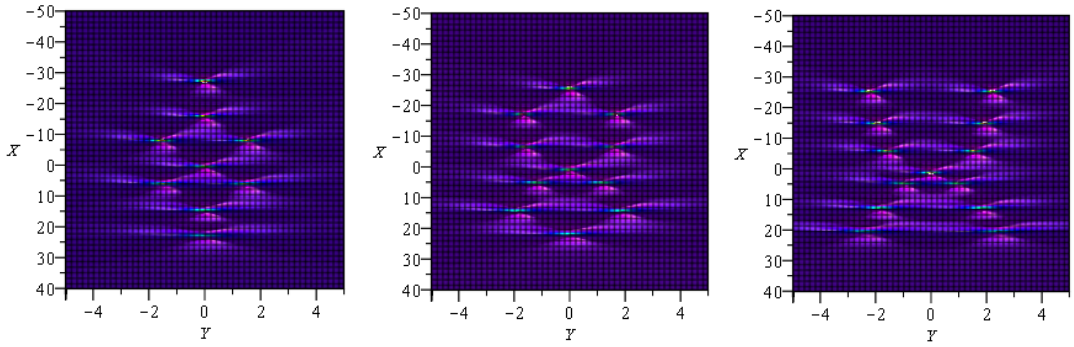

Figure 6.7: $u_{[m_1,8]}$ for $m_1 \in \{2,4,6\}$ at $t=-2$.

We explore what happens at $m_2 = 12$ to ascertain if this is the correct pattern, see Figure 6.8. For $u_{[2,12]}$ the sequence at $t=-2$ is $[1,1,1,1,2,1,2,1,1,1,1]$ and for $u_{[4,12]}$ the sequence at $t=-2$ is $[1,1,2,1,2,1,2,2,1,1,1]$. It seems that this latest function does not follow the pattern. Of course, as the functions near $t=0$ the placement of some of the waves seems to change so it could be that by increasing the modulus of t it may be possible to find a pattern before any alterations occur. Upon further inspection though, this doesn't seem to have changed the sequences already discovered.

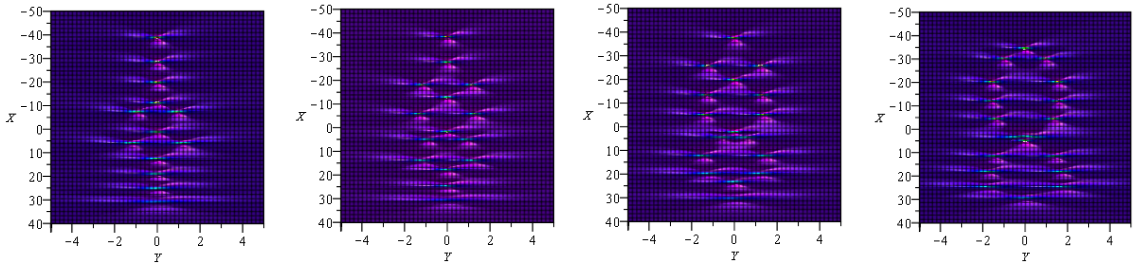

Figure 6.8: $u_{[m_1,12]}$ for $m_1 \in \{2,4,6,8\}$ at $t=-2$.

A more complex pattern may be occurring though for which more data is required. As such we consider $u_{[6,12]}$ which has the sequence $[1,2,1,2,2,1,2,2,2,1,1]$. For $u_{[8,12]}$ the sequence is $[1,2,2,2,2,1,2,2,2,2,1]$ (as expected by (6.37)).

If we consider that base behaviour as a line of waves on $Y=0$, then for m_2 even, the value of m_1 pertains to the number of paired waves that sit off this line.

Considering positive time, unlike as will be seen in the odd m_1 case, we now have an additional wave (since the combination of m_1 and m_2 gives us an odd number of waves) at the origin. If we were to exclude this wave then the behaviour exhibited in the even m_1 case is the same as that in the odd m_1 case with a duplicate of waves peeling off the original arc for each increase in m_1 by 2.

The structure of the waves at $t = 1$ for m_1 odd is shown in Figure 6.9. Figure 6.10 more explicitly shows how increasing the value of m_1 adds waves into the formation by the addition of red lines to show any altered structure from the previous function in the sequence.

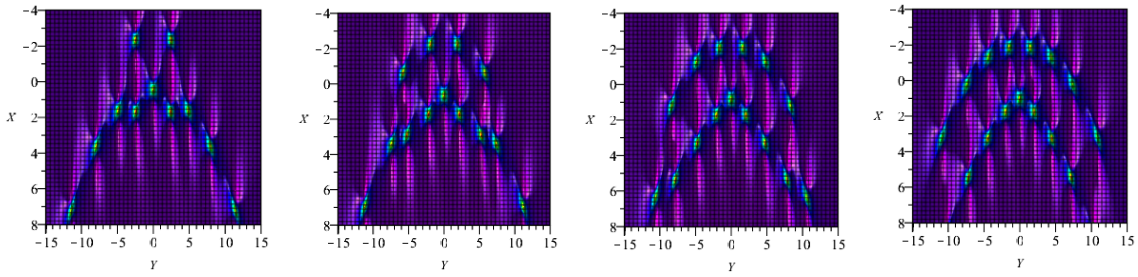

Figure 6.9: $u_{[m_1,10]}$ for $m_1 \in \{2, 4, 6, 8\}$ at $t = 1$.

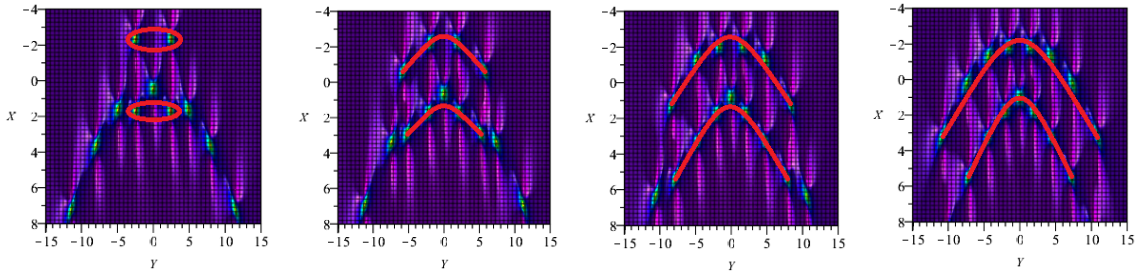

Figure 6.10: $u_{[m_1,10]}$ for $m_1 \in \{2, 4, 6, 8\}$ at $t = 1$ with the pattern identified.

6.4.2.2 Odd m_1

The pairs of waves are not as regimented for negative time as may be expected from this kind of solution. Given the previous behaviour, it would be natural to expect the paired waves to group together looking at large negative time, i.e to all be the ones nearest the origin or to be at either end of the X-axis. It seems

that instead, in the $u_{[3,8]}$ case, there is one duo of waves, followed by a singular wave, followed by two paired waves and finally another single wave; a sequence of $[1,2,1,2,2,1,1]$. Looking on to $u_{[5,8]}$ though and the sequence is $[2,1,2,2,2,2,1]$, and then at $u_{[7,8]}$ all the waves are in pairs, see Figure 6.11.

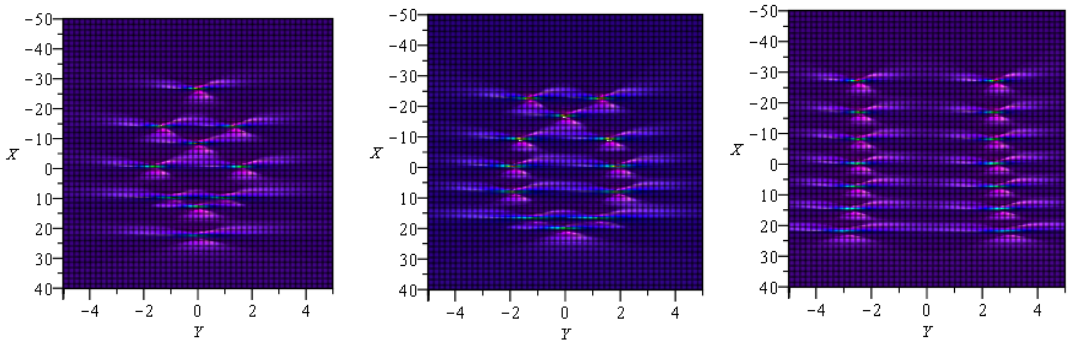

Figure 6.11: $u_{[m_1,8]}$ for $m_1 \in \{3,5,7\}$ at $t=-2$.

If we consider $m_2 = 12$ instead then we have more waves to investigate. For $u_{[3,12]}$, from negative X to positive and for negative time, see Figure 6.12, we have 3 singular waves, a double wave, a single wave, a double wave, a single wave, a double wave and 3 single waves. So let us think of this as the following sequence $[1,1,1,2,1,2,1,2,1,1,1]$. If we move up to $u_{[5,12]}$ then the sequence becomes $[1,1,2,2,1,2,2,1,2,1,1]$, so it seems that there are always the same number of singular waves at the beginning and the end of the sequence. For $u_{[7,12]}$ the sequence is $[1,2,2,1,2,2,2,2,1,2,1]$ and $u_{[9,12]}$ $[2,2,1,2,2,2,2,2,2,1,2]$.

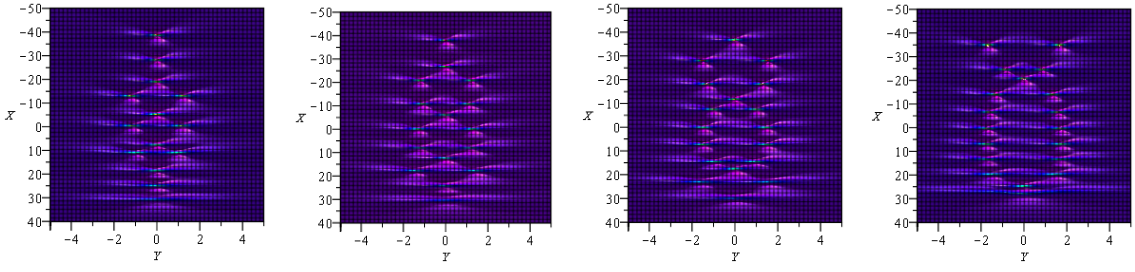

Figure 6.12: $u_{[m_1,12]}$ for $m_1 \in \{3,5,7,9\}$ at $t=-2$.

When the value of m_1 is only 1 less than the value of m_2, then all the waves will be paired up. This can be verified by substituting $m_2 = m_1 + 1$ into (6.16)

and halving the result to find that the number of waves will be twice the value of m_1 and thus the number of paired waves at its maximum must be the value of m_1.

The behaviour for positive time is very different from that for negative time. When $m_1 = 1$ then there are two waves that differ in behaviour from the others and sit on $Y = 0$. The rest of the waves sit in a single arc which intersects the chord between these two points. When m_1 is only 1 less than m_2 then there are two distinct arcs with the waves moving out on almost fixed lines in X. If we consider $m_2 = 8$ then as we move from $u_{[1,8]}$ through m_1 odd to $u_{[7,8]}$ then at each step another 2 waves peel off the first arc and head into the negative X area. It also deforms the original arc though so it is no longer a smooth arc but could be considered an arc in the neighbourhood of that from $u_{[1,8]}$. This can be seen in Figure 6.13 with the patterns identified in Figure 6.14

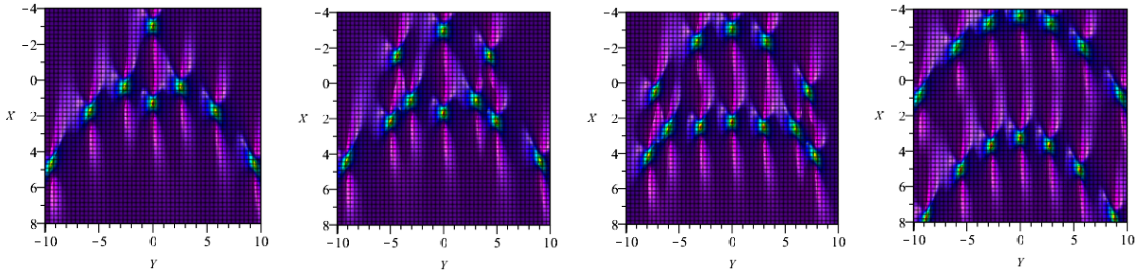

Figure 6.13: $u_{[m_1,8]}$ for $m_1 \in \{1, 3, 5, 7\}$ at $t = 1$.

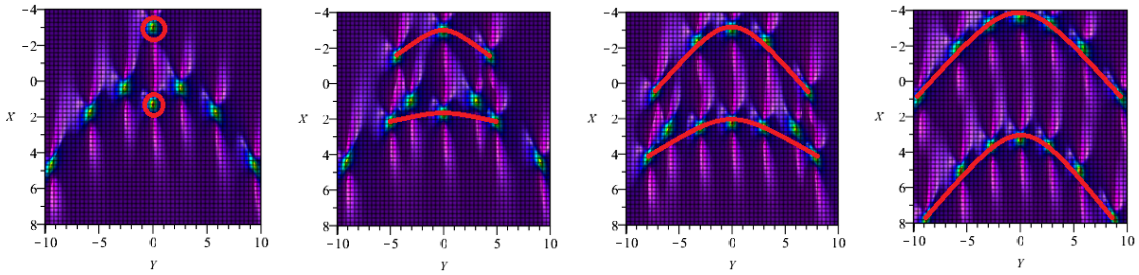

Figure 6.14: $u_{[m_1,8]}$ for $m_1 \in \{1, 3, 5, 7\}$ at $t = 1$ with the pattern identified.

As before, if we increase m_2 to 12 we can assess whether this pattern is maintained. This does occur for $m_2 = 12$ as well but the deformation of the original

arc is far more pronounced and may contain a pattern of its own. It seems that perhaps for each level of m_2 that we go up another two waves are also peeled onto the singular wave in positive X and this arc is flatter.

6.4.3 Fix $m_1 = 1$ and $m_2 = 2$ in the 3×3 Case

Starting with the simplest criteria in the 3×3 case and gradually increase m_3. Even and odd m_3 will be dealt with separately in order to ascertain whether there is a distinct difference between the two cases. Positive time seems to have more obvious patterns to examine so this will be considered for this section.

The waves in the 3×3 case are shifted from their relevant locations in the 2×2 case. That is, the range of X is much larger than it was previously and the graphs need to be adjusted accordingly. The arcs are still present as before however and much of the movement seems similar.

6.4.3.1 Odd m_3

The beginning position, i.e when $m_3 = 3$ is a trio of waves in an arc around the origin orientated like x^2. For each increment in m_3 another duo of waves appears on the $Y = 0$ for negative time. The arc of waves also move closer to $X = 0$. It seems that the apex of the curve comes closer to $X = 0$ but does not seem to pass this and move into positive X. This can be seen in Figure 6.15.

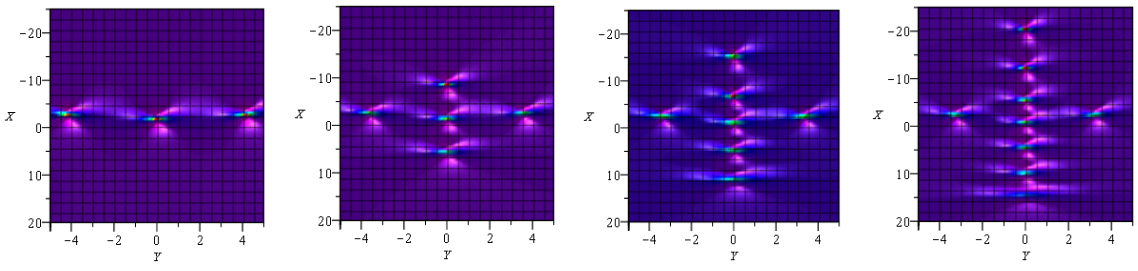

Figure 6.15: $u_{[1,2,m_3]}$ for $m_3 \in \{3, 5, 7, 9\}$ at $t = -1$.

If instead positive time is considered then the behaviour is as shown in Figure

6.16. That is, a trio of waves are now on a line seemingly $Y = 0$ and for each increment in m_3 a duo of waves appears on an arc around the central original wave.

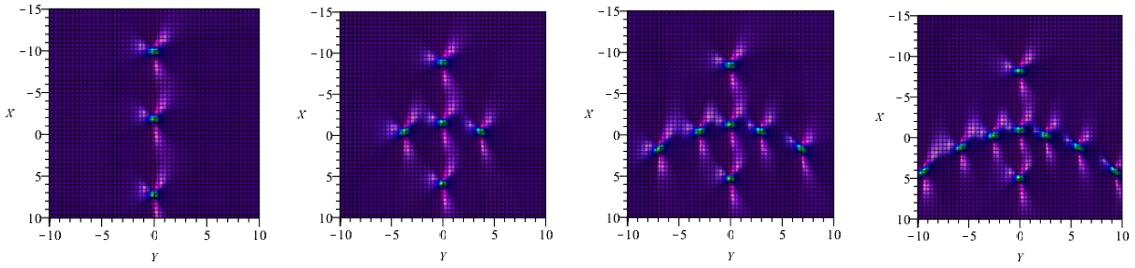

Figure 6.16: $u_{[1,2,m_3]}$ for $m_3 \in \{3, 5, 7, 9\}$ at $t = 1$.

6.4.3.2 Even m_3

For even m_3, as we increase its value then an additional 2 waves are added to the arc from the base case when $m_3 = 4$. As mentioned in the previous section, the behaviour seems very similar to that of the 2×2 case excepting that now there are waves at greater values of X for the same value of time. This is shown in Figure 6.17.

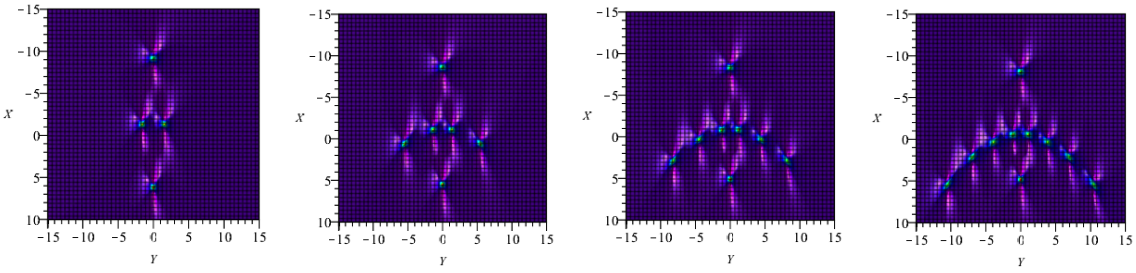

Figure 6.17: $u_{[1,2,m_3]}$ for $m_3 \in \{4, 6, 8, 10\}$ at $t = 1$.

6.4.4 Fix $m_1 = 1$ and $m_2 = 3$ in the 3×3 Case

It is advisable to explore what happens when m_1 and m_2 are both odd instead of just look at one odd and one even. As such the first two variables are fixed as

odd but as low as possible and m_3 is varied in both even and odd cases. Now only the positive time is considered.

6.4.4.1 Even m_3

When m_3 is even there are an odd number of waves. The behaviour noted is that with each increment in m_3 the two waves that reside next to each other in the negative X area of the graph seem to come closer to together. While this happens, they also move nearer to the origin as their partners in the positive X area do so as well. Additional waves at each stage are added to the "arc" but its apex is distorted by the 4 waves aforementioned and thus does not form a clean parabola. These graphs are given in Figure 6.18.

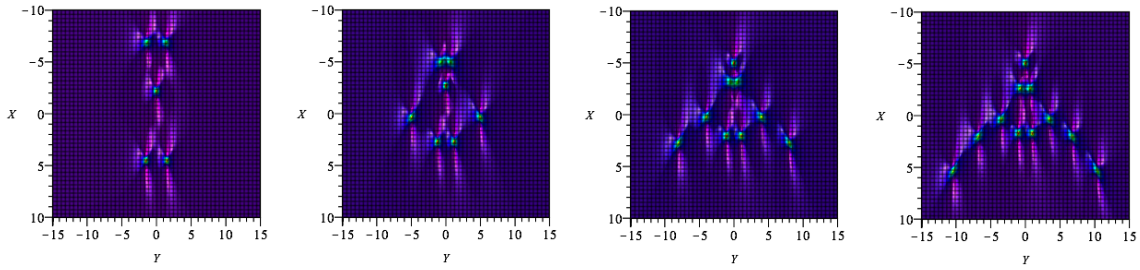

Figure 6.18: $u_{[1,3,m_3]}$ for $m_3 \in \{4, 6, 8, 10\}$ at $t = 1$.

6.4.4.2 Odd m_3

When m_3 is odd there is a very structured formation that is mentioned further in §6.4.7.6. This central formation does not seem to change but the increasing of m_3 only serves to add waves onto the parabola that would intersect the triangle formation between the second and third row. This behaviour is seen in Figure 6.19.

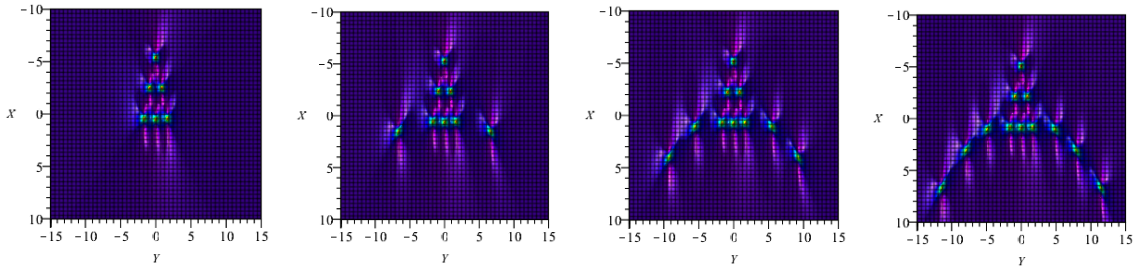

Figure 6.19: $u_{[1,3,m_3]}$ for $m_3 \in \{5, 7, 9, 11\}$ at $t = 1$.

6.4.5 Fix $m_1 = 2$ and $m_2 = 3$ in the 3×3 Case

In order to establish that $m_1 = 1$ does not restrict the wave behaviour too much, now select $m_1 = 2$ and $m_2 = 3$ and vary m_3 once more. This also ensure that for m_3 even then the case relates to when the sum of m_i is odd and for m_3 odd the converse is true. This is expected to be very similar to the behaviour shown in §6.4.4 however the will be an additional wave now. Positive time is considered for behaviour, as such all graphs displayed are at $t = 1$.

6.4.5.1 Even m_3

As always, the increasing of m_3 adds waves onto the parabola of waves. Unlike in the case explained in §6.4.4.2, now the parabola intersects the center of the original formation, but this original formation is a rectangle. Increasing m_3 causes this rectangle to shrink and the central 2 waves from the $m_3 = 4$ case come closer to the origin. The graphs are shown in Figure 6.20.

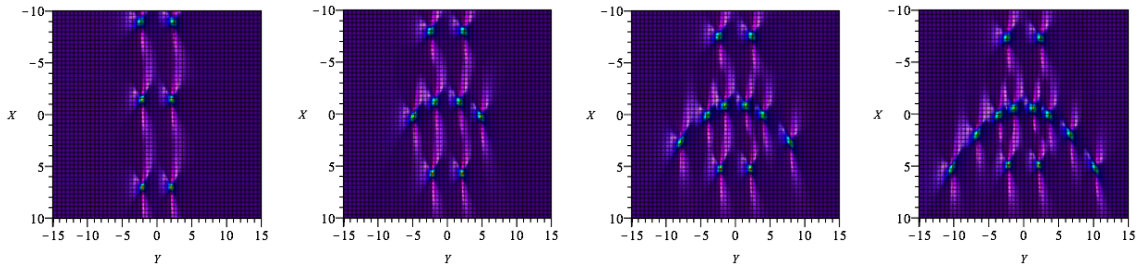

Figure 6.20: $u_{[2,3,m_3]}$ for $m_3 \in \{4, 6, 8, 10\}$ at $t = 1$.

6.4.5.2 Odd m_3

When m_3 is odd the original rectangular structure now has a central wave that distorts the rectangle somewhat so that its width in the centre is not the same as that at the edges. If this central wave was to be ignored then the behaviour is very close to that observed in §6.4.5.1, and this central wave merely moves incrementally from its original position to form a convex shape at the top of the parabola. The graphs are shown in Figure 6.21.

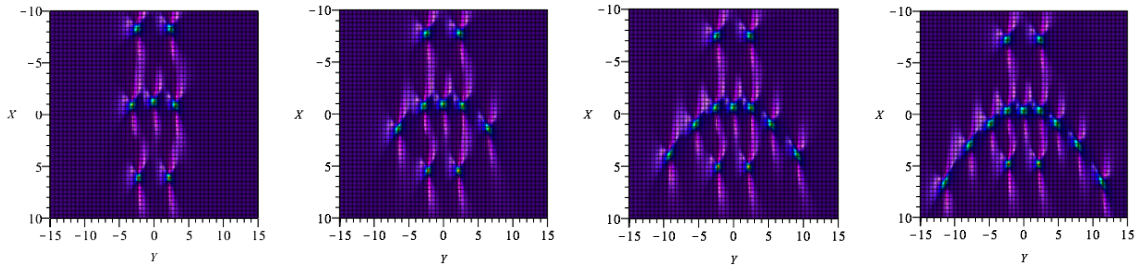

Figure 6.21: $u_{[2,3,m_3]}$ for $m_3 \in \{5, 7, 9, 11\}$ at $t = 1$.

6.4.6 Fix $m_1 = 2$ and $m_2 = 4$ in the 3×3 Case

Given the justification of including §6.4.5, this section will be concerned with the cases where if m_3 is even then all the m_i's are even and if m_3 is odd then the sum of the m_i is odd. This is the final section in which the behaviour is detailed and this is only completed for positive time $t = 1$. A good deal of information has been found already but it can be extended to both higher rank matrices, larger values of time and the exploration of negative time to name but a few.

6.4.6.1 Even m_3

With the number of waves that are now included, along with the difference between all the m_i's, the patterns become much more complex. The central structure has now become a triangle in negative X formed of 3 waves and with its

apex pointing towards the origin, coupled with another triangle-like object formed of 4 points with the same orientation of the apex. Additionally, at $m_3 = 6$ there are two waves which create a cross with the negative X triangle and it is these waves that are the initial parabola waves. As the value of m_3 is increased, the structure shrinks and at each point 2 waves are added to the parabola. This seems to be a new form of structure that derivations of are not clear from the previous cases. The graphs are shown in Figure 6.22.

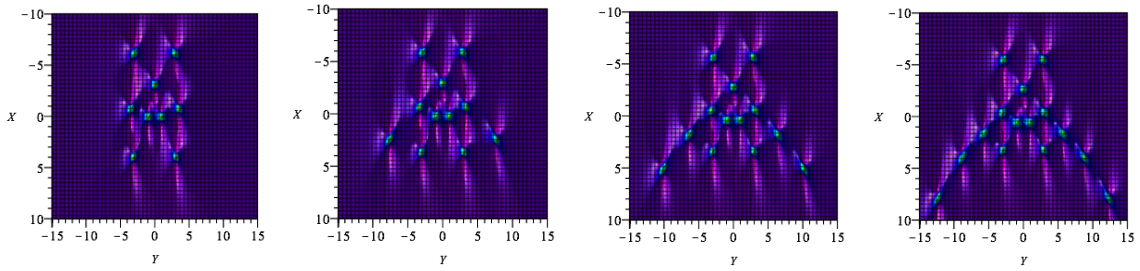

Figure 6.22: $u_{[2,4,m_3]}$ for $m_3 \in \{6, 8, 10, 12\}$ at $t = 1$.

6.4.6.2 Odd m_3

In some respects, the behaviour when m_3 is odd seems clearer than that when m_3 is even. The structure is a bowed rectangle and with increasing m_3 the curve in the shortest edges becomes more pronounced until it resembles a sharply pointed bowing. The parabola intersects with the central 2 waves and waves are added in increasing distance from the previous parabolic waves. The graphs are shown in Figure 6.23.

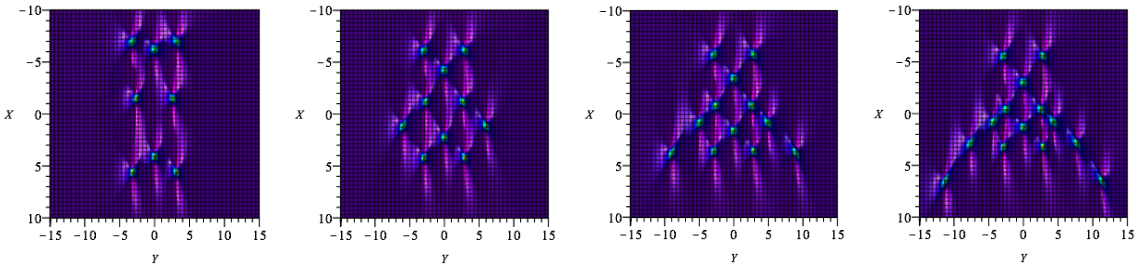

Figure 6.23: $u_{[2,4,m_3]}$ for $m_3 \in \{5, 7, 9, 11\}$ at $t = 1$.

6.4.7 Interesting Cases

During the investigation there were certain functions of m_i that gave repeated patterns. Some of those found are considered below. These were observed for both positive and negative values of t so in each case it will be specified at what value the behaviour was observed.

6.4.7.1 Fix $m_i = i$

In some respects it is easier to think of the 1×1 case as a special case. If then we increase the matrix rank, the behaviour mirrors that of the 1×1 case but with additional waves. For example, with $u_{[1,2,3]}$, this is the same as $u_{[1]}$ but with two additional waves. However they are all oriented on $Y = 0$ as can be seen in first image of Figure 6.16. Also the behaviour of the waves is exactly that of letting $t \to -t$ in this special case.

6.4.7.2 Fix $m_2 = m_1 + 2$

It seems that when $m_2 = m_1 + 2$ the pattern mimics the union of some positive and negative quadratic function, much like $y = x^2 \cup -x^2$. This behaviour has been checked for all values of m_2 up to 12 again and much like when $m_2 = m_1 + 4$, as will be seen later, the oval in the negative X area has a greater area than that in the positive X area. This behaviour was observed for negative time, see Figure 6.24.

6.4.7.3 Fix $m_2 = m_1 + 3$

For $m_1 + m_2 \leq 9$ then the pattern is just a circle or oval, that is for $m_1 = 1, 2$ or 3, where at each increase of the values, additional waves appear. Once values above this threshold are used then there are an additional two peaks who sit above the oval in the $-X$ region up to and including $m_1 + m_2 = 19$. Therefore there

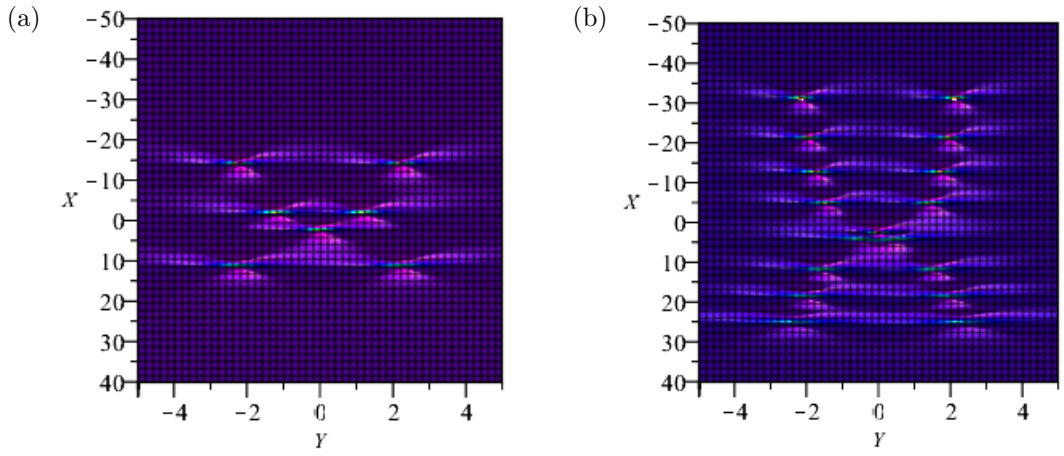

Figure 6.24: $u_{[3,5]}$ and $u_{[8,10]}$ respectively at $t = -2$.

are 5 different combinations of (m_1, m_2) as $(4, 7), (5, 8), (6, 9), (7, 10)$ and $(8, 11)$ that only have 2 additional waves sitting above the oval. Obviously as the value of m_1, and thus m_2, is increased, the oval gains additional waves. Considering the case $u_{[9,12]}$ though, there are now 4 peaks that form a quadratic pattern above the oval. This could be extended to establish when the 4 peaks adjusts to be 6 peaks and if there is some integer pattern that can be used to predict when behaviours change. These behaviours are shown in Figure 6.25.

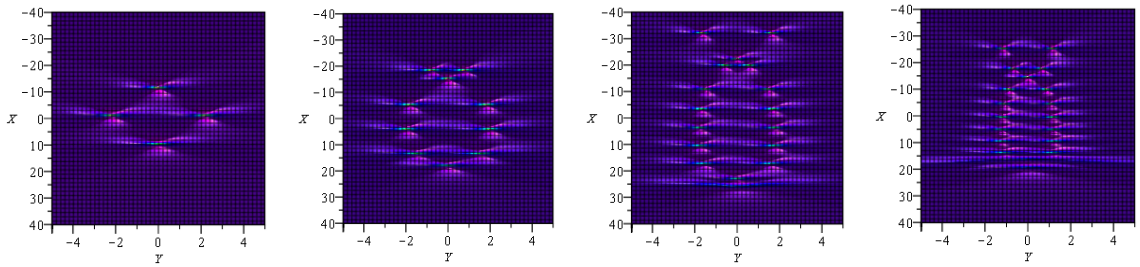

Figure 6.25: $u_{[1,4]}, u_{[4,7]}, u_{[8,11]}$ and $u_{[9,12]}$ at $t = -2$.

6.4.7.4 Fix $m_2 = m_1 + 4$

Another point to note is that for $u_{[8,12]}$ and $u_{[4,8]}$ the pattern of the waves mirrors a figure of 8. Perhaps when $m_2 = m_1 + 4$ this pattern is always retrieved. This has been checked for all values of m_2 up to $m_2 = 12$. The figure of eight

formation is visible in all cases for negative time with the circle located in negative X space being slightly larger than that in positive X space, see Figure 6.26. When m_2 is odd, and therefore m_1 is odd as well, there are an additional two waves in the negative X circle than the positive X and when m_1 and m_2 are even there is an equal number in each.

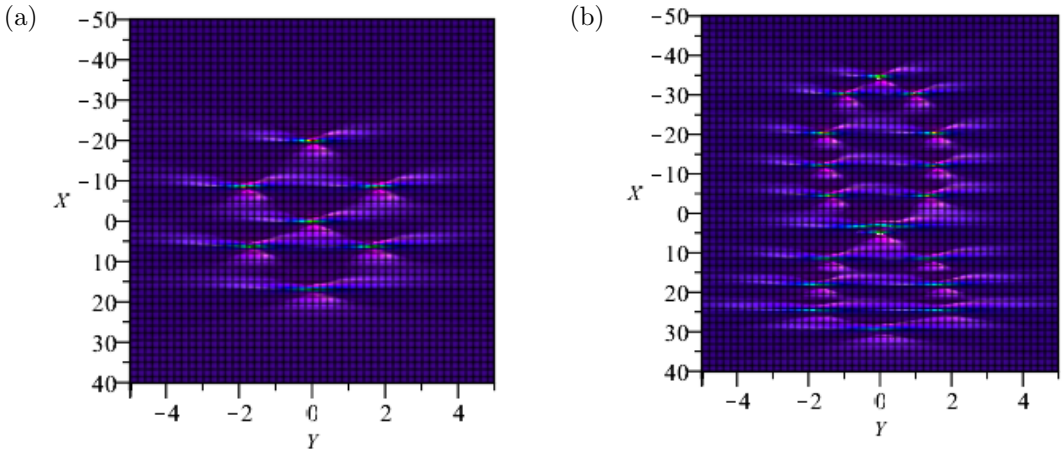

Figure 6.26: $u_{[2,6]}$ and $u_{[8,12]}$ respectively at $t = -2$.

6.4.7.5 $u_{[1,2]}$ and $u_{[1,4]}$

At first it seemed changing from $u_{[1,2]}$ to $u_{[1,4]}$ was a time shift. This was observed in the graphs as shown in Figure 6.27. In order to explore analytically, the coordinates of the maximums were found at a fixed value of Y. Selecting $Y = -2.5$, the maximums appear at $(X, t) = (-1.49, -1.06)$ to 2d.p. If $u_{[1,4]}$ is then considered at the point $(X, Y) = (-1.49, -2.5)$ to 2d.p. It transpired that there was no point in time where the maximum occupied this space. As such, despite seeming evidence of a timeshift this is not true analytically.

It is worth noting that even though the patterns are similar (if not exact), the peaks appear to be higher in the $u_{[1,4]}$ case. This is probably due to the fact that the time is nearing 0 and the waves rise near here.

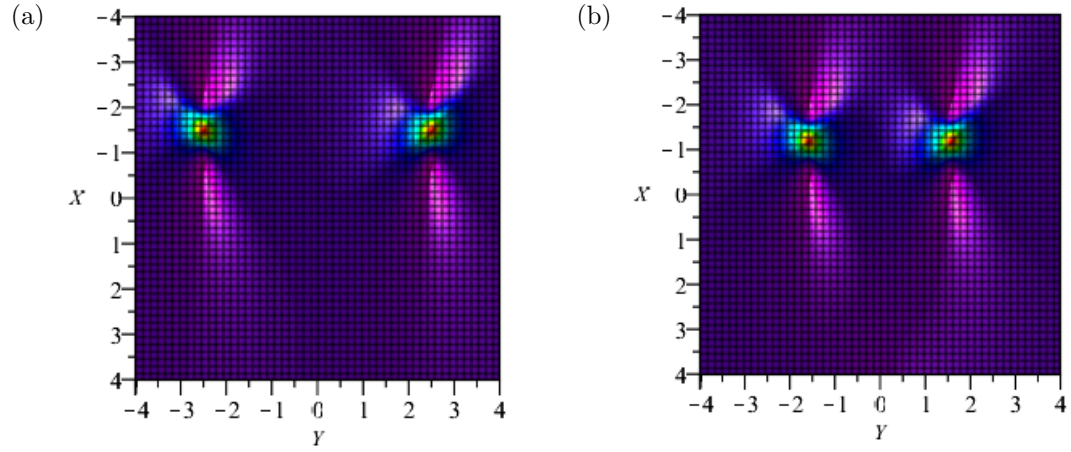

Figure 6.27: 3D graphs of $u_{[1,2]}$ and $u_{[1,4]}$ at $t = -1.062$ to 3d.p

6.4.7.6 Triangular Structure for Odd m_i at Positive Time

Consider situations when all m_i are odd, the pattern of the waves is mirrored even as the matrix rank is increased. From Figure 6.5 it is possible to see that the central structure remains a triangle with base 2 and from Figure 6.19 the same formation is seen but now the triangle has base 3. One can go further and look at higher ranked matrices as in Figure 6.28.

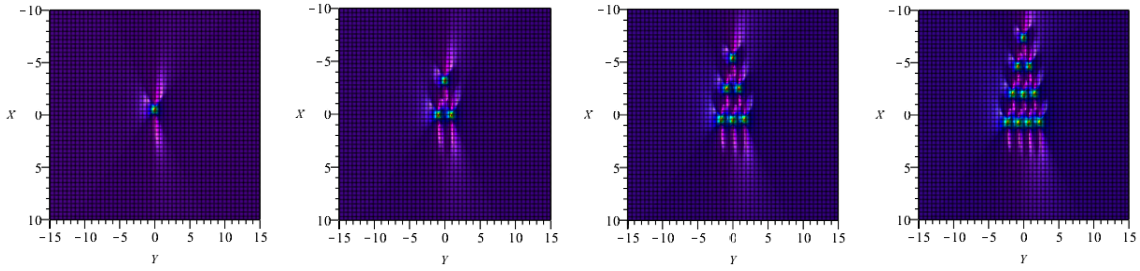

Figure 6.28: 3D graphs of $u_{[1]}$, $u_{[1,3]}$, $u_{[1,3,5]}$ and $u_{[1,3,5,7]}$ at $t = 1$

Conjecture 6.1. *If the value of* $m_1 = 1$ *and* $|m_{i+1} - m_i| = 2$ *then at positive time all waves will be structured in a triangle. The base of the triangle is formed of the same number of waves as the rank of the matrix and each row above this is* 1 *less than the row before until you reach the apex which resides in negative* X*.*

It is worth noting that despite the graphs making it look like the base of the triangles may all sit on the same line in X, this is not the case analytically.

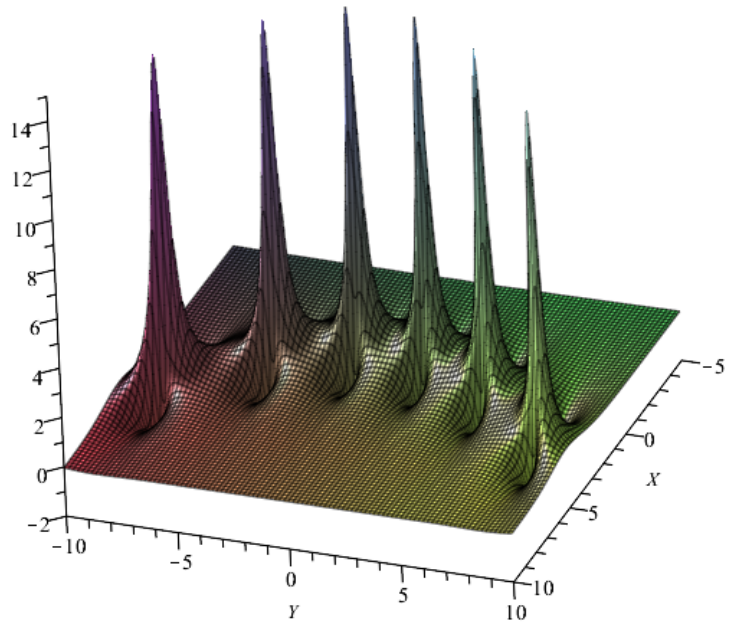

Figure 6.29: 3D graph of $u_{[6]}$ at $t = 1$

6.5 Behaviour for Fixed Matrix Rank

It has been mentioned that using the matrix formulation described in §6.3.1 can retrieve more than one polynomial of the same degree dependant on the rank of the matrix used. The fact that the lower order term coefficients change alters the formation of the waves, particularly around the origin. Where in the 1×1 case the waves would approach each other along $Y = 0$ and then travel off at right angles along a given line in X as time moved from negative, through $t = 0$ to positive time, for a different matrix rank the waves on $Y = 0$ stay on that line but the other waves move triangularly towards the origin. The waves then emanate out in a circular way for increasing positive time.

As such the rank of the matrix will impact the wave behaviour so there is enough of a change in the lower order coefficients that this behaviour is visible in the graphs. Such an impact can be seen in Figure 6.30 where there are still only 4 waves in each graph but the formations are very different dependant on matrix

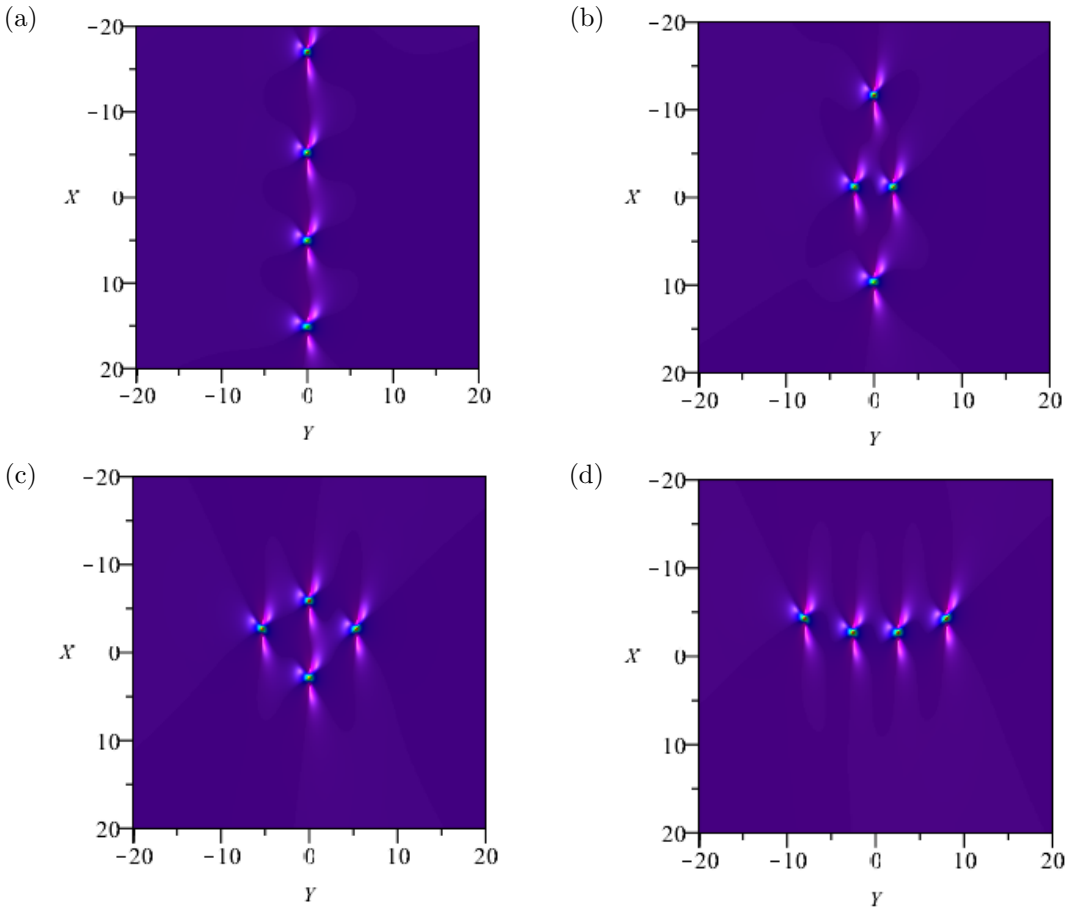

Figure 6.30: $u_{[4]}, u[1,4], u[1,2,4]$ and $u_{[1,2,3,4]}$ at $t = 1$ viewed from above.

rank.

6.5.1 The Effect of m_i on the Wave Formation

When working in the 1×1 case the value of m_1 merely determines the number of peaks for the function. When considering the formation, for negative time the waves move towards the origin along $Y = 0$ and then, after a transition in formation, fan out in along given lines in X but in a parabolic structure with relation to each other. This behaviour was detailed in Figure 6.29.

The more intriguing behaviour can be seen when we increase the rank of the matrix. Moving only up to the 2×2 case we now have m_1 and m_2 as variables.

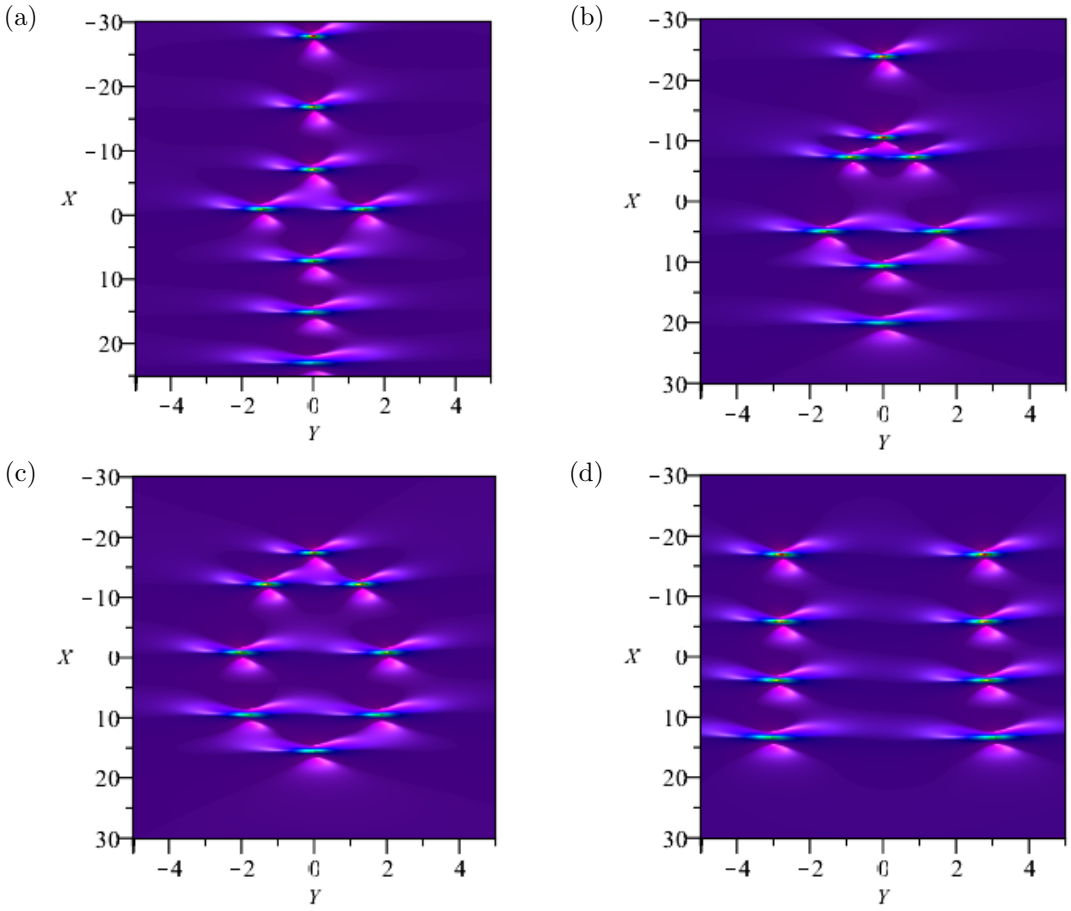

Figure 6.31: $u_{[1,8]}, u_{[2,7]}, u_{[3,6]}$ and $u_{[4,5]}$ at $t = -2$ viewed from above.

If we consider $u_{[1,8]}$, see Figure 6.31, then we have two waves that break for-

mation of the other waves. For negative t, instead of moving with the other waves along $Y = 0$, two waves are perpendicular to the others and move along $X = -1$. For positive t these travel along $Y = 0$ while the other waves fan out in a parabolic pattern and travel along designated lines in X.

However, if we consider $u_{[2,7]}$ the same behaviour is not seen. Now, the waves that are pulled off the $Y = 0$ for negative time do not move together towards that line but instead move towards the origin with the other waves. For positive time they do not seem to stay on a given line in X either but travel linearly away from the origin in another way. Moving on to $u_{[3,6]}$ though, and once more there are a pair of waves that for positive time move away from the origin on $Y = 0$. This can be seen in Figure 6.32.

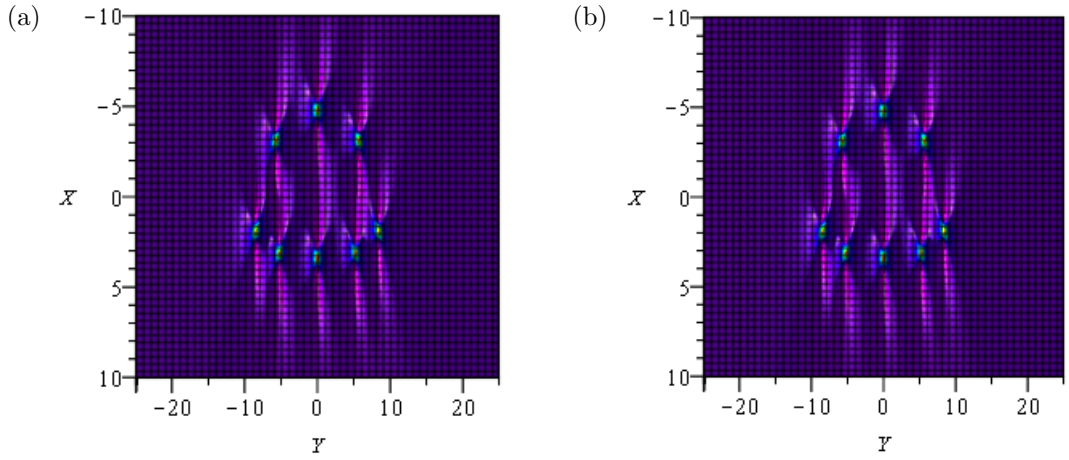

Figure 6.32: $u_{[2,7]}$ and $u_{[3,6]}$ for $t = 2$.

In the 2×2 case, if $m_1 = 1$ then you always have a line of waves for negative t with two waves (the central ones) sat off that line and perpendicular. If $m_1 + m_2$ is even then these two waves move towards the origin, if it is odd then they move towards each other to form on the same line. For positive t there is always a downward facing arc whose center is around the origin (if not exactly at the origin). If $m_1 + m_2$ is even then there is a singular wave off this arc on negative X, and if it's odd then there are a pair of waves who sit on $Y = 0$, one at positive

X and one at negative. This could also just be because the nature of $m_1 + m_2$ dictates the number of waves.

6.5.2 Effect of Increasing the Rank of the Matrix on the Solutions Behaviour

Consider an odd number of waves with m_i even (using u_9 here). It seems that for the 1×1 case all the waves behave in the same way. In the 2×2 case for positive t there are two arcs of waves and for negative t there are m_1 number of pairs of waves that sit slightly off the $Y = 0$ line but come towards the origin. In the 3×3 case consider $(m_1, m_2, m_3) = (2, 4, 6)$ and now there are 2 pairs of waves off the $Y = 0$ line, a pair who stay on the $Y = 0$ line and a trio of waves that arc along it, the central one being on the $Y = 0$ line. All waves move towards the origin - then there is a triangle whose base sits near the $X = 0$ line which has two lines of waves on the outer.

In the 5×5 case with $(m_1, m_2, m_3, m_4, m_5) = (1, 2, 3, 4, 5)$ and this reverses the time behaviour; the arc happens at negative t and the waves all form on a line for positive t with u_5.

6.6 Limit of the Wave Heights

Since establishing the behaviour of the maximums requires them to reside on some singular line in the (X, Y) plane for simplicity, in this section only the 1 matrix case has been considered and within that only certain wave heights have been proven. The waves that move in a parabolic way are harder to determine and this is still an open problem. Only low values of n in u_n have been considered but this method should work for specific waves at higher values of n though the location of the wave maximums will most likely reside on different values of Y or

X.

Considering the 1×1 case, as this is the easiest to investigate given where the maximums lie, an interesting situation occurs as $t \to \pm\infty$ for the maxima of these functions. The behaviour of the peaks is different for positive and negative t yet they both seem to tend to a limit. In Figure 6.33 we can see the graphs of $u_{[2]}$ and $u_{[3]}$ plotted for various values of t. For t positive the peaks always occur along a given value of X, similarly for negative t they occur at $Y = 0$. When working with $u_{[3]}$ there is a slight split as two of the waves repel away along $X = \frac{5}{6}$ while the third peak remains stationary at $Y = 0$. Not all of the maximums are considered since some of them do not lie on a fixed line throughout time and the function of such waves movements was could not to be found.

It can also be seen that with positive t the two peaks both increase to attain a value, whereas when t is negative at least two of the peaks travel in opposing directions; one decreasing and one increasing, until they reach what appears to be the same limit.

Once again, the images in Figure 6.34 have been created in Maple whereby there is no heat map coded into the programme already. These graphs have been created using a 3D plot and altering the colouring of the graph as can be found in Appendix E.5.

In Figure 6.34, the maximums of $u_{[2]}$ and $u_{[3]}$ have been plotted against t. We have taken cuts of the graphs for specific values of X and Y at which it is known that the maximums remain on as given above. There are always a pair of maximums that have parabolic development with respect to t except in the case of $u_{[1]}$ which has a stationary maximum at $X = Y = 0$. The factor of these parabolas differs and not all are centred around 0 even though it may look that way from the graphs. For positive t the parabolas are always symmetric around the $Y = 0$ but for negative t they are symmetric around $X = -\frac{1}{2}$ and $X = -\frac{2}{3}$

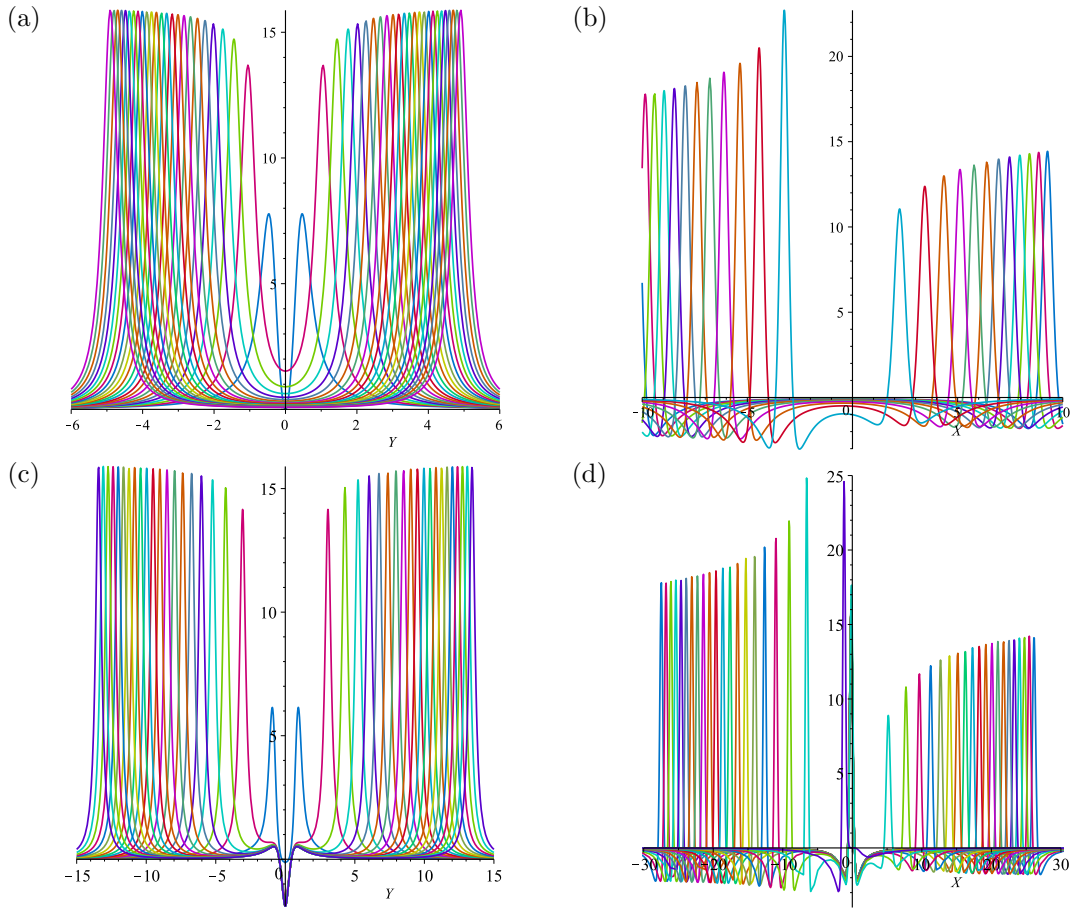

Figure 6.33: Time evolution plots of the maximums of u_2 for positive time at $X = 0$ (6.33(a)) and negative time (6.33(b)) at $Y = 0$. Likewise for u_3 taken at $X = \frac{5}{6}$ for positive time and $Y = 0$ for negative time.

for $u_{[2]}$ and $u_{[3]}$ respectively. This behaviour has been referred to in [61] but this paper was found subsequent to the research.

For $u_{[3]}$ there is also a third maximum that develops linearly in X and remains stationary on $Y = 0$. This linear wave does not bisect the parabolic wave in $u_{[3]}$ but intersects the X axis at a different point which will be shown below.

The graphs used in this section have been produced in Maple via the code provided in Appendix E.5. They can sometimes look rather simple given that the coding had to be manually adapted in order to produce a heat graph as shown.

Lemma 6.1. *The limit of the height maxima or maximums of* $u_{[m_1]}$ *tend to* 16 *as* $t \to \pm\infty$.

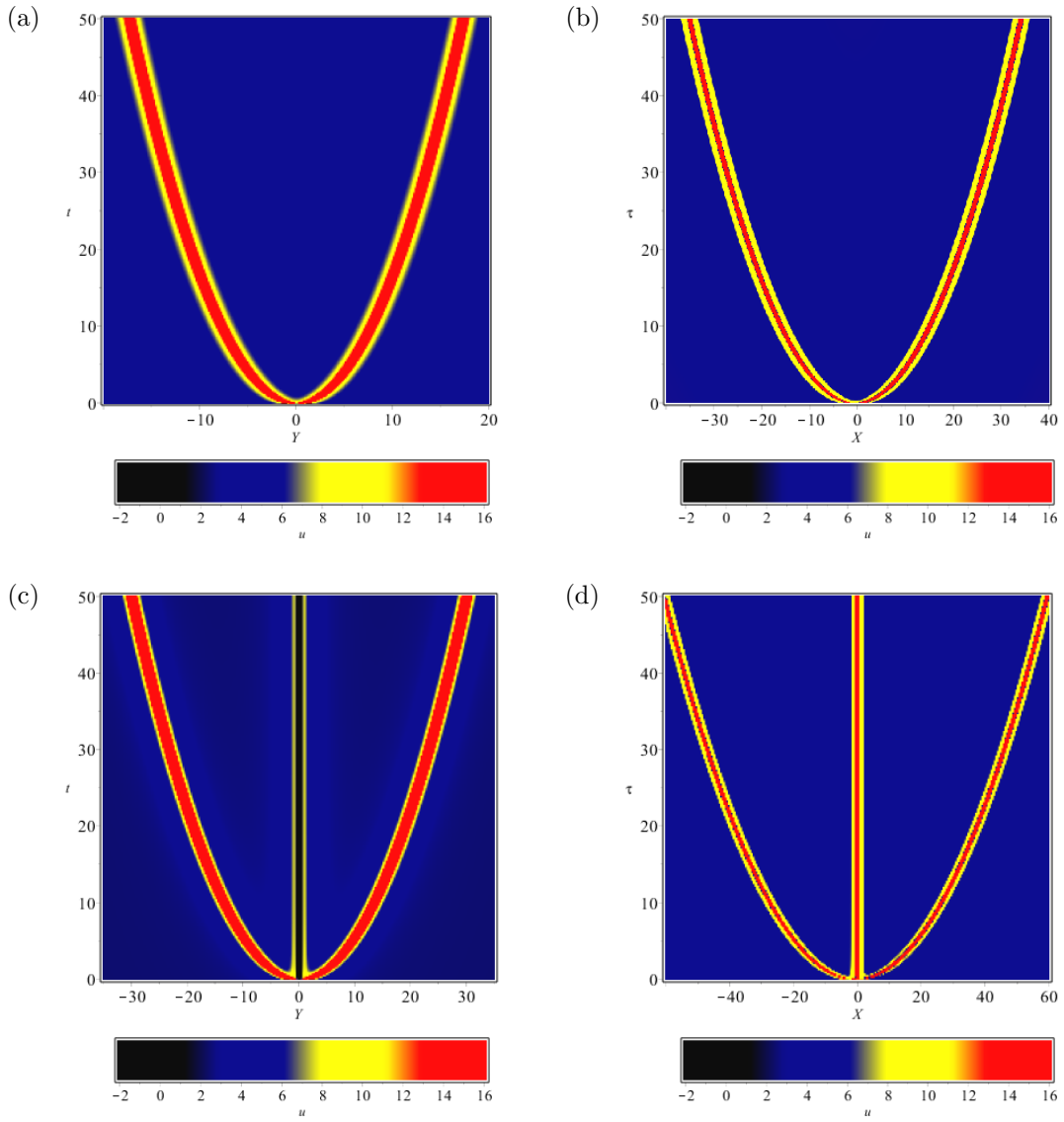

Figure 6.34: Development of the maxima of $u_{[2]}$ for positive (6.34(a)) and negative (6.34(b)) time. Likewise for $u_{[3]}$. Negative time is represented by τ.

The behaviour regarding limits of KP being 16 was postulated in [28] but this discovered subsequent to the investigation. Provided below are proofs of the limits of the central waves if they exist in the function $u_{[1]}, u_{[2]}$ and $u_{[3]}$, and the waves that reside on a fixed line in X or Y.

Proof of $u_{[1]}$, $u_{[2]}$ and $u_{[3]}$ as $t \to \infty$. Firstly let us consider as $t \to \infty$ in which the maximums of the functions $u_{[1]}, u_{[2]}$ and $u_{[3]}$ all occur for fixed X. The maximums all tend up to a limit in a symmetric fashion around fixed values of

X as seen in Figures 6.33(a) and 6.33(c). In all cases except for $u_{[1]}$ where the wave is unaltered by time, the symmetric maximums grow like a quadratic so we consider the functions for the value of X at which the maximums occur and for $Y = c\sqrt{t} + \xi$, for c and ξ constants to be determined. Where there is a central wave this grows linearly in X so we must alter the process slightly for this.

As mentioned, in the case of $u_{[1]}$, there is a a stationary, single peak at $X = Y = 0$ and $u_{[1]}(0, 0, t) = 16$.

For the symmetric moving waves in $u_{[2]}$ and $u_{[3]}$ we consider $X = 0$ with $u_{[2]}$ and $X = \frac{5}{6}$ with $u_{[3]}$ since the maximums always occur on these, and $Y = ct^{1/2} + \xi$ which have Taylor series in the limit as

$$u_{[2]}(0, ct^{1/2} + \xi, t) \sim \frac{2(c^2+6)}{t(c^2-6)^2} - \frac{4c\xi(c^2+18)}{t^{3/2}(c^2-6)^3} + \mathcal{O}(t^{-2}), \tag{6.38}$$

$$u_{[3]}(\tfrac{5}{6}, ct^{1/2} + \xi, t) \sim \frac{3(c^4+108)}{c^2t(c^2-18)^2} + \frac{6i\xi(c^6+18c^4+324c^2-1944)}{c^3t^{3/2}(c^2-18)^3} + \mathcal{O}(t^{-2}). \tag{6.39}$$

These have critical values that relate to maximums at $c = \sqrt{6}$ and $c = \sqrt{18}$ respectively. Substituting these values in and recalculating the series they become

$$u_{[2]}(0, \sqrt{6t} + \xi, t) \sim \frac{16}{16\xi^2+1} + \frac{8}{3}\frac{\sqrt{6}\xi}{t^{1/2}(16\xi^2+1)^2} + \mathcal{O}(t^{-1}), \tag{6.40}$$

$$u_{[3]}(\tfrac{5}{6}, \sqrt{18t} + \xi, t) \sim \frac{16}{16\xi^2+1} + \mathcal{O}(t^{-1/2}), \tag{6.41}$$

where the leading terms are maximal when $\xi = 0$.

There is another wave in $u_{[3]}$ whose maximum occurs on $Y = 0$ in the limit and moves in a straight line. Consider $Y = 0$ and $X = ct + \xi$ which has a Taylor series in the limit as

$$u_{[3]}(ct + \xi, 0, t) \sim -\frac{12}{c^2t^2} + \frac{12(2c\xi + c + 144)}{c^4t^3} + \mathcal{O}(t^{-4}), \tag{6.42}$$

which has a critical value at $c = 0$. With this substituted in the series becomes

$$u_{[3]}(\xi, 0, t) \sim -\frac{144(3\xi - 1)(3\xi + 2)}{(18\xi^2 + 6\xi + 5)^2} + \mathcal{O}(t^{-1}), \tag{6.43}$$

which has a maximal point for $\xi = -\frac{1}{6}$, and for which the maximum height of the wave is 16.

□

Proof of $u_{[1]}$, $u_{[2]}$ and $u_{[3]}$ as $\tau \to \infty$ with $\tau = -t$.

Since $u_{[1]}$ is independent of time then the same rational as used for $t \to \infty$ holds as to why the limit of the wave height is 16 for $\tau \to \infty$. The maximums now tend to the limit one from above, and one from below when we consider the symmetric waves around $Y = 0$ as seen in Figures 6.33(b) and 6.33(d). Once more, the symmetric waves grow as a quadratic and so we use $X = c\tau^{1/2} + \xi$ and the central wave grows linearly.

Firstly consider the symmetric waves, thus $Y = 0$ and $X = c\tau^{1/2} + \xi$ which results in $u_{[2]}$ and $u_{[3]}$ have Taylor series in the limit as

$$u_{[2]}(c\tau^{1/2} + \xi, 0, \tau) \sim -\frac{8(c^2 + 24)}{\tau(c^2 - 24)^2} + \frac{8c(c^2 + 72)(2\xi + 1)}{(c^2 - 24)^3\tau^{3/2}} + \mathcal{O}(\tau^{-2}), \tag{6.44}$$

$$u_{[3]}(c\tau^{1/2} + \xi, 0, \tau) \sim -\frac{12(c^4 + 1728)}{c^2\tau(c^2 - 72)^2} + \mathcal{O}(\tau^{-3/2}), \tag{6.45}$$

whose critical values that relate to the maximums are $c = \sqrt{24}$ and $c = \sqrt{72}$ respectively. Substituting these values in and recalculating the series, they become

$$u_{[2]}(\sqrt{24\tau} + \xi, 0, \tau) \sim -\frac{16\xi(\xi + 1)}{(2\xi^2 + 2\xi + 1)^2} + \mathcal{O}(\tau^{-1/2}), \tag{6.46}$$

$$u_{[3]}(\sqrt{72\tau} + \xi, 0, \tau) \sim -\frac{144(6\xi - 1)(6\xi + 5)}{(36\xi^2 + 24\xi + 13)^2} + \mathcal{O}(\tau^{-1/2}), \tag{6.47}$$

which have leading terms maximal at $\xi = -\frac{1}{2}$ and $\xi = -\frac{1}{3}$ respectively, and the

maximum height of the wave in both cases is 16.

For the additional wave in $u_{[3]}$ whose maximum occurs on $Y = 0$ in the limit and moves in a straight line. Again consider $Y = 0$ and $X = c\tau + \xi$ which has a Taylor series in the limit as

$$u_{[3]}(c\tau + \xi, 0, \tau) \sim -\frac{12}{c^2\tau^2} + \frac{12(2c\xi + c - 144)}{c^4\tau^3} + \mathcal{O}(\tau^{-4}), \tag{6.48}$$

which has a critical value at $c = 0$. With this substituted in the series becomes

$$u_{[3]}(\xi, 0, \tau) \sim -\frac{144(3\xi + 1)(3\xi + 4)}{(18\xi^2 + 30\xi + 17)^2} + \mathcal{O}(\tau^{-1}), \tag{6.49}$$

which has a maximal point for $\xi = -\frac{5}{6}$, and for which the maximum height of the wave is 16.

□

A list of the values of c was composed in order to see if there was a recognisable pattern just from this. That would then assist with proofs of later functions. This work can be found in Appendix D.2.

Interestingly if instead, of making the substitution of $t = -\tau$, you take the limit as $t \to -\infty$ then the Taylor series for positive t and negative t for the additional wave is exactly the same. However making that slight alteration seems to change the numbers in ξ and c.

This work was only evaluated for $u_{[1]}, u_{[2]}$ and $u_{[3]}$ however it should be possible to extend this to $u_{[n]}$ subject to different values of X for positive time and ultimately the hope would be to extend the proofs to any matrix rank solution. Consideration of $u_{[4]}$ and $u_{[5]}$ was considered however finding out precisely where the waves would lie, particularly as numerical error was having a greater impact.

6.7 Relation Between other Nonlinear PDE's and the KP-I Equation

In [55] Pelinovskii and Stepanyants consider the KP equation in the form

$$(U_t + UU_x - \beta U_{xxx})_x = -U_{yy}, \tag{6.50}$$

which they then consider steady-state solutions of by assuming $U(x, y, t) = U(x + Vt, y)$ for $V > 0$, $\xi = X\sqrt{V/\beta}, \eta = YV/\sqrt{\beta}$ and $\mu = -U/V$. In order to make (6.50) equivalent to (6.1), we find $\beta = \frac{1}{36}$. Further to this, if we let $x = \xi/\sqrt{3}$ and $y = \eta/\sqrt{3}$ we retrieve a set of solutions that are the same as solutions of (3.1). This is evidence of the well-known link between the solutions of the KP-I equation and solutions of the Boussinesq equation. All solutions of the Boussinesq equation can, by simple scalings, be solutions of the KP-I equation. It is not always possible to go the other way since there are solutions of KP-I which are not found as symmetry reductions of the Boussinesq.

Dubard and Matveev [27, 28] derive rational solutions of (6.1) from the generalised rational solution $\widehat{\psi}_2(x, t; \alpha, \beta)$ of the focusing NLS equation

$$F_2^{GNLS}(x, t; \alpha, \beta) = \left\{ 1 - 12\frac{\widehat{G}_2(x, t; \alpha, \beta) + \mathrm{i}\widehat{H}_2(x, t; \alpha, \beta)}{\widehat{D}_2(x, t; \alpha, \beta)} \right\} \exp\left(\tfrac{1}{2}\mathrm{i}t\right), \tag{6.51}$$

where

$$\widehat{G}_2(x, t; \alpha, \beta) = G_2(x, t) - 2\alpha t + 2\beta x, \tag{6.52a}$$

$$\widehat{H}_2(x, t; \alpha, \beta) = tH_2(x, t) + \alpha(x^2 - t^2 + 1) + 2\beta xt, \tag{6.52b}$$

$$\widehat{D}_2(x, t; \alpha, \beta) = D_2(x, t) + 2\alpha t(3x^2 - t^2 - 9) - 2\beta x(x^2 - 3t^2 - 3) + \alpha^2 + \beta^2, \tag{6.52c}$$

with α and β arbitrary constants, G_2, H_2 and D_2 as given in Appendix A, see also [41, 42]. Specifically Dubard and Matveev show that

$$\begin{aligned} v(\xi,\eta,\tau) &= 2\frac{\partial^2}{\partial\xi^2}\ln\widehat{D}_2(\xi-3\tau,\eta;\alpha,-48\tau) \\ &= \tfrac{1}{2}\left(|F_2^{GNLS}(x,t;\alpha,\beta)|^2-1\right)\Big|_{x=\xi-3\tau,t=\eta,\beta=-48\tau}, \end{aligned} \tag{6.53}$$

is a solution of (6.1). If we define $F_2^{\rm nls}(\xi,\eta,\tau;\alpha)=\widehat{D}_2(\xi-3\tau,\eta;\alpha,-48\tau)$, then

$$\begin{aligned} F_2^{\rm nls}(\xi,\tau;\alpha) = {}& \xi^6-18\tau\xi^5+3\left(45\tau^2+\eta^2+1\right)\xi^4-12\left(45\tau^2+3\eta^2-5\right)\tau\xi^3 \\ &+\left\{3\eta^4+18\left(9\tau^2-1\right)\eta^2+1215\tau^4-702\tau^2+27\right\}\xi^2 \\ &-\left\{18\tau\eta^4+36\left(9\tau^2+5\right)\tau\eta^2+1458\tau^5-2268\tau^3+450\tau\right\}\xi \\ &+\eta^6+27\left(\tau^2+1\right)\eta^4+9\left(27\tau^4+78\tau^2+11\right)\eta^2+729\tau^6 \\ &-2349\tau^4+3411\tau^2+9. \end{aligned} \tag{6.54}$$

The polynomial $F_2^{\rm nls}(\xi,\tau;\alpha)$ satisfies

$$\left(\mathrm{D}_\xi^4+\mathrm{D}_\xi\mathrm{D}_\tau-3\mathrm{D}_\eta^2\right)F_2\cdot F_2=0, \tag{6.55}$$

which is the bilinear form of the (6.1), and so

$$v_2^{\rm nls}(\xi,\eta,\tau;\alpha)=2\frac{\partial^2}{\partial\xi^2}\ln F_2^{\rm nls}(\xi,\eta,\tau;\alpha), \tag{6.56}$$

is a rational solution of (6.1).

6.8 Generalised KP

It is possible to introduce parameters into the solutions $F^{GKP}_{[m_1,..,m_n]}$ from (6.11) by altering the form of ϕ_1.

Conjecture 6.2. *An infinite number of parameters can be introduced into the bilinear form solutions from* (6.11) *by changing* ϕ *to,*

$$\phi_N = -kx - k^2 y - 4k^3 t + \sum_{j=3}^{N+2} (a_j + \mathrm{i}b_j)(\mathrm{i}k)^j, \tag{6.57}$$

where $(a_j, b_j) \in \mathbb{R}^2$ *are parameters. For each* $N \in \mathbb{Z}$ *there are solutions to the bilinear form for* $F^{GKP}_{[m_1,..,m_n]}$*, where* n *still denotes the rank of the matrix* $\mathbf{M}$*.*

This conjecture was mentioned in [28] in a slightly different form where here the lowest order terms have been explicitly given and the ψ_l from the paper has been written as $a_j + \mathrm{i}b_j$ since it can be complex.

For $F^{GKP}_{[1]}$ it is always possible to translate out these additional parameters however at higher orders this is not the case. In fact, the translation required is always as follows,

$$\begin{aligned} x &\to x - \frac{1}{2}\left(\partial_x^2 \left(F^{GKP}_{[1]}\right)\Big|_{x=0} + 24t - 1\right) \\ y &\to y - \frac{1}{8}\left(\partial_y^2 \left(F^{GKP}_{[1]}\right)\Big|_{y=0}\right). \end{aligned}$$

Interestingly the functions $\partial_x^2 \left(F^{GKP}_{[1]}\right)\Big|_{x=0}$ and $\partial_y^2 \left(F^{GKP}_{[1]}\right)\Big|_{y=0}$ are highly structured and can be written as,

$$\begin{aligned} \partial_x^2 \left(F^{GKP}_{[1]}\right)\Big|_{x=0} &= 1 - 24t + 2\sum_{j=4}^{n} j b_j \\ \partial_y^2 \left(F^{GKP}_{[1]}\right)\Big|_{y=0} &= 4\sum_{j=4}^{n} j a_j \end{aligned}$$

which is not intuitive from the equation.

6.9 Discussion

There are many links between the KP-I equation solutions and other mathematical phenomena. For one, it is possible to express (6.21) from §6.3.1.2 as Young diagrams. It is also possible to express the number of variations of m_i not as partitions of an integer into distinct parts, as was done in §6.3.1.3 but as Young diagrams. This may reformat the problem in such a way that it is possible to not only establish what the generating function is doing but also why this generating function works and what the impact of the values of m_i are. In a similar way, it is possible to think of the k_i values of the multinomials given in (6.22) from §6.3.1.2 as all the partitions of the integer n. Essentially, given that the precise reason as to why this method works has not been found yet, it may be wise to consider different expressions of the problem since there are links with both partitions and Young diagrams at least; potentially many other useful expressions as well. If this does not simplify the problem, then a continuation of the work regarding the Hessenberg matrices may solve it still.

The categorisation work from §6.4 could also be extended to analysis of much large m_i's as well as higher ranked matrices. This would then establish another branch of the categorisation problem. It also remains to conjecture and prove the behaviour for the 1×1, 2×2 and 3×3 cases such that given m_1, m_2 and m_3 the behaviour will be easily predicted. Within this, the proof of Conjecture 6.1 remains to be found. Much of the categorisation work focussed on positive time behaviour as well as this seemed to be the most patterned, thus it would be interesting to focus on the negative time more and establish the behaviour here. It would also be worth investigating large values of $|t|$ to ensure that the behaviour does not alter drastically later.

The limit work shown in §6.6 needs to be extended to higher values of n in u_n or to be generalised to all functions. The generalisation would require some

knowledge of the leading order behaviour and coefficients of these leading order terms however in order to complete.

Chapter 7

Relation between KP, Boussinesq and NLS

It has been shown in previous chapters that there are multiple links between the NLS, Boussinesq and KP-I solutions. This chapter gives an equation solution in terms of 3 parameters such that specific selection of the parameters leads to separate solutions of all 3 of these equations.

7.1 The Equation

If we compare the polynomials $F_2^{GNLS}(\xi,\tau;\alpha,\beta)$ and $F_2^{GBE}(\xi,\eta,\tau;\alpha,\beta)$, respectively given by

$$F_2^{GNLS}(\xi,t;\alpha,\beta)=\left\{1-12\frac{\widehat{G}_2(\xi,t;\alpha,\beta)+\mathrm{i}\widehat{H}_2(\xi,t;\alpha,\beta)}{\widehat{D}_2(\xi,t;\alpha,\beta)}\right\}\exp\left(\tfrac{1}{2}\mathrm{i}t\right), \tag{7.1}$$

where

$$\widehat{G}_2(\xi,\tau;\alpha,\beta)=G_2(\xi,\tau)-2\alpha\tau+2\beta\xi, \tag{7.2a}$$

$$\widehat{H}_2(\xi,\tau;\alpha,\beta)=\tau H_2(\xi,\tau)+\alpha(\xi^2-\tau^2+1)+2\beta\xi\tau, \tag{7.2b}$$

$$\widehat{D}_2(\xi,\tau;\alpha,\beta) = D_2(\xi,\tau) + 2\alpha\tau(3\xi^2 - \tau^2 - 9) - 2\beta\xi(\xi^2 - 3\tau^2 - 3) + \alpha^2 + \beta^2, \tag{7.2c}$$

and

$$\begin{aligned} F_n^{GBE}(\xi,\tau;\alpha,\beta) =& F_n^{BE}(\xi,\tau) + 2\alpha\tau P_{n-1}(\xi,\tau) + 2\beta\xi Q_{n-1}(\xi,\tau) \\ &+ (\alpha^2+\beta^2)F_{n-2}^{BE}(\xi,\tau),, \end{aligned} \tag{7.3}$$

then we see that they are fundamentally different. As we shall now demonstrate, they are special cases of a more general polynomial. Consider the polynomial $\mathcal{F}_2(\xi,\eta,\tau;\mu,\alpha,\beta)$, with parameters μ, α and β, given by

$$\begin{aligned} \mathcal{F}_2(\xi,\eta,\tau;\mu,\alpha,\beta) =& \xi^6 - 18\tau\xi^5 + (3\eta^2 + 135\tau^2 - 6\mu^2 + 9)\xi^4 \\ &- \left\{36\eta^2 + 540\tau^2 - 12(6\mu^2 + 6\mu - 7)\right\}\tau\xi^3 \\ &+ \left\{3\eta^4 + 18(9\tau^2 - 2\mu + 1)\eta^2 + 1215\tau^4\right. \\ &\left. - 54(6\mu^2 + 12\mu - 5)\tau^2 + 9\mu(\mu+2)(\mu^2 - 2\mu + 2)\right\}\xi^2 \\ &- \left\{18\eta^4 + 36(9\tau^2 + 5)\eta^2 + 1458\tau^4 - 324(2\mu^2 + 6\mu - 1)\tau^2\right. \\ &\left. + 18\mu(3\mu^3 + 12\mu^2 - 2\mu + 12)\right\}\tau\xi + \eta^6 \\ &+ (27\tau^2 + 6\mu^2 + 12\mu + 9)\eta^4 \\ &+ \left\{243\tau^4 + 54(6\mu+7)\tau^2 + 9(\mu^4 + 4\mu^3 + 6\mu^2 - 4\mu + 4)\right\}\eta^2 \\ &+ 729\tau^6 - 81(\mu^2 + 24\mu - 1)\tau^4 \\ &+ 9(9\mu^4 + 72\mu^3 + 150\mu^2 + 132\mu + 16)\tau^2 + 9(\mu^2 - 2\mu + 2)^2 \\ &+ 2\alpha\left\{3\eta\xi^2 - 18\tau\eta\xi - \eta^3 + 3\left[9\tau^2 - \mu(\mu+2)\right]\eta\right\} \\ &+ 2\beta\left\{\xi^3 - 9\tau\xi^2 - 6(\eta^2 - 9\tau^2 + \mu^2)\xi + 9\tau\eta^2 - 27\tau^3\right. \\ &\left. + 3(3\mu^2 + 12\mu + 4)\tau\right\} + \alpha^2 + \beta^2. \end{aligned} \tag{7.4}$$

Then (7.4) has both the polynomials of $F_2^{GNLS}(\xi,\eta,\tau;\alpha)$ and $F_2^{GBE}(\xi,\eta,\tau;\alpha,\beta)$ as special cases, specifically

$$F_2^{GNLS}(\xi,\eta,\tau;\alpha) = \mathcal{F}_2(\xi,\eta,\tau;1,\alpha,0),$$
$$F_2^{GBE}(\xi,\eta,\tau;\alpha,\beta) = \mathcal{F}_2(\xi,\eta,\tau;-\tfrac{1}{3},\alpha,\beta).$$

Furthermore

$$u(\xi,\eta,\tau;\mu,\alpha,\beta) = 2\frac{\partial^2}{\partial\xi^2}\ln\mathcal{F}_2(\xi,\eta,\tau;\mu,\alpha,\beta), \tag{7.5}$$

with $\mathcal{F}_2(\xi,\eta,\tau;\mu,\alpha,\beta)$ given by (7.4), is a solution of the KP-I equation

$$u_{tx} + 6u_x^2 + 6uu_{xx} + u_{xxxx} + 3\sigma^2 u_{yy} = 0, \tag{7.6}$$

which includes as special cases the bilinear solution of the NLS, when $\mu = 1$ and $\beta = 0$, and the bilinear solution of the Boussinesq, when $\mu = -\frac{1}{3}$, as is easily shown.

In Figure 7.1, the initial solution $u(\xi,\eta,0;\mu,0,0)$ given by (7.5) is plotted for various choices of the parameter μ. When $\mu = 1$, then this arises from the solution (6.56) derived from the focusing NLS equation

$$\mathrm{i}u_t + u_{xx} + 2|u|^2 u = 0, \tag{7.8}$$

whilst when $\mu = -\frac{1}{3}$, then this arises from the solution derived from the Boussinesq equation (7.3). From Figure 7.1 we can see that for $\mu < \mu^*$, the solution $v(\xi,\eta,0;\mu,0,0)$ has two peaks on the line $\eta = 0$, which coalesce when $\mu = \mu^*$ to form one peak at $\xi = \eta = 0$. By considering when

$$\frac{\partial^2}{\partial\xi^2}v(\xi,0,0;\mu,0,0)\bigg|_{\xi=0} = -\frac{8(3\mu^4+12\mu^3+16\mu^2-6)}{(\mu^2-2\mu+2)^2} = 0, \tag{7.9}$$

then μ^* is the real positive root of

$$\begin{aligned} 3\mu^4 + 12\mu^3 + 16\mu^2 - 6 =& 3\left[\mu^2 + 2(1 - \tfrac{1}{3}\sqrt{6})\mu + 2 - \sqrt{6}\right] \\ & \times \left[\mu^2 + 2(1 + \tfrac{1}{3}\sqrt{6})\mu + 2 + \sqrt{6}\right] = 0, \end{aligned} \tag{7.10}$$

i.e. $\mu^* = -1 + \frac{1}{3}\sqrt{6} + \frac{1}{3}\sqrt{-3 + 3\sqrt{6}} \approx 0.5115960325$. For $\mu > \mu^*$, it can be shown that

$$v(0, 0, 0; \mu, 0, 0) = \frac{4\mu(\mu + 2)}{\mu^2 - 2\mu + 2}, \tag{7.11}$$

increases until it reaches a maximum height of $4(2 + \sqrt{5})$ when $\mu = \frac{1}{2}(1 + \sqrt{5})$, which is the golden mean!

7.2 Discussion

This work has been very recent and as such, there is much that can be done to extend it. It would be interesting to see the effect of the parameters on the wave formations so that it can be characterised as to what they do. It is known that these will all be solutions of the KP-I solution, but these solutions are not ones that have been investigated in detail as they differ from the solutions found in Chapter 6.

Additionally, it would be worth determine whether this equation could solve other nonlinear PDEs that have not been considered in this thesis. There are often many links between the integrable nonlinear PDEs so it may be that solutions exist already for certain parameter choices or that this equation could be extended with additional parameters in order to accommodate this.

Since only the degree 6 functions have been considered, extending this to degree 12 and further may help to enlighten some generic form or combination of the solutions so that they could be generated more readily.

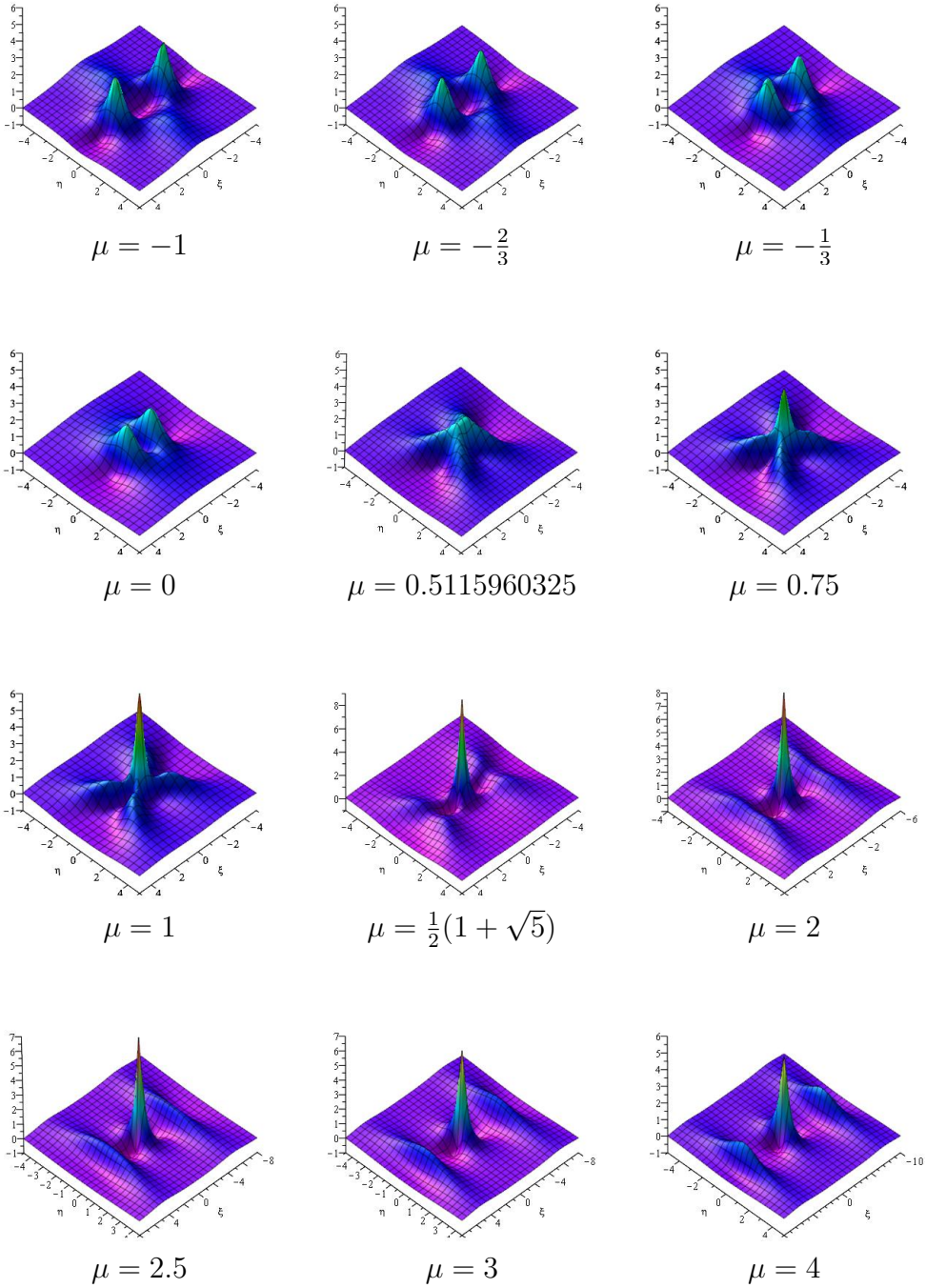

(7.7)

Figure 7.1: The initial solution $v(\xi, \eta, 0; \mu, 0, 0)$ given by (7.5) is plotted for various choices of the parameter μ. When $\mu = -\frac{1}{3}$ the initial solution corresponds to that arising from the Boussinesq equation (7.3) and when $\mu = 1$ to the initial solution from the focusing NLS equation $\mathrm{i}u_t + u_{xx} + 2|u|^2 u = 0$.

Chapter 8

Conclusion

The aim of this thesis was to explore the rational solutions of 3 nonlinear PDEs. During this time, multiple queries came up regarding the inherent structure of such solutions across all of the equations. While it has been known that solutions of integrable PDEs often exhibit such behaviour, the reasoning behind this is not always clear. Through the applications of combinatorics, characterisation and simplifications of these solutions, this thesis has progressed in its understanding of why such solutions may act in this way. Additionally, given that there are often similarities between such equations, an equation has been found which links solutions of the KP-I equation with both the Boussinesq and the NLS equations, subject to specific selections of the parameters. As well as this, a theorem regarding nonlinear superposition of functions that solve the Boussinesq bilinear form to produce new functions from old was also found. This theorem, that pulls together 2 known rational solutions of the bilinear form with another function, is a pivotal find that is unexpected in such nonlinear equations.

Given the high similarities seen between the rational solutions of the NLS equation and the Boussinesq equation, it would be beneficial to spend more time trying to develop the generating function that exists for the NLS. While this

thesis was not aimed at focussing very much on the NLS equation solutions, as they have been widely researched, the link between the NLS and the Boussinesq could be extended in further work. The behaviour of the complex roots of the bilinear solutions has been of much interest, not just for the NLS equation but for the others in this thesis. It was interesting to see how the behaviour of the roots differed from the other equation solutions and ultimately it would be beneficial if their structure could be fully explained as to how they affect the overall solution of the PDE.

The work on KP-I has been the most extensive given that the generating function already existed, but there was not much context regarding why the functions worked. In order to understand the function so that this could hopefully be applied to other equations, characterisation of solutions was completed. While a complete characterisation still eludes us, it gave a lot of information as to how the different parts of the generating function were influencing the solutions. If this was fully understood, then the ability to adapt it in order to apply it to the Boussinesq equation would be much easier.

Within this analysis of the generating function, the opportunity to work on more combinatorics was presented. Subject to this, further links with Young diagrams, integer partitions and other topics were discovered. Ultimately, the wealth of structure provided by the integrable nonlinear PDE's considered have links with many other areas of mathematics. There was not enough time to extend this exploration but it may be that in another area is the solution to the generating function problem. The ability to reformat the problem in a different setting gives us a further chance of solving it.

The work in this predominantly experimental thesis has widened the understanding of some of the rational solutions of the nonlinear PDEs investigated. It has also lead to a number of queries relating further behaviour or relations

between these equations and most likely others. Proofs have been completed for certain limits in functions that, while it has been hinted at in other works, has not been produced until now. Extension of these proofs is but one of the extensions that can be worked on in order to further our understanding. The experimental work has been fundamental in highlighting these questions and others that may not have been found without it.

There is much that can be done with regard to future work, not only within the work that has been completed thus far but also in extensions to other nonlinear PDEs. When working with the Boussinesq equation it was established that the solutions of the bilinear form for rogue wave solutions are of degree $n(n+1)$ in x and t. Moving on to work with the KP-I equation, the fact that this equation is a $(2+1)$ dimensional equation meant that there were many more solutions of varying degrees that still satisfied the relevant equation. There are equations such as the Davey-Stewartson equation [49, 50] which is a system of two PDEs and is an analogue of the NLS equation. This equation is also solvable via inverse scattering and as such gives another avenue of exploration of the function and the justification behind the wave behaviour. Additionally it is a generalisation of the KP-I and NLS equations which further supports the case that, along with its integrability and the fact that there are some exact solutions, there are likely to be many more undiscovered solutions in our polynomial form.

Considering the asymptotics of solutions is also something that has been briefly visited in my PhD but that I wish to extend further, as well as consideration of perturbations of the solutions and the resulting stability which I have been unable to explore thus far.

It is of great interest to me to extend the work conducted on the KP-I equation. Following from this should help the Boussinesq problem more as well as offering the chance to firmly determine different patterns and groupings of waves derived

from the KP-I equation. The extension of the characterisation to fully understand the solutions is the first aim as this will no doubt inform the workings of the generating function. Additionally, further work on the complex roots and their influence on the full solution is likely to be best worked with in terms of KP-I since there are a greater number of waves and roots to consider than that of the Boussinesq equation at present.

Appendix A

Focusing NLS Equation

A.1 Polynomial Functions of Degree $n(n+1)$

These are some of the polynomial functions of the NLS as defined in [23]. As mentioned in Chapter 2 these can be related to the method used by Dubard and Matveev [28] via some simple translations.

$$
\begin{aligned}
F_1 =& x^2 + t^2 + 1, \\
G_1 =& 1, \\
H_1 =& 1, \\
F_2 =& x^6 + 3\left(t^2+1\right)x^4 + 3\left(t^2-3\right)^2 x^2 + t^6 + 27\,t^4 + 99\,t^2 + 9, \\
G_2 =& 3\,x^4 + 18\left(t^2+1\right)x^2 + 15\,t^4 + 54\,t^2 - 9, \\
H_2 =& 3\,x^4 + \left(6\,t^2 - 18\right)x^2 + 3\,t^4 + 6\,t^2 - 45, \\
F_3 =& x^{12} + \left(6\,t^2+6\right)x^{10} + \left(15\,t^4 - 90\,t^2 + 135\right)x^8 + \left(20\,t^6 - 180\,t^4 + 540\,t^2\right. \\
& \left. +2340\right)x^6 + \left(15\,t^8 + 60\,t^6 - 1350\,t^4 + 13500\,t^2 + 3375\right)x^4 + \left(6\,t^{10}\right. \\
& \left. +270\,t^8 + 13500\,t^6 + 78300\,t^4 - 36450\,t^2 + 12150\right)x^2 + t^{12} + 126\,t^{10} \\
& + 3735\,t^8 + 15300\,t^6 + 143775\,t^4 + 93150\,t^2 + 2025,
\end{aligned}
$$

$$
\begin{aligned}
G_3 =& 6\,x^{10} + \left(90\,t^2 + 90\right) x^8 + \left(300\,t^4 - 360\,t^2 + 1260\right) x^6 + \left(420\,t^6 - 900\,t^4\right. \\
&\left. + 2700\,t^2 - 2700\right) x^4 + \left(270\,t^8 + 2520\,t^6 + 40500\,t^4 - 81000\,t^2 - 4050\right) x^2 \\
&+ 66\,t^{10} + 2970\,t^8 + 13140\,t^6 - 45900\,t^4 - 12150\,t^2 + 4050, \\
H_3 =& 6\,x^{10} + \left(30\,t^2 - 90\right) x^8 + \left(60\,t^4 - 840\,t^2 - 900\right) x^6 + \left(60\,t^6 - 1260\,t^4\right. \\
&\left. - 2700\,t^2 - 8100\right) x^4 + \left(30\,t^8 - 360\,t^6 + 10260\,t^4 - 37800\,t^2 + 28350\right) x^2 \\
&+ 6\,t^{10} + 150\,t^8 - 5220\,t^6 - 57780\,t^4 - 14850\,t^2 + 28350.
\end{aligned}
$$

Appendix B

Boussinesq Equation Solutions

These are solutions of the bilinear form of the Boussinesq equation (3.31) as mentioned in Chapter 3. Solutions of the Boussinesq equation (3.1) are found by taking twice the second logarithmic derivative in x of these. Both the main solutions of degree $n(n+1)$ are given as well as some monic solutions.

B.1 Degree $n(n+1)$ Polynomial Solutions of (3.31)

The solutions below are all of the currently known polynomial solutions of (3.31) that are of even degree.

$$
\begin{aligned}
F_1 =& x^2 + t^2 + 1, \\
F_2 =& x^6 + \left(3\,t^2 + \frac{25}{3}\right) x^4 + \left(3\,t^4 + 30\,t^2 - \frac{125}{9}\right) x^2 + t^6 + \frac{17}{3}\,t^4 + \frac{475}{9}\,t^2 \\
& + \frac{625}{9}, \\
F_3 =& x^{12} + \left(6\,t^2 + \frac{98}{3}\right) x^{10} + \left(15\,t^4 + 230\,t^2 + \frac{245}{3}\right) x^8 + \\
& \left(20\,t^6 + \frac{1540}{3}\,t^4 + \frac{18620}{9}\,t^2 + \frac{75460}{81}\right) x^6 + \\
& \left(15\,t^8 + \frac{1460}{3}\,t^6 + \frac{37450}{9}\,t^4 + \frac{24500}{3}\,t^2 - \frac{5187875}{243}\right) x^4 +
\end{aligned}
$$

$$\left(6\,t^{10}+190\,t^{8}+\frac{35420}{9}\,t^{6}-\frac{4900}{9}\,t^{4}+\frac{188650}{27}\,t^{2}+\frac{159786550}{729}\right)x^{2}$$
$$+\,t^{12}+\frac{58}{3}\,t^{10}+\frac{1445}{3}\,t^{8}+\frac{798980}{81}\,t^{6}+\frac{16391725}{243}\,t^{4}+\frac{300896750}{729}\,t^{2}$$
$$+\,\frac{878826025}{6561},$$

$$F_4 = x^{20}+\left(10\,t^{2}+90\right)x^{18}+\left(45\,t^{4}+1010\,t^{2}+1845\right)x^{16}+$$
$$\left(120\,t^{6}+4600\,t^{4}+30600\,t^{2}+13000\right)x^{14}+$$
$$\left(210\,t^{8}+11480\,t^{6}+151900\,t^{4}+393400\,t^{2}-\frac{2097550}{9}\right)x^{12}+$$
$$\left(252\,t^{10}+17500\,t^{8}+367640\,t^{6}+2095800\,t^{4}+\frac{11948300}{9}\,t^{2}+\right.$$
$$\left.\frac{232696100}{27}\right)x^{10}+\left(210\,t^{12}+16940\,t^{10}+501550\,t^{8}+5010600\,t^{6}\right.$$
$$\left.+\frac{39702250}{3}\,t^{4}+\frac{180407500}{9}\,t^{2}-\frac{6596112250}{27}\right)x^{8}+$$
$$\left(120\,t^{14}+10360\,t^{12}+400120\,t^{10}+5601400\,t^{8}+\frac{141659000}{3}\,t^{6}+\right.$$
$$\left.\frac{23569000}{9}\,t^{4}-\frac{19319573000}{27}\,t^{2}+\frac{86014747000}{27}\right)x^{6}+$$
$$\left(45\,t^{16}+3800\,t^{14}+179900\,t^{12}+3504200\,t^{10}+\frac{98796250}{3}\,t^{8}+\right.$$
$$\frac{1675457000}{9}\,t^{6}-\frac{15031607500}{27}\,t^{4}+\frac{410944625000}{27}\,t^{2}+$$
$$\left.\frac{2352823598125}{81}\right)x^{4}+\left(10\,t^{18}+730\,t^{16}+39400\,t^{14}+1320200\,t^{12}+\right.$$
$$\frac{74612300}{9}\,t^{10}+\frac{1165839500}{9}\,t^{8}+\frac{73409791000}{27}\,t^{6}+\frac{1122199715000}{27}\,t^{4}$$
$$\left.+\frac{10744980496250}{81}\,t^{2}-\frac{8594611821250}{243}\right)x^{2}+t^{20}+50\,t^{18}+2565\,t^{16}$$
$$+\,122200\,t^{14}+\frac{40078850}{9}\,t^{12}+\frac{2423740900}{27}\,t^{10}+\frac{44477105750}{27}\,t^{8}+$$
$$\frac{177775871000}{9}\,t^{6}+\frac{4304738108125}{81}\,t^{4}+\frac{42895279813750}{243}\,t^{2}$$
$$+\,\frac{73054200480625}{729},$$

$$F_5(x,t) = x^{30}+\left(15\,t^{2}+\frac{605}{3}\right)x^{28}+\left(105\,t^{4}+3290\,t^{2}+12705\right)x^{26}+$$
$$\left(455\,t^{6}+\frac{71575}{3}\,t^{4}+\frac{2265725}{9}\,t^{2}+\frac{25939375}{81}\right)x^{24}+$$

$$\left(1365\,t^{8}+\frac{309260}{3}\,t^{6}+\frac{17897950}{9}\,t^{4}+\frac{26849900}{3}\,t^{2}+\frac{374564575}{243}\right)x^{22}+$$
$$\left(3003\,t^{10}+298375\,t^{8}+\frac{79208990}{9}\,t^{6}+\frac{725413150}{9}\,t^{4}+\frac{1327947775}{9}\,t^{2}+\right.$$
$$\left.\frac{45146222275}{729}\right)x^{20}+\left(5005\,t^{12}+\frac{1842610}{3}\,t^{10}+\frac{74936225}{3}\,t^{8}+\right.$$
$$\frac{30256387700}{81}\,t^{6}+\frac{416681967625}{243}\,t^{4}+\frac{1062878489750}{729}\,t^{2}-$$
$$\left.\frac{29949453408875}{6561}\right)x^{18}+\left(6435\,t^{14}+929005\,t^{12}+\frac{145887805}{3}\,t^{10}+\right.$$
$$\frac{9444440425}{9}\,t^{8}+\frac{716701225625}{81}\,t^{6}+\frac{4765327769125}{243}\,t^{4}-$$
$$\left.\frac{16069741485875}{729}\,t^{2}+\frac{1572487588700875}{6561}\right)x^{16}+\left(6435\,t^{16}+\right.$$
$$1049400\,t^{14}+\frac{201729500}{3}\,t^{12}+\frac{17384033800}{9}\,t^{10}+\frac{679848919750}{27}\,t^{8}+$$
$$\frac{29329239247000}{243}\,t^{6}+\frac{56763015732500}{729}\,t^{4}+\frac{877079786275000}{729}\,t^{2}-$$
$$\left.\frac{145319532381244375}{19683}\right)x^{14}+\left(5005\,t^{18}+888965\,t^{16}+\frac{201107900}{3}\,t^{14}\right.$$
$$+\frac{7268596300}{3}\,t^{12}+\frac{397343633750}{9}\,t^{10}+\frac{3094794221750}{9}\,t^{8}+$$
$$\frac{877248309206500}{729}\,t^{6}+\frac{7522818112617500}{2187}\,t^{4}-\frac{338877246089256875}{6561}\,t^{2}$$
$$\left.-\frac{1153508042510140625}{177147}\right)x^{12}+\left(3003\,t^{20}+\frac{1682450}{3}\,t^{18}+\right.$$
$$\frac{144448885}{3}\,t^{16}+\frac{18942077000}{9}\,t^{14}+49769993350\,t^{12}+$$
$$\frac{16141595185100}{27}\,t^{10}+\frac{2217737551163750}{729}\,t^{8}+\frac{9963380300797000}{729}\,t^{6}-$$
$$\frac{1297656625261390625}{6561}\,t^{4}+\frac{4533029626565151250}{19683}\,t^{2}+$$
$$\left.\frac{4174111038326870361875}{531441}\right)x^{10}+$$
$$\left(1365\,t^{22}+258335\,t^{20}+\frac{73529225}{3}\,t^{18}+\frac{11361306425}{9}\,t^{16}+\right.$$
$$\frac{976840075750}{27}\,t^{14}+\frac{17752164295250}{27}\,t^{12}+\frac{3658725849605750}{729}\,t^{10}+$$
$$\frac{3515840993183750}{243}\,t^{8}-\frac{195785332934489375}{729}\,t^{6}+$$
$$\frac{24978207925819946875}{6561}\,t^{4}+\frac{1159166663661630903125}{19683}\,t^{2}+$$

$$\frac{4904143764303914178125}{531441}\Big)\,x^8+\Big(455\,t^{24}+\frac{251020}{3}\,t^{22}+\frac{76657070}{9}\,t^{20}$$
$$+\frac{41289423700}{81}\,t^{18}+\frac{1362831787625}{81}\,t^{16}+\frac{98913216479000}{243}\,t^{14}+$$
$$\frac{4366923310634500}{729}\,t^{12}+\frac{14325694558021000}{729}\,t^{10}+$$
$$\frac{164980602695610625}{729}\,t^8+\frac{38543006652688037500}{2187}\,t^6+$$
$$\frac{12142620899858806568750}{59049}\,t^4+\frac{84368406785489229287500}{177147}\,t^2+$$
$$\frac{10336329254752185028093 75}{4782969}\Big)\,x^6+\Big(105\,t^{26}+\frac{53375}{3}\,t^{24}+$$
$$\frac{16915150}{9}\,t^{22}+\frac{1171587550}{9}\,t^{20}+\frac{1229272389625}{243}\,t^{18}+$$
$$\frac{32275315890125}{243}\,t^{16}+\frac{2128271542512500}{729}\,t^{14}+\frac{110365606933697500}{2187}\,t^{12}$$
$$+\frac{6125181130562869375}{6561}\,t^{10}+\frac{184494438219511371875}{6561}\,t^8+$$
$$\frac{1882955442893218491875 0}{59049}\,t^6+\frac{30319073658670395156250}{19683}\,t^4+$$
$$\frac{7679010260208620229531 25}{531441}\,t^2-\frac{37763631956445485447328125}{14348907}\Big)\,x^4+$$
$$\Big(15\,t^{28}+2170\,t^{26}+\frac{2043125}{9}\,t^{24}+\frac{163177700}{9}\,t^{22}+\frac{8631985775}{9}\,t^{20}+$$
$$\frac{17793313441750}{729}\,t^{18}+\frac{584377965527125}{729}\,t^{16}+\frac{7043820768985000}{243}\,t^{14}+$$
$$\frac{6235281337588043125}{6561}\,t^{12}+\frac{437562641832806971250}{19683}\,t^{10}+$$
$$\frac{5034320101951909278125}{19683}\,t^8+\frac{2968161816471785115875 00}{177147}\,t^6$$
$$-\frac{3055018615255839912968 75}{531441}\,t^4+\frac{1390140747020592706562 50}{531441}\,t^2+$$
$$\frac{6340831615246872352587 34375}{43046721}\Big)\,x^2+t^{30}+\frac{325}{3}\,t^{28}+10185\,t^{26}+$$
$$\frac{71587775}{81}\,t^{24}+\frac{16294723375}{243}\,t^{22}+\frac{2934806885675}{729}\,t^{20}+$$
$$\frac{1145785364618125}{6561}\,t^{18}+\frac{44166106891704875}{6561}\,t^{16}+$$
$$\frac{4108707388089775625}{19683}\,t^{14}+\frac{774149365283245634375}{177147}\,t^{12}+$$
$$\frac{24580063449195140376875}{531441}\,t^{10}+\frac{26692043796741170082 8125}{531441}\,t^8+$$
$$\frac{18940589955229082293759375}{4782969}\,t^6+\frac{19643200369899165158979 6875}{14348907}\,t^4+$$

$$\frac{16545990206422666839308593 75}{43046721}\,t^2+$$
$$\frac{29327795222257014720376562 5}{43046721}.$$

$$F_6(x,t) = x^{42}+\left(21\,t^2+\frac{1183}{3}\right)x^{40}+\left(210\,t^4+8820\,t^2+\frac{508690}{9}\right)x^{38}+\Big(1330\,t^6$$
$$+\frac{274610}{3}t^4+\frac{12788230}{9}t^2+3821090\Big)x^{36}+\Big(5985\,t^8+588980\,t^6+$$
$$\frac{47375650}{3}t^4+\frac{1044234100}{9}t^2+\frac{1101580025}{9}\Big)x^{34}+\Big(20349\,t^{10}+$$
$$2643585\,t^8+\frac{315853510}{3}t^6+\frac{12869088050}{9}t^4+\frac{46713328025}{9}t^2+$$
$$\frac{52703389375}{27}\Big)x^{32}+\Big(54264\,t^{12}+8817424\,t^{10}+477541960\,t^8+$$
$$\frac{90697722080}{9}t^6+\frac{2023126141400}{27}t^4+\frac{10677484963600}{81}t^2-$$
$$\frac{18449248181000}{729}\Big)x^{30}+\Big(116280\,t^{14}+22709960\,t^{12}+\frac{4730096840}{3}t^{10}+$$
$$\frac{420870165800}{9}t^8+\frac{15521441007800}{27}t^6+\frac{191853007255000}{81}t^4+$$
$$\frac{334252884511000}{243}t^2+\frac{6409667048057000}{2187}\Big)x^{28}+\Big(203490\,t^{16}+$$
$$46295760\,t^{14}+3947383160\,t^{12}+\frac{1385956450480}{9}t^{10}+$$
$$\frac{24986660017900}{9}t^8+\frac{184787782270000}{9}\,t^6+\frac{3522137350459000}{81}\,t^4+$$
$$\frac{7077480053462000}{243}t^2-\frac{505994906281114250}{2187}\Big)x^{26}+\Big(293930\,t^{18}+$$
$$75911290\,t^{16}+\frac{23071430200}{3}\,t^{14}+\frac{3386918974600}{9}\,t^{12}+$$
$$\frac{248667948865700}{27}\,t^{10}+\frac{2844740151662500}{27}\,t^8+$$
$$\frac{114282158050151000}{243}\,t^6+\frac{130857435176195000}{243}\,t^4-$$
$$\frac{1559522065545193750}{729}\,t^2+\frac{6541917347970321 36250}{59049}\Big)x^{24}+$$
$$\Big(352716\,t^{20}+\frac{303397640}{3}\,t^{18}+\frac{35559121780}{3}\,t^{16}+\frac{6315930964000}{9}\,t^{14}+$$
$$\frac{596228929709000}{27}\,t^{12}+\frac{28864067489238800}{81}\,t^{10}+$$
$$\frac{23867708727863000}{9}\,t^8+\frac{5204725442990164000}{729}\,t^6-$$

$$\frac{171882373232918075002187}{}\,t^4+\frac{2292090862911349045019683}{}\,t^2+\frac{13248866554462384982500177147}{}\Big)\,x^{22}+\big(352716\,t^{22}+110065956\,t^{20}+\frac{131342431220}{9}\,t^{18}+\frac{9144134924540}{9}\,t^{16}+\frac{355252391817400}{9}\,t^{14}+\frac{68378910769169000}{81}\,t^{12}+\frac{2260368009271972600}{243}\,t^{10}+\frac{10863031144502537000}{243}\,t^8+\frac{78544749617454620500}{2187}\,t^6+\frac{13808886200832600377500}{19683}\,t^4-\frac{12934524968912559512500}{19683}\,t^2-\frac{27771380912032848002412500}{531441}\Big)\,x^{20}+\Big(293930\,t^{24}+\frac{293991880}{3}\,t^{22}+\frac{129744835220}{9}\,t^{20}+\frac{10377500348600}{9}\,t^{18}+53572820774550\,t^{16}+\frac{13065704465198000}{9}\,t^{14}+\frac{15987203586473119000}{729}\,t^{12}+\frac{368550382777130554000}{2187}\,t^{10}+\frac{9447034190513732312187}{}\,t^8+\frac{175826232378634712875000}{59049}\,t^6-\frac{3225589197078194008562500}{177147}\,t^4-\frac{26874207494234805767562500}{531441}\,t^2+\frac{40516627046452373768826875}{177147}\Big)\,x^{18}+\big(203490\,t^{26}+71208410\,t^{24}+\frac{34262480980}{3}\,t^{22}+\frac{9263172082780}{9}\,t^{20}+\frac{167157956122850}{3}\,t^{18}+\frac{5548040292814250}{3}\,t^{16}+\frac{977895647675947000}{27}\,t^{14}+\frac{98796645394546099000}{243}\,t^{12}+\frac{4796486572313698512250}{2187}\,t^{10}+\frac{53949259281978384073750}{6561}\,t^8-\frac{72007665606274683910625006561}{59049}\,t^6-\frac{38720041443505991467648750}{177147}\,t^4+\frac{12236568998998042486493956250}{531441}\,t^2+\frac{29612659579871878066788481250}{531441}\Big)\,x^{16}+\big(116280\,t^{28}+41954640\,t^{26}+\frac{21654014200}{3}\,t^{24}+\frac{6487987066400}{9}\,t^{22}+\frac{400431559820600}{9}\,t^{20}+\frac{15842597995070000}{9}\,t^{18}+\frac{387881509931377000}{9}\,t^{16}+$$

$$\frac{52065471534516440000}{81}\,t^{14}+\frac{13340946813139820875000}{2187}\,t^{12}+$$
$$\frac{16769579350325260459000}{6561}\,t^{10}-\frac{77777192371888579319750000}{19683}\,t^{8}-$$
$$\frac{650856092767480713813700000}{177147}\,t^{6}+$$
$$\frac{772584095703354541342986250000}{531441}\,t^{4}+$$
$$\frac{18683211813953947136451575000}{177147}\,t^{2}+$$
$$\frac{3515442901067136917196068750000}{531441}\Big)\,x^{14}+\big(54264\,t^{30}+19815880\,t^{28}+$$
$$3599992760\,t^{26}+\frac{3535390934600}{9}\,t^{24}+\frac{732832492771400}{27}\,t^{22}+$$
$$\frac{101228428792090600}{81}\,t^{20}+\frac{27370708689515191000}{729}\,t^{18}+$$
$$\frac{170942329321206443000}{243}\,t^{16}+\frac{20207635390942154155000}{2187}\,t^{14}+$$
$$\frac{54323923384598442575000}{729}\,t^{12}-\frac{84652259354721712704050000}{19683}\,t^{10}+$$
$$\frac{44254063693754686188917500 0}{59049}\,t^{8}+$$
$$\frac{34032578513612094160297052500 0}{531441}\,t^{6}+$$
$$\frac{11214905814539048318037966625000}{1594323}\,t^{4}+$$
$$\frac{66938714349325879543197840125000}{4782969}\,t^{2}-$$
$$\frac{49648614435150545238896784812500 0}{43046721}\Big)\,x^{12}+\big(20349\,t^{32}+7370384\,t^{30}$$
$$+\frac{4175192840}{3}\,t^{28}+\frac{1474902065840}{9}\,t^{26}+\frac{337402973593700}{27}\,t^{24}+$$
$$\frac{52955521397069200}{81}\,t^{22}+\frac{5796598700963270200}{243}\,t^{20}+$$
$$\frac{1231989028743827354000}{2187}\,t^{18}+\frac{19331925392497315848250}{2187}\,t^{16}$$
$$+\frac{7103148781467394155500 00\,t^{14}}{6561}+\frac{16604666383183532408755000\,t^{12}}{19683}$$
$$+\frac{9741429479396098659675500 00\,t^{10}}{19683}+$$
$$\frac{96689882575212403619991598750 0\,t^{8}}{531441}$$
$$+\frac{38869440974605335709680915850000\,t^{6}}{1594323}+$$

$$\frac{427206289275180085895959109375000\,t^4}{4782969}+$$
$$\frac{433893468319006960931185268750000\,t^2}{14348907}+$$
$$+\left(5985\,t^{34}+2100945\,t^{32}+405469960\,t^{30}+\frac{458704157800\,t^{28}}{9}+\right.$$
$$\frac{38257142877100\,t^{26}}{9}+\frac{6655221161886500\,t^{24}}{27}+$$
$$\frac{290043365177293000\,t^{22}}{27}+\frac{79906863097974913000\,t^{20}}{243}+$$
$$\frac{1397848018419046319125 0\,t^{18}}{2187}+\frac{691787098499321408333750\,t^{16}}{6561}+$$
$$\frac{5075812594018448164382500 0\,t^{14}}{19683}+$$
$$\frac{690407358964170001672017500 0\,t^{12}}{59049}+$$
$$\frac{178061631206617270042239058750 0\,t^{10}}{531441}+$$
$$\frac{880875494598322142789575956250 0\,t^8}{177147}+$$
$$\frac{425611566376910377760538116875000\,t^6}{1594323}+$$
$$\frac{255716521573770519512649711812500 0\,t^4}{4782969}+$$
$$\frac{105312775710846364036536547105468 75\,t^2}{14348907}-$$
$$\left.\frac{165303868342551177798903647037109375}{43046721}\right)x^8+\left(1330\,t^{36}+440020\,t^{34}\right.$$
$$+\frac{255465910\,t^{32}}{3}+\frac{101835163360\,t^{30}}{9}+\frac{27839829798200\,t^{28}}{27}+$$
$$\frac{195173340698000\,t^{26}}{3}+\frac{793937870170991000\,t^{24}}{243}+$$
$$\frac{93497936075368916000\,t^{22}}{729}+\frac{8067284989927579916500\,t^{20}}{2187}$$
$$+\frac{5143752792067415040515000\,t^{18}}{59049}+$$
$$\frac{1971595706674548111532375 00\,t^{16}}{59049}$$
$$+\frac{2495172012804924058996390000 0\,t^{14}}{177147}+$$
$$+\frac{9842397570889593537590788025000 0\,t^{10}}{1594323}+$$

$$\frac{7731893138662149328740897778750000\,t^{8}}{1594323}$$
$$+\frac{3453926582309903966120517162500000\,t^{6}}{1594323}+$$
$$\frac{1106258645429815455904534411328125 0\,t^{4}}{43046721}-$$
$$\frac{19787724705519904413718263216015625 00\,t^{2}}{129140163}+$$
$$\frac{7806909581043151408593466642392578125 0}{3486784401}\Bigg)x^{6}+\Big(210\,t^{38}+$$
$$\frac{189490\,t^{36}}{3}+\frac{35909650\,t^{34}}{3}+\frac{14981399650\,t^{32}}{9}+\frac{4520197971800\,t^{30}}{27}+$$
$$\frac{943387657415000\,t^{28}}{81}+\frac{51651141194611000\,t^{26}}{81}+$$
$$\frac{7502510197238875000\,t^{24}}{243}+\frac{2944961558842115312500\,t^{22}}{2187}+$$
$$\frac{1094716544015072936457500\,t^{20}}{19683}+\frac{4156171022211643623563375 00\,t^{18}}{177147}$$
$$+\frac{1631510672898336531552501 2500\,t^{16}}{177147}+$$
$$\frac{1296580044821647817703096625000\,t^{14}}{531441}+$$
$$\frac{6912596567627896756277429262500 0\,t^{12}}{1594323}+$$
$$\frac{2104539412822602705384844784375000\,t^{10}}{4782969}+$$
$$\frac{1037515177725120759119883240312500 0\,t^{8}}{4782969}+$$
$$\frac{1871772963735645018625934677632812 50\,t^{6}}{43046721}-$$
$$\frac{3747063417256555658124396401054687 50\,t^{4}}{14348907}+$$
$$\frac{1722418219199126224053433188040820312 50\,t^{2}}{1162261467}+$$
$$\frac{2296165252273808625473936117942089843750}{10460353203}\Bigg)x^{4}+\Big(21\,t^{40}+5460\,t^{38}$$
$$+\frac{8815030\,t^{36}}{9}+\frac{1264694900\,t^{34}}{9}+\frac{143286898825\,t^{32}}{9}+$$
$$\frac{107472139686800\,t^{30}}{81}+\frac{19113680572231000\,t^{28}}{243}+$$
$$\frac{1166058628437430000\,t^{26}}{243}+\frac{2151001000264478862 50\,t^{24}}{729}+$$

$$\frac{335144166243836015885000\,t^{22}}{19683}+\frac{551264896318780692298250 0\,t^{20}}{6561}+$$
$$\frac{16921307853928066209195575000\,t^{18}}{531441}+$$
$$\frac{44666020829263147470577045625 0\,t^{16}}{531441}+$$
$$\frac{86436099533037207187426692500 00\,t^{14}}{531441}+$$
$$\frac{90409932530899648480447446312 5000\,t^{12}}{4782969}+$$
$$\frac{10581733599205122998294829928750000\,t^{10}}{14348907}+$$
$$\frac{10468380944493892085976126183554 6875\,t^{8}}{14348907}+$$
$$\frac{11132484872863479901707200292460937500\,t^{6}}{129140163}+$$
$$\frac{77645513554018408690183677405923828 1250\,t^{4}}{1162261467}+$$
$$\frac{13816292532860541437890469861927734 37500\,t^{2}}{1162261467}-$$
$$\frac{67810168755232716118919756568718261 71875}{31381059609}\Bigg)\,x^2+t^{42}+\frac{623\,t^{40}}{3}+$$
$$\frac{298690\,t^{38}}{9}+\frac{42592130\,t^{36}}{9}+\frac{5471772425\,t^{34}}{9}+\frac{1840236638975\,t^{32}}{27}+$$
$$\frac{4646271972911800\,t^{30}}{729}+\frac{1071194036163601000\,t^{28}}{2187}+$$
$$\frac{73077160861345117750\,t^{26}}{2187}+\frac{1160566131863029390362 50\,t^{24}}{59049}+$$
$$\frac{16622946598174278228002500\,t^{22}}{177147}+$$
$$\frac{17929622698339763296360475 00\,t^{20}}{531441}+$$
$$\frac{47449313453716467895257906250\,t^{18}}{531441}+$$
$$\frac{11642980235607678680773362812 50\,t^{16}}{531441}+$$
$$\frac{80469014025449969075792886250 00\,t^{14}}{177147}+$$
$$\frac{30627329797561880522657099456875000\,t^{12}}{43046721}+$$
$$\frac{99912921025813536114651672455898 4375\,t^{10}}{129140163}+$$
$$\frac{30615375950471269505467863854066 40625\,t^{8}}{43046721}+$$

$$\frac{1444919423625289681163097716325894531250\,t^6}{3486784401}+$$
$$\frac{7168271840945207899663953737380683593750\,t^4}{10460353203}+$$
$$\frac{4090969780646034191369353841088833007812 5\,t^2}{31381059609}+$$
$$\frac{1398762058423838035423742258927954101562 5}{31381059609}.$$

B.2 Monic Polynomial Solutions of (3.31)

The following solutions and their complex conjugates all satisfy the bilinear form of the Boussinesq equation (3.31) with a_i, b_i and c_i all constants.

$$\begin{aligned}
F_1^{mon} =& x + \mathrm{i}t + a_0,\\
F_2^{mon} =& \left(x + \frac{b_0}{2}\right)^2 + \left(t + \frac{b_1}{2}\right)^2 + 1,\\
\sim& x^2 + t^2 + 1,\\
F_3^{mon} =& x^3 + (3\mathrm{i}t + c_0)x^2 + \left(-3t^2 + 2\mathrm{i}tc_0 + \frac{c_0^2}{3} - \frac{1}{3}\right)x - \mathrm{i}t^3 - c_0t^2\\
&+ \frac{\mathrm{i}(c_0^2+5)}{3}t + c_1,
\end{aligned}$$

Appendix C

Generalised Solutions to the Boussinesq Equation

The section below gives the polynomial solutions P_n and Q_n that are currently known for the generalised Boussinesq equation (4.3) as mentioned in Chapter 4.

C.1 P and Q Functions of (4.3)

It is possible to see that not only do these equations have a high structure within themselves but they also have many similarities with the solutions given in Appendix B.1.

$$
\begin{aligned}
P_1 =& 3x^2 - t^2 + \frac{5}{3}, \\
Q_1 =& x^2 - 3t^2 - \frac{1}{3}, \\
P_2 =& 5\,x^6 + \left(-5\,t^2 + 35\right) x^4 + \left(-9\,t^4 - \frac{190}{3}\,t^2 - \frac{665}{9}\right) x^2 + t^6 - \frac{7}{3}\,t^4 - \frac{245}{9}\,t^2 \\
& + \frac{18865}{81}, \\
Q_2 =& x^6 + \left(-9\,t^2 + \frac{13}{3}\right) x^4 + \left(-5\,t^4 - \frac{230}{3}\,t^2 - \frac{245}{9}\right) x^2 + 5\,t^6 + 15\,t^4 + \frac{535}{9}\,t^2
\end{aligned}
$$

$$+\frac{12005}{81},$$

$$P_3 = 7\,x^{12}+\left(-14\,t^2+210\right)x^{10}+\left(-63\,t^4-630\,t^2+\frac{875}{3}\right)x^8+\left(-36\,t^6-2044\,t^4-\frac{16100}{3}\,t^2+\frac{16100}{3}\right)x^6+\left(25\,t^8+260\,t^6-\frac{39550}{3}\,t^4-\frac{91700}{3}\,t^2-\frac{1066975}{9}\right)x^4+\left(18\,t^{10}+\frac{1310}{3}\,t^8+\frac{26140}{3}\,t^6+\frac{146300}{3}\,t^4+\frac{1835050}{9}\,t^2+\frac{32655350}{27}\right)x^2-t^{12}-\frac{10}{3}\,t^{10}+25\,t^8-\frac{1900}{3}\,t^6-\frac{1230775}{9}\,t^4-\frac{2070250}{3}\,t^2+\frac{32680375}{81},$$

$$Q_3 = x^{12}+\left(-18\,t^2+\frac{74}{3}\right)x^{10}+\left(-25\,t^4-\frac{1870}{3}\,t^2-\frac{275}{3}\right)x^8+\left(36\,t^6-580\,t^4-\frac{8860}{3}\,t^2+\frac{4700}{3}\right)x^6+\left(63\,t^8+1820\,t^6-\frac{2450}{3}\,t^4-\frac{37100}{3}\,t^2-\frac{247625}{9}\right)x^4+\left(14\,t^{10}+630\,t^8+\frac{49700}{3}\,t^6+48300\,t^4+\frac{1877750}{9}\,t^2+\frac{2898350}{9}\right)x^2-7\,t^{12}-98\,t^{10}-\frac{5075}{3}\,t^8-23100\,t^6-\frac{2108225}{9}\,t^4-\frac{43900150}{27}\,t^2-\frac{4998175}{81},$$

$$P_4 = 9\,x^{20}+\left(-30\,t^2+770\right)x^{18}+\left(-243\,t^4-3390\,t^2+14245\right)x^{16}+\left(-360\,t^6-24360\,t^4-107800\,t^2+\frac{754600}{9}\right)x^{14}+\left(130\,t^8-23720\,t^6-\frac{2278220}{3}\,t^4-\frac{4419800}{3}\,t^2-\frac{51285850}{27}\right)x^{12}+\left(780\,t^{10}+\frac{94820}{3}\,t^8-\frac{759640}{3}\,t^6-\frac{82510120}{9}\,t^4+\frac{16762900}{27}\,t^2+\frac{5563180700}{81}\right)x^{10}+\left(690\,t^{12}+58700\,t^{10}+\frac{3917450}{3}\,t^8+\frac{79849000}{9}\,t^6-\frac{1064659750}{27}\,t^4-\frac{5795597500}{27}\,t^2-\frac{1367658734750}{729}\right)x^8+\left(152\,t^{14}+\frac{65800}{3}\,t^{12}+\frac{11986520}{9}\,t^{10}+\frac{120221500081}{}t^8+\frac{8625185800}{81}\,t^6+\frac{69758781400}{243}\,t^4+\frac{1077743975000}{243}\,t^2+\frac{55941010279000}{2187}\right)x^6+\left(-75\,t^{16}-\frac{10360}{3}\,t^{14}-\frac{66500}{9}\,t^{12}+\frac{69057800}{9}\,t^{10}+\frac{20996610250}{243}\,t^8+\frac{275830555000}{243}\,t^6+\frac{5620866905500}{729}\,t^4-\frac{9843829765000}{729}\,t^2+\frac{404610075244375}{2187}\right)x^4+\left(-30\,t^{18}-1790\,t^{16}-\frac{803320}{9}\,t^{14}-\frac{28869400}{9}\,t^{12}-\frac{1473856300}{27}\,t^{10}-\frac{629478426500}{729}\,t^8-\right.$$

$$\frac{11032069279000}{729}\,t^6 - \frac{133702667483000}{729}\,t^4 - \frac{112127684226250}{243}\,t^2 - \frac{5297582110686250}{19683}\Bigg)\,x^2 + t^{20} + \frac{70}{3}\,t^{18} + \frac{1855}{3}\,t^{16} + \frac{1899800}{81}\,t^{14} + \frac{438095350}{243}\,t^{12} + \frac{88186059500}{729}\,t^{10} + \frac{14094153477250}{6561}\,t^8 + \frac{138847640239000}{6561}\,t^6 - \frac{823906531765625}{19683}\,t^4 - \frac{20487539830546250}{177147}\,t^2 + \frac{266883842659905625}{531441},$$

$$Q_4 = x^{20} + \left(-30\,t^2 + \frac{230}{3}\right)x^{18} + \left(-75\,t^4 - 2830\,t^2 + \frac{2695}{3}\right)x^{16} + \Big(152\,t^6 - \frac{18680}{3}\,t^4 - \frac{615640}{9}\,t^2 + \frac{237160}{81}\Bigg)\,x^{14} + \left(690\,t^8 + \frac{63560}{3}\,t^6 - \frac{1276100}{9}\,t^4 - \frac{1832600}{3}\,t^2 - \frac{60772250}{243}\right)x^{12} + \left(780\,t^{10} + 62860\,t^8 + \frac{8213240}{9}\,t^6 - 586600\,t^4 + \frac{116801300}{27}\,t^2 + \frac{8356925500}{729}\right)x^{10} + \left(130\,t^{12} + \frac{117700}{3}\,t^{10} + \frac{4962650}{3}\,t^8 + \frac{1352661800}{81}\,t^6 + \frac{179352250}{243}\,t^4 - \frac{117373448500}{729}\,t^2 - \frac{2249680490750}{6561}\right)x^8 + \left(-360\,t^{14} - 15400\,t^{12} + \frac{1286600}{3}\,t^{10} + \frac{82943000}{9}\,t^8 + \frac{8897211400}{81}\,t^6 + \frac{65165639000}{243}\,t^4 + \frac{3029653781000}{729}\,t^2 + \frac{31684368485000}{6561}\right)x^6 + \left(-243\,t^{16} - 19560\,t^{14} - \frac{2325260}{3}\,t^{12} - \frac{29280440}{9}\,t^{10} - \frac{59473750}{27}\,t^8 + \frac{61024825400}{243}\,t^6 - \frac{320631426500}{729}\,t^4 - \frac{37020326189000}{729}\,t^2 + \frac{425463980932375}{19683}\right)x^4 + \left(-30\,t^{18} - 2910\,t^{16} - 191800\,t^{14} - \frac{23294600}{3}\,t^{12} - \frac{2501523500}{27}\,t^{10} - \frac{34775471500}{27}\,t^8 - \frac{1233890119000}{81}\,t^6 - \frac{9121143955000}{81}\,t^4 - \frac{114976450146250}{243}\,t^2 - \frac{153076114099562 50}{177147}\right)x^2 + 9\,t^{20} + 370\,t^{18} + 15325\,t^{16} + \frac{5192600}{9}\,t^{14} + \frac{475032950}{27}\,t^{12} + \frac{35488950700}{81}\,t^{10} + \frac{6433079133250}{729}\,t^8 + \frac{234408499325000}{2187}\,t^6 + \frac{315145911994375}{2187}\,t^4 + \frac{4908421805113750}{19683}\,t^2 + \frac{140298620844930625}{531441}.$$

Appendix D

KP Equation Solutions

This chapter is concerned with the solutions of the KP-I equation as mentioned in Chapter 6.

D.1 Polynomial Functions as in [1]

These solutions are the non-matrix solutions given in [1] up to 3 with $a = 0$ and $b = 1$. It seems that F_3 does not solve the KP-I equation.

$$
\begin{aligned}
F_1 =& x^2 - 24\,xt + 4\,y^2 + 144\,t^2 + \frac{1}{4},\\
F_2 =& x^4 + (-48\,t + 2)\,x^3 + \left(8\,y^2 + 864\,t^2 - 24\,t + 3\right)x^2 + \left((-192\,t - 8)\,y^2 - \right.\\
& \left. 6912\,t^3 - 288\,t^2 - 24\,t + 3\right)x + 16\,y^4 + \left(1152\,t^2 - 96\,t\right)y^2 + 20736\,t^4\\
& + 3456\,t^3 + 432\,t^2 - 12\,t + \frac{3}{2},\\
F_3 =& x^6 + (-72\,t + 3)\,x^5 + \left(12\,y^2 + 2160\,t^2 - 36\,t + \frac{15}{2}\right)x^4 + \left((-576\,t - 24)\,y^2\right.\\
& \left. -34560\,t^3 - 2592\,t^2 - 24\,t + \frac{27}{2}\right)x^3 + \left(48\,y^4 + \left(10368\,t^2 + 864\,t\right)y^2\right.\\
& \left. +311040\,t^4 + 72576\,t^3 - 432\,t^2 + 18\,t + \frac{81}{4}\right)x^2 + \left((-1152\,t - 144)\,y^4 + \right.\\
& \left.\left(-82944\,t^3 - 10368\,t^2 - 576\,t + 18\right)y^2 - 1492992\,t^5 - 684288\,t^4 - 31104\,t^3\right.
\end{aligned}
$$

$$+2376\,t^2 - 90\,t + \frac{81}{4}\Big)\,x + 64\,y^6 + \big(6912\,t^2 - 576\,t + 72\big)\,y^4 + \big(248832\,t^4$$
$$+41472\,t^3 + 27648\,t^2 + 72\,t - 9\big)\,y^2 + 2985984\,t^6 + 2239488\,t^5 + 321408\,t^4$$
$$- 54432\,t^3 + 3060\,t^2 - 81\,t + \frac{171}{16}.$$

D.2 Method for Limit Work

This additional work aimed to find a pattern behind the scaling and translation that was required for proof of the KP-I limit work in §6.6. This would aid in the finding of a proof for all waves, not just those on a specific line.

D.2.1 'Paired' Waves at Negative t

Considering only the waves that paired up at negative time and those that had a solution as $X = \sqrt{ct} + \xi$, the following was found.

function	value of c from $\sqrt{ct}$	value of ξ
$u_{[2]}$	24	$-\frac{1}{2}$
$u_{[3]}$	72	$-\frac{2}{3}$
$u_{[4]}$	$72 + 24\sqrt{6}$	$-\frac{1}{2} - \frac{\sqrt{6}}{6}$
$u_{[5]}$	$120 + 24\sqrt{10}$	$-\frac{2}{3} - \frac{\sqrt{10}}{6}$
$u_{[1,2]}$	-24	-1
$u_{[1,4]}$	$24 + 24\sqrt{2}$	-1
$u_{[1,5]}$	120	$-\frac{13}{10}$
$u_{[2,3]}$	$24\mathrm{i}\sqrt{3}$	$-\frac{\mathrm{i}}{6}\sqrt{3} - 1$
$u_{[2,4]}$	$24 + 24\mathrm{i}\sqrt{2}$	$-\frac{\mathrm{i}}{2}\sqrt{3} - \frac{7}{6}$

The absence of $u_{[1,3]}$ in the table above is due to the fact that there was no solution for $X = \sqrt{ct} + \xi$ but there was a solution for $X = (ct)^{1/3} + \xi$ for which the results are below.

function	value of c from $(ct)^{\frac{1}{3}}$	value of ξ
$u_{[1,3]}$	12	-1

Some of the values of c and ξ are complex as in the case of $u_{[2,3]}$ and $u_{[2,4]}$. This may mean that another ansatz needs to be used rather than the square root.

D.2.2 'Paired' Waves at Positive t

Moving to positive time and considering the functions in which there were paired waves gave the following.

function	value of c from $\sqrt{ct}$	value of ξ
$u_{[1,2]}$	24	-1
$u_{[1,4]}$	$-24 + 24\sqrt{2}$	-1
$u_{[1,5]}$	-120	$-\frac{13}{10}$

Where the solution given for $u_{[1,5]}$ has a square root that is imaginary which again may require refining of the ansatz.

Appendix E

Maple Code

This chapter gives some samples of the code used in parts of this thesis. There are times where the full detail has been given in some commands but that is optional, for instance regarding the lighting and colour alterations in a plot.

E.1 Calculating F^{BE}

It was necessary to use the packages "linalg" and "CodeTools" in the following code. For simplicity the alias command was used as well with regard to F to speed up coding time.

```
>restart:
>with(linalg):with(CodeTools):alias(F=F(x,t)):
```

Below is the bilinear form of the Boussinesq equation after substitution of $u = 2\left[\ln(F)\right]_{xx}$, as given in (3.31).

```
>BLF:=F*diff(F,t$2)-diff(F,t)^2+F*diff(F,x$2)-diff(F,x)^2-
(1/3)*F*diff(F,x$4)+(4/3)*diff(F,x)*diff(F,x$3)-diff(F,x$2)^2:
```

Now the aim is to construct a polynomial of only even powers of x and t such that the order of the polynomial is $n(n+1)$ and all possible elements are included.

Consider a polynomial defined as

$$\sum_{i=0}^{6}\sum_{j=0}^{6} A_{i,j}x^i t^j.$$

This will have order 12 and will include odd powers of x and t so in order to remove anything of order greater than 6 and any odd powers, utilise a three level for loop. Firstly require that $i+j \leq 6$ and if not set the function inside the sums to be 0. If this condition is met then require that $i+j$ is even else set the function to 0. Finally it is required that j (or indeed i) is even so that any odd powers are removed. Then sum over the 0 to 6 for both indexes and are only left with the coefficients that are wanted.

```
>printlevel:=3:
 for i from 0 to 6 do
 for j from 0 to 6 do
 if i+j<=6 then
 if type(i+j,even)=true then
 if type(j,even)=true then
 p[i,j]:=A[i,j]*x^i*t^j
 else p[i,j]:=0 end if
 else p[i,j]:=0 end if
 else p[i,j]:=0
 end if end do
 enddo:
>f2:=collect(sum(sum(p[k,l],k=0..6),l=0..6),x):
```

It still remains to calculate what the coefficients need be in order to satisfy the equation named "BLF". In order to do this, substitute the polynomial into the equation and assume that $A_{6,0}$, which is the coefficient of x^6, to be non-zero.

One could pick either $A_{6,0}$ or $A_{0,6}$ to keep something of order 6. Since both x^6 and t^6 share the same coefficient, it seems that if you set them to 0 and try and find a solution of the "BLF" then the solution collapses to F_1. Similarly with higher order polynomials, they collapse to the prior solution. Then substitute these solutions back into the function $f2$ so that all coefficients are in terms of $A_{6,0}$.

```
>coeffs(collect(expand(subs(F=f2,BLF)),[t,x],'distributed'),[t,x]):
 solve({%},useassumptions) assuming A[6,0]<>0:
 F2:=subs(%,f2):
>expand(subs(F=F2,BLF)):
```

If this is substituted back into "BLF" then the solution is 0. As such, it is possible to any value of $A_{6,0}$ here and it will satisfy the equation, however as this is just a scaling the simplest thing to do is set $A_{6,0} = 1$ and have a monic polynomial.

```
>subs(A[6,0]=1,F2):
```

This is now the polynomial F_2 of degree $n(n+1)$ where $n = 2$ that satisfies the "BLF" equation and is the unique monic polynomial solution.

E.2 Root Trajectory Graphs

For the graphs shown in Figure 3.6 the digits in Maple had to be increased in order to achieve the correct accuracy. The graphs were formed via the following code with the polynomial solutions of the Boussinesq bilinear form being read in from a separate file and F_n being denoted as $F[n]$.

```
>restart:
>with(plots):Digits:=50:
>currentdir():
```

```
>read"Ffunctionsto5.txt":
>A[3]:=eval(allvalues(RootOf(F[3],x))):
 for n from 1 to 12 do
 A[3][n]
 end do:
>F3roots:=complexplot({A[3]},t=-10..10,style=point,symbol=
 solidcircle,color="Purple",symbolsize=5,numpoints=500,
 view=[-6..6,-15..15]):
>display([F3roots]):
```

Using the "RootOf" command to compute the roots of the polynomial F_3 in the form $x(t)$. It is necessary to use "allvalues" to keep all, in this case 12, roots. Once these roots have been assigned to a name; $A[3]$, then one can create a complex plot that varies t to create the trajectories. It is equally possible to calculate the roots as $t(x)$ but this seemed less intuitive.

E.3 KP Limit Work

The maximums are generally found when either $X = 0$ or $Y = 0$. The template below shows how the limits were established when the roots where not so easily determined, namely for positive time F_3^{KP} for the paired maximums that move with time rather than the central maximum. Note that F_3^{KP} is denoted in the code as $F(3)$.

```
>restart:
>with(linalg):
>Digits:=50:
>with(plots):
>with(RootFinding):
```

```
>phi:=k->-k*x-y*k^2-4*k^3*t:
>psi:=m->subs(k=-I,diff(exp(I*phi(k)),k$m)):
>p:=m->simplify(psi(m)*exp(-I*phi(-I))):q:=m->subs(I=-I,p(m)):
>F:=m->sort(collect(simplify(expand(p(m)*q(m))+sum(diff(expand(
 p(m)*q(m)),x$j)/(2)^j,j=1..2*m),symbolic),[x,y,t],factor),order=
 plex(x,y,t)):
>F(3):sort(collect(expand(subs(x=X+12*t,y=Y,F(3))),[X,Y,t]),order
 =plex(X,Y,t)):
>animate(plot3d,[2*diff(ln(F(3)),X$2),X=-10..10,Y=-5..5],t=-10..10,
 grid=[10,10],orientation=[90,0,0]):
```

The animated plot is used to establish an estimate of where the maximums move along and to verify that it is positive time that is being considered. With this information it is possible to now use numerical testing to progress with the problem.

```
>Spat:=diff(2*diff(ln(F(3)),X$2),X):
>Time:=diff(2*diff(ln(F(3)),X$2),Y):
>Spat1:=subs(t=1,Spat):
 Time1:=subs(t=1,Time):
 evalf((solve([Spat1,Time1])[2])[1]):
>Spat10:=subs(t=10,Spat):
 Time10:=subs(t=10,Time):
 evalf((solve([Spat10,Time10])[2])[1]):
>Spat100:=subs(t=100,Spat):
 Time100:=subs(t=100,Time):
 evalf((solve([Spat100,Time100])[2])[1]):
>Spat1000:=subs(t=1000,Spat):
 Time1000:=subs(t=1000,Time):
```

```
evalf((solve([Spat1000,Time1000])[2])[1]):
```

Select input 2 from the "solve" to select one of the pairs of maximums that do not sit on $Y = 0$ and then input 1 of this to give the value of X at this point alone. From the numerical results above, it seems that the waves are not stationary on X but that they may tend to a limit. Seen as the concern is with the behaviour in the limit $t \to \infty$ then this can still be used.

If the limit is $0.8\dot{3}$ as it seems to be from testing then X is tending to $\frac{5}{6}$. Assuming this, one can substitute this into the equations and see if a reasonable limit is obtained.

```
>diff(subs(X=5/6,t=50,u3),X):
>diff(subs(X=5/6,t=500,u3),X):
>diff(subs(X=5/6,t=10000000,u3),X):
>seq(Isolate(numer(factor(diff(subs(X=5/6,t=50,u3),Y))),[Y])[i],
 i={1,7}):
>seq(Isolate(numer(factor(diff(subs(X=5/6,t=500,u3),Y))),[Y])[i],
 i={1,7}):
>seq(Isolate(numer(factor(diff(subs(X=5/6,t=10000000,u3),Y))),[Y])
 [i], i={1,7}):
```

By running the code one can see that the differences for the solutions of Y at each time are getting smaller, suggesting that the assumption that $X = 5/6$ is correct. It transpires that it is the solutions 1 and 7 from the sequence output that pertain to the maximums. Since only real solutions are wanted, the command "Isolate" from "RootFinding" has been used but due to the restrictions when using this it is necessary to take the numerator of $(\widehat{u}_3)_Y$ first in order for it to calculate. Now that this assumption has numerical evidence to support it, consider the evolution of the waves which is believed to be of a quadratic nature.

```
>eq:=factor(subs(Y=0,2*diff(ln(F(3)),X$2))):
 subs(X=c*sqrt(t)+xi,%):
 series(%,t=-infinity,7):
 factor(op(1,%))+factor(op(2,%))+factor(op(3,%));
```

Since the behaviour is quadratic in t it is necessary to take $X = c\sqrt{t} + \xi$. This is different from the notation used in Appendix D.2 as it is often easier for Maple to compute e.g. c rather than $\sqrt{c}$. Using the ansatz and considering $t \to -\infty$ the first few terms are selected. The use of the "op" function was merely due to the fact that often the series had to be taken to quite a high order in order to get solutions but it was only necessary to print the first 2 or 3 terms. All terms where functions of $1/t$ which is not what is wanted, but letting $c = \sqrt{-72}$ will alter this behaviour and hopefully give a different asymptotic behaviour so this substitution is used.

```
>subs(X=sqrt(-72*t)+xi,eq):
 series(%,t=-infinity,7):
 factor(op(1,%))+factor(op(2,%));
 solve(diff(op(1,%),xi));
```

As was thought, the new series now has an initial term that is independent of t but is a function of ξ. The critical point of this function is what is required so the differential is taken in terms of ξ and then solved to give 3 solutions. Of these solutions, 2 pertain to the troughs on that same trajectory and the other is the peak. The solution in this case is $\xi = -2/3$.

```
 subs(X=sqrt(-72*t)-2/3,eq):
 series(%,t=-infinity,7):
 factor(op(1,%))+factor(op(2,%));
```

This is substituted in and the series taken again with now the result of the first term, which is the only term independent of t and the only term that will remain in the limit $t \to -\infty$, is 16. A proof that the waves that evolve in pairs on the path $(X + 2/3)^2 + 72t = 0$ have a limit as $t \to -\infty$ of 16. It is also possible to compute this by letting $t = -\tau$ and taking the limit as $\tau \to \infty$ which gives the same result but different values for c and ξ. The same process is used for $t \to \infty$ as has been shown for $t \to -\infty$.

There is also the central wave to consider which evolves in a linear way. This method is shown in the code below.

```
>eq:=factor(subs(Y=0,2*diff(ln(F(3)),X$2))):
 subs(X=c*t+xi,%):
 series(%,t=-infinity,20):
 factor(op(1,%))+factor(op(2,%))+factor(op(3,%));
```

Much as before but here the solution for c that will give a term independent of t in the limit is $c = 0$.

```
 subs(X=xi,eq):
 series(%,t=-infinity,7):
 factor(op(1,%))+factor(op(2,%));
 solve(diff(op(1,%),xi));
```

In this case the solution found is $\xi = -1/6$.

```
 subs(X=-1/6,eq):
 series(%,t=-infinity,7):
 factor(op(1,%))+factor(op(2,%));
```

Again the first term is now 16, so the central wave evolves on the line $X = -1/6$ and has a limit of 16 as $t \to -\infty$.

E.4 KP Limit Graphs

Having completed the limiting work described in Appendix E.3, it still remains to produce the graphs. The following code describes how these graphs were formed.

```
>restart:
>with(linalg):Digits:=20:
 with(plots):
>phi:=k->-k*x-y*k^2-4*k^3*t:
>psi:=m->subs(k=-I,diff(exp(I*phi(k)),k$m)):
>p:=m->simplify(psi(m)*exp(-I*phi(-I))):q:=m->subs(I=-I,p(m)):
>F:=m->sort(collect(simplify(expand(p(m)*q(m))+sum(diff(expand(
 p(m)*q(m)),x$j)/(2)^j,j=1..2*m),symbolic),[x,y,t],factor),order=
 plex(x,y,t)):
>F(3):
 newF(3):=sort(collect(expand(subs(x=X+12*t,y=Y,F(3))),[X,Y,t]),
 order=plex(X,Y,t));
```

Beginning by defining the function as usual, this will be a work through of $u_{[3]}$. Since the waves reside on different lines for positive and negative time, the two cases will be dealt with separately. The aim is to have multiple lines corresponding to different values of t plotted on the same axis so it is possible to see if there's any evidence that a limit is reached as $|t| \to \infty$. Since the maximums that are being considered for negative t occur on $Y = 0$, the following code is used.

```
>setcolors("Spring"):
>plot({seq(subs(Y=0,t=n,2*diff(ln(newF(3)),X$2)),n=-50..0,1/2)},
X=-30..30);
```

This produces the plot as given in Figure 6.33(d). Now consider positive time whereby the maximums considered occur on $X = 5/6$.

```
>plot({seq(subs(X=5/6,t=n,2*diff(ln(newF(3)),X$2)),n=0..10,1/2)},
Y=-15..15);
```

This code produces the plot as in Figure 6.33(c). The code can also be used for the Figures 4.8 and 4.9.

E.5 KP Heat Graphs

In this code the KP solutions are generated within the file as described in §6.3.1. In order to produce the graphs as in Figure 6.34, the solutions are plotted with time varying. In order to see how the maximums of the graph develop as time increases, it is easiest to have the maximums appearing in red and the standard sea state in blue. This is achieved with the "colorscheme" and "densityplot" commands below.

```
>restart:
>with(linalg):Digits:=20:with(plots):
>phi:=(-k*x-k^2*y-4*k^3*t):
>psi:=(j,m)->subs(k=-I,diff(exp(I*phi),k$m)):
>psibar:=(j,n)->subs(I=-I,psi(j,n)):
>M:=(i,j,m,n)->simplify(int(psi(i,m)*psibar(j,n),x)):
>A1:=(m)->simplify(det(matrix([[M(1,1,m,m)]])),symbolic):
>factor(diff(ln(A1(3)),x)): denom(%):
 f3:=collect(%/coeff(%,x,degree(%,x)),[x,y,t],factor):
>F3:=sort(collect(expand(subs(x=X+12*t,y=Y,f3)),
 [X,Y,t]),order=plex(X,Y,t));
>u3:=2*diff(ln(F3),X$2):
```

This code uses the 2x2 matrix method for $u_{[3]}$. It is necessary to differentiate the determinant of the logarithm of the matrix and take its denominator in order to retrieve the polynomial. Then this is simplified as '$f3$' and '$F3$' represents the same polynomial but in the moving coordinates.

```
>X:=5/6:
 densityplot(u3,Y=-35..35,t=0..50,colorscheme=["Black","Black",
 "Black","DarkBlue","DarkBlue","DarkBlue","Yellow",
 "Yellow","Yellow","Red","Red","Red"],style=polygon,
 transparency=0.05,axes=boxed,grid=[250,250]);
 densityplot((u,gamma)->0.2*u,-2..16,0..2,style=PATCHNOGRID,
 colorscheme=["Black","Black","Black","DarkBlue","DarkBlue",
 "DarkBlue","Yellow","Yellow","Yellow","Red","Red","Red"],
 scaling=constrained,axes=boxed,labels=[u,""],
 transparency=0.05,numpoints=5000);
 unassign('X'):
```

For $u_{[3]}$, it is known that the maximums reside on $X = 5/6$ and the code above uses this to produce the graph. As mentioned in the thesis, since Maple does not have this code pre-programmed and the idea is to have the peaks appear in red and the steady sea state appear in blue, the colour scheme has to be selected quite carefully in the density plot. The second command is a scaled version of the colour scheme which provides the key for the graph.

Bibliography

[1] M.J. Ablowitz, S. Chakravarty, A.D. Trubatch and J. Villarroel, A novel class of solutions of the non-stationary Schrödinger and the Kadomtsev-Petviashvili I equations, *Phys. Lett. A*, **267** 132–146 (2000).

[2] M.J. Ablowitz and P.A. Clarkson, "*Solitons, Nonlinear Evolution Equations and Inverse Scattering*", *L.M.S. Lect. Notes Math.*, vol. **149**, C.U.P., Cambrdige (1991).

[3] M.J. Ablowitz and R. Haberman, Resonantly coupled nonlinear evolution equations, *J. Math. Phys.*, **16** 2301–2305 (1975).

[4] M.J. Ablowitz and H. Segur, On the evolution of packets of water waves, *J. Fluid Mech.*, **92** 691-715 (1979).

[5] M.J. Ablowitz and H. Segur, "*Solitons and the Inverse Scattering Transform*", SIAM, Philadelphia (1981).

[6] M.J. Ablowitz and J. Satsuma, Solitons and rational solutions of nonlinear evolution equations, *J. Math. Phys.*, **19** 2180–2186 (1978).

[7] A. Ankiewicz and N. Akhmediev, Multi-rogue waves and triangle numbers, *Australian and New Zealand Conference on Optics and Photonics (2015,Adelaide,South Australia) Engineers Australia/Australian Optical Society.*

[8] A. Ankiewicz, A.P. Bassom, P.A. Clarkson and E. Dowie, Conservation laws and integral relations for the Boussinesq equation, *arXiv:nlin/1611.09505v1.*

[9] A. Ankiewicz, P.A. Clarkson and N. Akhmediev, Rogue waves, rational solutions, the patterns of their zeros and integral relations, *J. Phys. A: Math. Theor.*, **43** 1–9 (2010).

[10] B. Baschek and J. Imai, Rogue wave observations off the US West Coast, *Oceanography*, **24** 158–165 (2011).

[11] D.J. Benney and A.C. Newell, The propogation of nonlinear wave envelopes, *J. Math. & Phys. (Stud. Appl. Math.)*, **46** 133–139 (1967).

[12] D.J. Benney and G.J. Roskes, Wave instabilities, *Stud. Appl. Math.*, **48** 377–385 (1969).

[13] Y.V. Bludov V.V. Konotop and N. Akhmediev, Matter rogue waves, *Phys. Rev. A*, **80** 033610 (2009).

[14] L.V. Bogdanov and V.E. Zakharov, The Boussinesq equation revisited, *Phys. D*, **165** 137–162 (2002).

[15] J. Boussinesq, Théorie de l'intumescence liquide, applele onde solitaire ou de translation, se propageant dans un canal rectangulaire, *Comptes Rendus*, **72** 1871 (755–759).

[16] J. Boussinesq, Théorie des ondes et des remous qui se propagent le long d'un canal rectangulaire horizontal, en communiquant au liquide contenu dans ce canal des vitesses sensiblement pareilles de la surface au fond, *J. Math. Pures Appl.*, **17** 55–108 (1872).

[17] N.D. Cahill, J.R. D'Errico, D.A. Narayan & J.Y. Narayan, Fibonacci determinants, *College Math. J.*, **33(3)** 221–225 (2002).

[18] P.J. Caudrey, The inverse problem for the third order equation $u_{xxx}+q(x)u_x+r(x)u = i\rho^3 u$, *Phys. Lett.*, **79A** 264–268 (1980).

[19] P.J. Caudrey, The inverse problem for a general NxN spectral equation, *Physica*, **6D** 51–66 (1982).

[20] C.A. Charalambides, "*Enumerative Combinatorics*", *CRC Press Series on Discrete Mathematics and its Applications*, Chapman & Hall/CRC, Boca Raton, FL (2002).

[21] O. Chvartatskyi and F. Muöller-Hoissen, NLS breathers, rogue waves, and solutions of the Lyapunov equation for Jordan blocks, *J. Phys. A: Math. Theor.*, **50** 1–20 (2017).

[22] P.A. Clarkson, Special polynomials associated with rational solutions of the Painlevé equations and applications to soliton equations, *Comput. Methods Funct. Theory*, **6** 329–401 (2006).

[23] P.A. Clarkson and E. Dowie, Rational solutions of the Boussinesq equation and applications to rogue waves, *arXiv:nlin/1609.00503v1.*

[24] P.A. Clarkson and M.D. Kruskal, New similarity reductions of the Boussinesq equation, *J. Math. Phys.*, **30** 2201–2213 (1989).

[25] A. Degasperis and S. Lombardo, "*Integrability in Action: Solitons, Instability and Rogue Waves*", *Lecture Notes in Physics*, **926**, Springer, London (2016).

[26] P. Deift, C. Tomei and E. Trubowitz, Inverse scattering and the Boussinesq equation, *Commun. Pure Appl. Math.*, **35** 567–628 (1982).

[27] P. Dubard and V.B. Matveev, Multi-rogue wave solutions to the focusing NLS equation and the KP-I equation, *Natural Hazards and the Earth System Sciences*, **11** 667–672 (2011).

[28] P. Dubard and V.B. Matveev, Multi-rogue waves solutions: from the NLS to the KP-I equation, *Nonlinearity*, **26** 93–125 (2013).

[29] J.M. Dudley, F. Dias, M. Erkintalo and G. Genty, Instabilites, breathers and rogue waves in optics, *Nature Photonics*, **8** 755–764 (2014).

[30] J.M. Dudley, G. Genty, F. Dias, B. Kibler and N. Akhmediev, Modulation instability, Akhmediev breathers and continuous wave supercontinuum generation, *Opt. Expr.*, **17** 21497–21508 (2009).

[31] A.S. Fokas and M.J. Ablowitz, On the inverse scattering of the time-dependent Schrödinger equation the associated Kadomtsev-Petviashvili equation, *Stud. Appl. Math.*, **69** 211–228 (1983).

[32] P. Gaillard, Families of quasi-rational solutions of the NLS equation and multi-rogue waves, *J. Phys. A: Math. Theor.*, **44** 1–15 (2011).

[33] P. Gaillard, Higher order Peregrine breathers, their deformations and multi-rogue waves, *J. Phys.: Conf. Ser.*, **482** 012016 (2014).

[34] A.N. Ganshin, V.B. Efimov, G.V. Kolmakov, L.P. Mezhov-Deglin and P.V.E. McClintock, Observation of an inverse energy cascade in developed acoustic turbulence in superfluid helium, *Phys. Rev. Lett.*, **101** 065303 (2008).

[35] S Haver, A possible freak wave event measured at the Draupner jacket January 1 1995, in "*Proceedings of Rogue Waves*", edited by M. Olagnon and M. Prevosta [Ifremer, Brest], 1–8 (2004).

[36] W. Hereman, P.J. Adams, H.L. Eklund, M.S. Hickman and B.M. Herbst, "*Direct Methods and Symbolic Software for Conservation Laws of Nonlinear Equations*", *Advances in nonlinear waves and symbolic computation*, Nova Sci. Publ., New York (2009).

[37] R Hirota, Exact N-soliton solutions of the wave equation of long waves in shallow-water and in nonlinear lattices, *J. Maths. Phys.*, **14** 810–814 (1973).

[38] E. Infeld and G. Rowlands, "*Nonlinear Waves, Solitons and Chaos*", C.U.P. Cambridge (1990).

[39] W.P. Johnson, The curious history of Faá di Bruno's formula, *Amer. Math. Monthly*, **109** 217–234 (2002).

[40] B.B. Kadomtsev and V.I. Petviashvili, On the stability of solitary waves in weakly dispersing media, *Soviet Phys. Dokl.*, **15** 539-541 (1970).

[41] D.J. Kedziora, A. Ankiewicz and N. Akhmediev, Circular rogue wave clusters, *Phys. Rev. E*, **84** 056611 (2011).

[42] D.J. Kedziora, A. Ankiewicz and N. Akhmediev, Triangular rogue wave cascades, *Phys. Rev. E*, **86** 056602 (2012).

[43] B. Kibler, J. Fatome, C. Finot, G. Millot, F. Dias, G. Genty, N. Akhmediev and J.M. Dudley, The Peregrine soliton in nonlinear fibre optics, *Nat. Phys.*, **6** 790–795 (2010).

[44] J. Hietarinta, Hirota's bilinear method and soliton solutions, *Physics AUC*, **15** 31–37 (2005).

[45] B.G. Konopelchenko, "*Introduction to Multidimensional Integrable Equations: The Inverse Spectral Transform in* $2+1$ *Dimensions*", Plenum Press, New York and London (1992).

[46] W.X. Ma, Wronskians, generalized wronskians and solutions to the Korteweg-de Vries equation, *Chaos, Solitons & Fractals*, **19** 163–170 (2004).

[47] S.V. Manakov, The inverse scattering transform for the time-dependent Schrödinger equation and the Kadomtsev-Petviashvili equation, *Physica*, **3D** 420–427 (1981).

[48] S. Novikov, S.V. Manakov, L.P. Pitaevski and V.E. Zakharov, "*Theory of Solitons. The Inverse Scattering Method*", Contemporary Soviet Math., Consultants Bureau [Plenum], New York (1984).

[49] Y. Ohta and J. Yang, Rogue waves in the Davey-Stewartson I equation, *Phys. Rev. E*, **86** 036604 (2012).

[50] Y. Ohta and J. Yang, Dynamics of rogue waves in the Davey Stewartson II equation, *J. Phys. A*, **46** 105202 (2013).

[51] A.R. Osborne, "*Nonlinear Ocean Waves and the Inverse Scattering Transform*", *International Geophysics Series*, vol. **97**, Academic Press, Boston (2010).

[52] D. Pelinovsky, Rational solutions of the Kadomtsev-Petviashvili hierarchy and the dynamics of their poles. I. New form of a general rational solution, *J. Math. Phys.*, **35** 5820–5830 (1994).

[53] D. Pelinovsky, Rational solutions of the KP hierarchy and the dynamics of their poles. II. Construction of the degenerate polynomial solutions, *J. Math. Phys.*, **39** 5377–5395 (1998).

[54] D.E. Pelinovsky and C. Kharif (Editors), "*Extreme Ocean Waves*", Second Edition, Springer (2016).

[55] D.E. Pelinovsky and Y.A. Stepanyants, New multisoliton solutions of the Kadomtsev-Petviashvili equation, *JETP Lett.*, **57** 25–29 (1993).

[56] H. Segur and A. Finkel, An analytical model of periodic waves in shallow water, *Stud. Appl. Math.*, **73** 183–220 (1985).

[57] D.R. Solli, C. Ropers, P. Koonath and B. Jalali, Optical rogue waves, *Nature*, **450** 1054–1057 (2007).

[58] N.J.A. Sloane, "*The On-Line Encyclopedia of Integer Sequences*", published electronically at https://oeis.org (2016).

[59] L. Stenflo and M. Marklund, Rogue waves in the atmosphere, *J. Plasma Physics*, **76** 293–295 (2010).

[60] S. Turitsyn and G. Falkovitch, Stability of magneto-elastic solitons and self-focusing of sound in antiferromagnet, *Soviet Phys. JETP*, **62** 146–152 (1985).

[61] J. Villarroel and M.J. Ablowitz, On the discrete spectrum of the nonstationary Schrödinger equation and multipole lumps of the Kadomtsev-Petviashvili I equation, *Comm. Math. Phys.*, **207** 1–42 (1999).

[62] Z.Y. Yan, Financial rogue waves, *Commun. Theor. Phys.*, **54** 947–949 (2010).

[63] Z.Y. Yan, Vector financial rogue waves, *Phys. Lett. A*, **375** 4274–4279 (2011).

[64] V.E. Zakharov and A.B. Shabat, A scheme for integrating the nonlinear equations of mathematical physics by the method of the inverse scattering problem, *Func. Anal. Appl.*, **8** 226–235 (1974).

[65] V.E. Zakharov and A.B. Shabat, Exact theory of two-dimensional self-focusing and one-dimensional of waves in nonlinear media, *Sov. Phys. JETP*, **34** 62–69 (1972).

[66] D. Zhang, Notes on solutions in wronskian form to soliton equations: KdV-type, *arXiv:nlin/0603008v3*.